

**WL-TR-97-1181**

**INTEGRATED OPTICAL TRANSCEIVER**

**GEOFFREY W. TAYLOR**

**UNIVERSITY OF CONNECTICUT  
PHOTONICS RESEARCH CENTER  
2600 GLENBROOK ROAD U-157  
STORRS, CT 06269**



**JUNE 1997**

**FINAL REPORT FOR PERIOD 09/16/95 - 03/31/97**

**Approved for public release; distribution unlimited**

**19980420 124**

**THIS QUALITY INSPECTED 4**

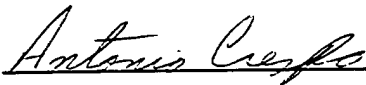
**AVIONICS DIRECTORATE  
WRIGHT LABORATORY  
AIR FORCE MATERIEL COMMAND  
WRIGHT-PATTERSON AIR FORCE BASE, OH 45433-7623**

## NOTICE

USING GOVERNMENT DRAWINGS, SPECIFICATIONS, OR OTHER DATA INCLUDED IN THIS DOCUMENT FOR ANY PURPOSE OTHER THAN GOVERNMENT PROCUREMENT DOES NOT IN ANY WAY OBLIGATE THE US GOVERNMENT. THE FACT THAT THE GOVERNMENT FORMULATED OR SUPPLIED THE DRAWINGS, SPECIFICATIONS, OR OTHER DATA DOES NOT LICENSE THE HOLDER OR ANY OTHER PERSON OR CORPORATION; OR CONVEY ANY RIGHTS OR PERMISSION TO MANUFACTURE, USE, OR SELL ANY PATENTED INVENTION THAT MAY RELATE TO THEM.

THIS REPORT IS RELEASABLE TO THE NATIONAL TECHNICAL INFORMATION SERVICE (NTIS). AT NTIS, IT WILL BE AVAILABLE TO THE GENERAL PUBLIC, INCLUDING FOREIGN NATIONS.

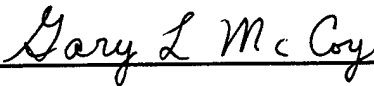
THIS TECHNICAL REPORT HAS BEEN REVIEWED AND IS APPROVED FOR PUBLICATION.



Antonio Crespo  
Project Manager  
Electro-Optical Components Branch



Charles H. Stevens  
Chief, WL/AADO  
Electro-Optical Components Branch



Gary L. McCoy  
Technical Director  
Electron Devices Division

IF YOUR ADDRESS HAS CHANGED, IF YOU WISH TO BE REMOVED FROM OUR MAILING LIST, OR IF THE ADDRESSEE IS NO LONGER EMPLOYED BY YOUR ORGANIZATION PLEASE NOTIFY WL/AADO WRIGHT-PATTERSON AFB OH 45433-7322 TO HELP MAINTAIN A CURRENT MAILING LIST.

Do not return copies of this report unless contractual obligations or notice on a specific document requires its return.

REPORT DOCUMENTATION PAGE			Form Approved OMB No. 0704-0188	
Public reporting burden for this collection of information is estimated to average 1 hour per response, including the time for reviewing instructions, searching existing data sources, gathering and maintaining the data needed, and completing and reviewing the collection of information. Send comments regarding this burden estimate or any other aspect of this collection of information, including suggestions for reducing this burden, to Washington Headquarters Services, Directorate for Information Operations and Reports, 1215 Jefferson Davis Highway, Suite 1204, Arlington, VA 22202-4302, and to the Office of Management and Budget, Paperwork Reduction Project (0704-0188), Washington, DC 20503.				
1. AGENCY USE ONLY (Leave blank)		2. REPORT DATE JUN 1997	3. REPORT TYPE AND DATES COVERED FINAL 09/16/95--03/31/97	
4. TITLE AND SUBTITLE INTEGRATED OPTICAL TRANSCEIVER			5. FUNDING NUMBERS C F33615-95-C-1632 PE 62204 PR 2001 TA 02 WU AN	
6. AUTHOR(S) GEOFFREY W. TAYLOR				
7. PERFORMING ORGANIZATION NAME(S) AND ADDRESS(ES) UNIVERSITY OF CONNECTICUT PHOTONICS RESEARCH CENTER 260 GLENBROOK ROAD U-157 STORRS, CT 06269			8. PERFORMING ORGANIZATION REPORT NUMBER	
9. SPONSORING/MONITORING AGENCY NAME(S) AND ADDRESS(ES) AVIONICS DIRECTORATE WRIGHT LABORATORY AIR FORCE MATERIEL COMMAND WRIGHT PATTERSON AFB OH 45433-7623 POC: ANTONION CRESPO, WL/AADO (937)255-7310 Ext 3359			10. SPONSORING/MONITORING AGENCY REPORT NUMBER WL-TR-97-1181	
11. SUPPLEMENTARY NOTES				
12a. DISTRIBUTION/AVAILABILITY STATEMENT APPROVED FOR PUBLIC RELEASE; DISTRIBUTION IS UNLIMITED.			12b. DISTRIBUTION CODE	
13. ABSTRACT (Maximum 200 words)  In previous work for the Air Force on the Three Terminal Optoelectronic Array program, a technology base was developed for the implementation of monolithic integrated optoelectronic circuits based upon the modulation doped inversion channel interface. In the Integrated Optical Transceiver program, that technology was adapted to the implementation of travelling wave devices that could operate at frequencies up to 100Gb/s. The concepts of a grating coupled vertical cavity laser and a grating coupled resonant cavity detector are introduced and designs were completed and implemented in photomasks. The performance of the second order grating was evaluated and models developed. The insertion of the grating into the vertical cavity waveguide was characterized and the laser performance was analyzed. A new approach to the implementation of the waveguide was developed. The speed of the detector was analyzed as a function of the velocity mismatch. A complete set of photomasks (14 levels) was developed including travelling wave devices, O/E test circuits and a variety of diagnostic test chips. The devices implemented include FET circuits-CCDs, switch based O/E interface circuits, HFET and DOES lasers as vertical emitters, directional couplers, and heterodyne laser sources.				
14. SUBJECT TERMS Vertical Cavity Lasers, Travelling Wave Operation Optoelectronic Switched, Grating Coupled			15. NUMBER OF PAGES 110	
			16. PRICE CODE	
17. SECURITY CLASSIFICATION OF REPORT UNCLASSIFIED	18. SECURITY CLASSIFICATION OF THIS PAGE UNCLASSIFIED	19. SECURITY CLASSIFICATION OF ABSTRACT UNCLASSIFIED	20. LIMITATION OF ABSTRACT SAR	

## TABLE OF CONTENTS

1. SUMMARY .....	1
2. BACKGROUND .....	2
3. LASER DESIGN REQUIREMENTS FOR 100GHz OPERATION .....	5
4. THE GRATING COUPLED VERTICAL CAVITY LASER .....	7
5. DETERMINATION OF DIFFRACTION EFFICIENCIES IN THE GRATING COUPLED VERTICAL CAVITY LASER .....	8
6. DETAILED DC OPERATION OF THE GCVCSEL .....	12
7. HIGH SPEED OPERATION OF THE GCVSEL .....	18
8. THE HFET VERTICAL CAVITY TRAVELING WAVE DETECTOR .....	21
8.1 General Design .....	21
8.2 Dynamic Response .....	25
8.2.1 Impulse Response and Small Signal Transfer Function .....	26
8.2.2 Parasitic Time Constant .....	30
9. FABRICATION AND PHOTOMASK DESIGN AND GENERATION .....	32
10. GROWTH AND TESTING .....	35
11. REFERENCES .....	37
12. Appendices .....	42
Appendix A. Determination of Diffraction Efficiency for a second order Corrugated Waveguide .....	42
Appendix B. Diffraction Into Corrugated Waveguide From Normally Incident Radiation .....	76

## LIST OF FIGURES

Fig.1 Grating Coupled Traveling Wave Laser .....	6
Fig.2 Traveling wave optoelectronic device cross-section in the ICT.....	6
Fig.3 Topologies for the diffraction of light normal to a corrugated waveguide.	
left, light incident externally upon a corrugated waveguide	
right, light incident upon corrugation from within guide (w or w/o grating) .....	9
Fig. 4 Diffraction efficiency versus grating angle in a three-layer dielectric guide.....	9
Fig. 5 Diffraction efficiency versus the grating angle in the vertical cavity waveguide. ....	11
Fig. 6 Waveguide photon density versus device length.....	15
Fig. 7 Effective velocity matching on the optical output response.....	19
Fig. 8 Current flow diagram for laser and detector .....	22
Fig. 9 Circuit model of transmission line for traveling wave optoelectronic devices .....	25
Fig. 10 Effective velocity matching on the optical input response .....	27
Fig. 11 Traveling Wave Detector Dynamic Response.....	30

## **PREFACE**

This final technical report describes the results of one and a half years of effort on the Integrated Optical Transceiver program to develop 100GHz operation in electro-optic transceivers. The program resulted in the development of new concepts in device operation and fabrication and growth for a unified set of components in the Inversion Channel Technology. The designs analyses, fabrication sequence design and photomask design are described in detail.

## 1. SUMMARY

The integrated Optical transceiver program was initiated on Sept. 16, 1995 and was concluded on March 31, 1997. This phase I effort was concerned with establishing the feasibility of implementing an electro-optic data link with a digital data capability of 100Gb/s or an analog transmission rate of 100GHz . To achieve this goal, three new concepts were introduced which included a grating coupled vertical cavity laser and detector, a traveling wave electro-optic device design that builds upon the existing inversion channel technology, and an implementation of the inversion channel bipolar transistor that can achieve very low parasitic resistance by virtue of its inverted structure. The effort in this program established a technology plan to achieve 100GHz operation in traveling wave operation. The principles of diffraction in second order corrugated waveguides were established and tools were developed to design the grating coupled laser. The principles of velocity matching in electro-optic devices was developed through the analysis of the grating coupled detector for high speed operation. The fabrication sequence of the Inversion Channel Technology was completely revised to enable waveguides and traveling wave operation. Growth and fabrication of these concepts is the next step.

## 2. BACKGROUND

The integrated optical transceiver program was designed to determine the feasibility of a high bandwidth, frequency-modulated transceiver for optical data communications to and from an electronic source. The E/O and O/E signal conversions need to be suitable for digital transmission at 100 Gb/s with a bit error rate of  $10^{-12}$  or analog transmission with a 3 dB cut-off frequency of 100 GHz. Our interpretation of the program requirements was that a single channel operating at 100 GHz was desired and therefore the goal was operation of electronic amplifying devices with cut-off frequencies of 150 GHz-200 GHz and optoelectronic devices with cut-off frequencies of 100 GHz. The higher frequency operation of transistors is needed to build circuits with this performance. Multiple channels could be considered to reduce the bandwidth requirement on the emitters and detectors but it would still require the same speed of electronics.

An analysis of these requirements indicates that the problems of interconnection of the electronic and optoelectronic components are major obstacles to these goals and that a monolithic approach that integrates all of these components on the same substrate is the only practical way to approach this performance. Above 20 GHz the problems of wire or even bump bonding of transistor circuits to opto devices becomes very difficult. The metal traces on the chips must be matched to 50 ohms and the solder bump impedance must appear as 50ohms. If wire bonding and MM wave connectors are used these must also be matched to the metal traces. To achieve a manufacturable (affordable) result monolithic integration is the only solution.

Our proposal to achieve these goals was based upon a monolithic integrated technology approach which was developed by WPAFB through funding to AT&T over the period from 1987-1994. This technology has been designated as the Inversion Channel Technology (ICT) because it utilizes the inversion channel formed at a modulation doped interface as the active element in transistor, laser, detector, and modulator devices. It also produces all of these devices with a single unified fabrication sequence which uses the same set of processing steps to realize all components simultaneously. The starting wafer is grown by MBE and a single layer sequence is used for all devices without the requirement for any regrowth steps. This technology is actually an optoelectronic version of the very successful PHEMT technology because it employs essentially the same growth structure. Both wafer growths utilize a modulation doped III-V interface in which a multiple quantum well of strained InGaAs forms a channel at a heterostructure interface. Both growths start from a SI GaAs substrate and place moderately p-doped AlGaAs below the quantum wells. In these respects they are essentially identical. Where they differ is above the quantum well(s). Whereas the PHEMT grows only a thin layer of undoped AlGaAs upon which a schottky gate is formed, the opto PHEMT grows layers of p doped AlGaAs which are terminated in p+ doping to form an ohmic contact. It is this innovation which allows the formation of the laser, the detector and the transistor simultaneously.

The ICT technology was developed at AT&T, first with edge emitting optical devices and then with vertical cavity optical devices. The vertical cavity technology version was barely to the point of full demonstration when this program was interrupted by AT&T and the PI moved to the University of Connecticut. What had been



demonstrated was the operation of the transistor, the switching laser and the detector all from the same epitaxial wafer. In terms of performance at that point in time, the transistor operated at 14 GHz using Be for p doping for a 1  $\mu$ m device gate length but when Carbon was used for the p doping in the growth and e-beam lithography was used to generate 0.5  $\mu$ m gates, we obtained 40 GHz cut-off frequencies. The vertical cavity laser 3dB frequency was 3.8 GHz. The resonant cavity detector from this epi growth was demonstrated with near unity quantum efficiency but speed measurements were not obtained. These component demonstrations were made from the same epitaxy and using the same fabrication sequence. Due to the success of the individual experiments, photomasks were designed to produce functional opto IC's. Initial fabrication had begun and a couple of chips made it almost to the end of the sequence. These chips however did not qualify for deposition of dielectric stacks to demonstrate the opto devices and so final testing of full IC's had only just begun. Testing was restricted to the FET electronic devices where divide by two circuits and flip flops were demonstrated and to individual laser devices where a threshold of 2 mA for the DOES laser with proton implant isolation was achieved.

We have proposed for the integrated optical transceiver program to use the ICT as a starting point to realize monolithically integrated components. However, to have a hope of achieving the very high bandwidth operation, several device innovations were required because there are no known device structures either within the ICT or elsewhere, that could achieve 100GHz operation in the laser. There are also no known detector structures that could achieve these bandwidths within the constraints of a monolithic integrated circuit. In addition, although the laser and detector were not required to be part of the same chip, our concept was to produce one integrated circuit which would perform the transceiver function at either end of an optical link so the integration would include the laser, detector and FET electronics. There were therefore, several challenges to be met in our program and these are listed

- Devise a laser structure within the ICT to achieve 100 GHz operation. This means reworking the DOES laser or HFET laser concept to circumvent the conventional limits
- Devise a detector within the ICT to achieve 100 GHz operation. The HFET detector concept must also be reworked to address the high speed requirement.
- The new concepts required on-chip waveguides. Therefore the processing flow sequence to build the ICT had to be totally redesigned. As it turned out, the photomask sequence and usage were altered substantially from the final AT&T version in order to accommodate the new concepts. Therefore a major mask redesign had to be implemented
- The new laser and detector designs required CAD design tools for gratings that did not exist and thus a major effort was needed to analyze and understand the performance parameters of second order gratings.
- To build these complex structures requires a state-of-the-art fabrication and growth facility. A major burden on the PI since arriving at UConn was to put this capability in place. The task was finished only as the program drew to a close and was the major reason why so little progress was made within the one year on the reduction to practice of these concepts.

In the next sections we describe the innovations , simulations , analyses and designs that were implemented resulting in the final photomasks that were made for the demonstration. We will also describe our efforts to reach a demonstration and how funding limitations have curtailed our attempts to move forward. Our present efforts to acquire these funds through other channels and the current status and plans will be mentioned briefly.

### 3. LASER DESIGN REQUIREMENTS FOR 100GHz OPERATION

The laser structure to achieve 100 GHz operation must be a vertical cavity device because it is only the vertical cavity in which

- (1) the separate confinement heterostructure (SCH) region can be made very short because optical confinement by the SCH region is not required (the optical confinement in the vertical cavity is the ratio of the quantum wells to the cavity length). When the SCH region is very short (a few hundred angstroms), the low frequency roll-off effects are minimized so that low frequency roll-off can be extended to beyond 100GHz.
- (2) The photon lifetime of the cavity can be made very short. Since the stimulated lifetime tracks the photon lifetime to within  $1/Q$  ( $Q$  is the quality factor of the laser) then this determines the ultimate laser speed. In calculations of the response the parameter of interest is the differential stimulated lifetime. In conventional laser jargon this is proportional to the differential gain.

When both these effects have been addressed for high speed operation then the remaining limitations on the laser response are the time constants presented by resistance and capacitance. First there is the time constant determined by the resistance and capacitance internal to the laser diode. In the vertical cavity laser, the resistance is primarily the contact resistance of the p type contact and its associated current crowding and the capacitance is that of the i region of the pin structure. The capacitance is fixed by design but the resistance can be minimized by innovations in the metallurgy and the geometry of the contact areas. Reducing this resistance becomes the ultimate limitation in increasing the bandwidth of the laser. The second time constant is the one determined by the laser capacitance and the load impedance driven by the laser. For discrete laser devices this is always 50 ohms. In order to address this issue, a traveling wave type of operation is required. A concept was therefore introduced by which the virtues of the vertical cavity laser could be maintained within the context of a traveling wave device. The physical implementation of the concept was within the ICT and the device is shown in cross-section along the direction of the traveling wave in Fig.1 and in a perspective view from the input port in Fig.2.

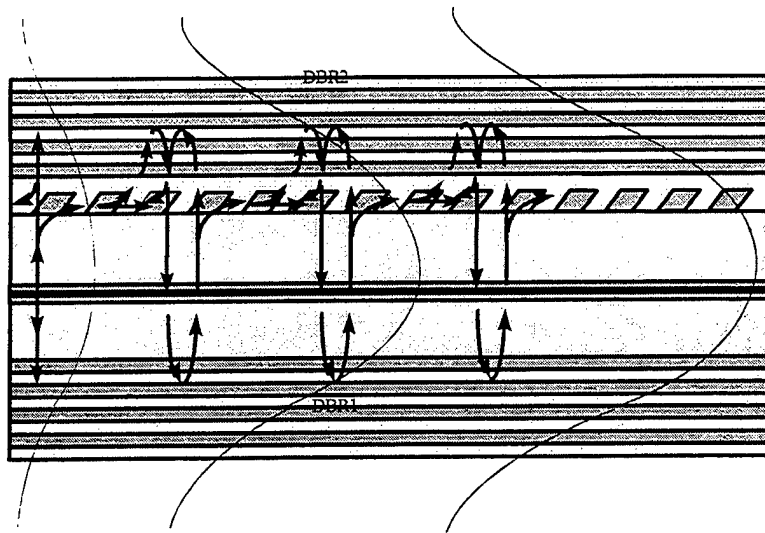


Fig.1 Grating Coupled Traveling Wave Laser

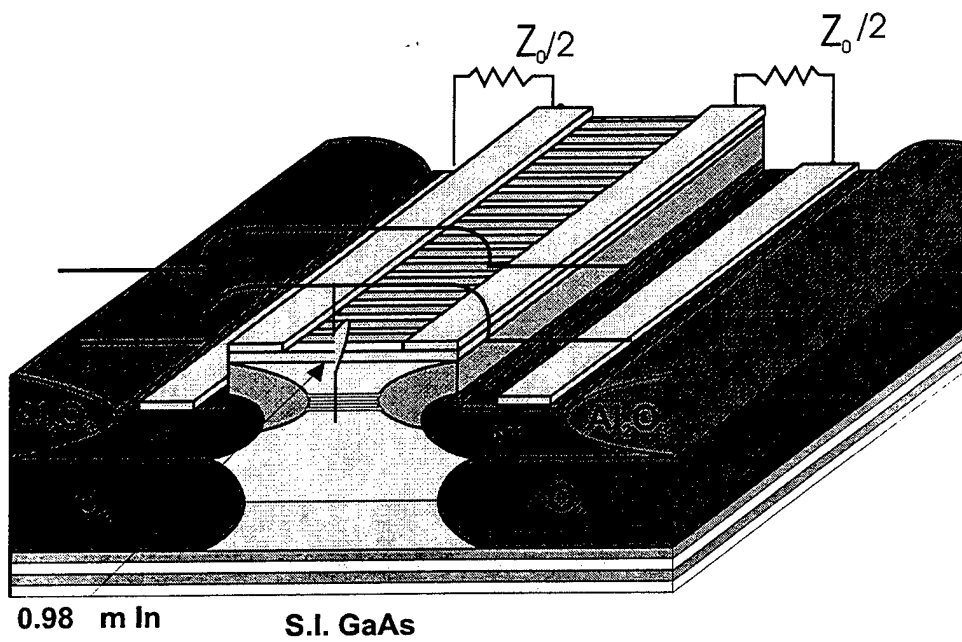


Fig.2 Traveling wave optoelectronic device cross-section in the ICT

#### 4. THE GRATING COUPLED VERTICAL CAVITY LASER

The innovation is to introduce a diffraction grating within the vertical cavity as shown in Fig.1. The grating is formed in the first layer of the mirror stack. It is a blazed grating which diffracts light preferentially in one direction. The DBR mirrors of the vertical cavity device are deposited on top of the mirror and of course the bottom mirror is formed under the device during the growth. We call this device the Grating Coupled Vertical Cavity Surface Emitting Laser (GC VCSEL). To understand the operation of the GC VCSEL consider the VCSEL operation at the back end of the device ( $x = 0$  in Fig.1) . The front end at  $x = L$  is the output port where light is to be emitted. The current is to be applied uniformly along the length of the device. When current is applied, light is generated vertically in the VCSEL at  $x = 0$ . Consider the optical wave in the cavity as it passes through the grating. A small fraction is diffracted to the left. Due to the asymmetry of the blaze a much smaller fraction is diffracted to the right (this is illustrated by the relative sizes of the arrows in Fig.1). Now if the grating were of zero thickness, then the remainder of the light, which is most of the energy, would pass through the grating, be reflected back and pass through the grating in the reverse direction. Due to the reversibility of the diffraction process, the majority of this light would be diffracted in the reverse direction with the net result that the light would be coupled fairly equally in both directions. However, the grating has a finite thickness and in addition the penetration of the light into the mirror is small for a high reflectivity mirror. Thus the intensity of the light traveling downward into the laser after reflection from the mirror decreases dramatically with penetration into the mirror. It follows then that the amplitude of the light incident on the grating from within the cavity is substantially greater than the amplitude of the light incident on the grating by reflection from the mirror. Therefore the fraction of light diffracted to the right is substantially less than the fraction of light diffracted to the left.

The design criterion that is followed is that the thickness of the diffraction grating should be approximately equal to the penetration depth of the mirror ( this is also determined by the standing wave effects in the grating which are found from the diffraction analysis). This situation is the one that will be implemented in practice because for a high reflectivity mirror, the decay of intensity to about 10% occurs within the first  $\frac{1}{4}$  wavelength of the mirror stack and additionally, it is most practical to form the grating by etching through approximately the first layer of the mirror stack. In the fabrication sequence, the dielectrics chosen to form the mirrors are  $\text{SiO}_2$  and undoped sputtered GaAs. This choice is dictated by the very large index difference which reduces the number of required pairs and the fact that our mirror must be deposited during the device processing. Given these layer components we have two choices to implement the grating 1)deposit a layer of GaAs and then pattern and etch this layer followed by a  $\frac{1}{4}$  wave of  $\text{SiO}_2$  and then GaAs etc. 2)deposit a  $\frac{1}{4}$  wave layer of  $\text{SiO}_2$ , pattern and etch this layer and then deposit a  $\frac{1}{4}$  wave of GaAs and then  $\text{SiO}_2$  and then GaAs etc. The second of these is the one we will start with in the fabrication. The choice of  $\frac{1}{4}$  wave thickness is also supported by the grating efficiency and its dependence on the index difference between the layers of the stack as discussed in the next section on grating efficiencies. In

Fig.1, the relative sizes of the arrows indicate that the majority of light is diffracted to the right.

## 5. DETERMINATION OF DIFFRACTION EFFICIENCIES IN THE GRATING COUPLED VERTICAL CAVITY LASER

The quantitative prediction of diffracted power has been a subject of much study over the years primarily because of its importance to the operation of the DFB laser. In these cases the gratings are usually designed to be first order since it is the first order forward and backward traveling waves which form the basis of coupled mode theory. There are some instances where second order has been used in the DFB to produce an optical loss mechanism in an effort to stabilize the mode position as described by Kazarinov and Henry [6](however, the laser output is still via the first order wave). More generally the second order grating has been used as the output reflector for DBR lasers in order to obtain vertical emission. Since the second order grating when implemented as a waveguide corrugation produces both first order diffraction in the guide and second order diffraction normal to the guide then it can be used in the DBR to provide both reflection for the guided wave and output coupling of the laser light.

At the beginning of this work, the best available description of waveguide diffraction was the work of Streifer [5] and Kazarinov [6]. All of the existing work describes the diffraction in a general way which includes all possible diffraction orders. The results are complicated, difficult to understand and require a full numerical analysis to implement to obtain the quantitative predictions required for this work. We needed a simpler design tool with the same level of accuracy. Therefore it was undertaken to solve this problem in a more direct manner to produce more useable results. We are only interested in ideal second order diffraction so this was used as a starting point. It turns out that for this case the equations can be simplified and only one differential equation needs to be solved for a symmetrical grating. With this approach a simple predictor for diffraction efficiency was produced for both exact or approximate second order gratings, i.e. the approximate second order grating is one in which the grating pitch is either slightly smaller or larger than the exact value. This solver runs on a 200 MHz PC in about 150 secs to produce a complete calculation of efficiency versus grating depth for example. The basis for the model was a three layer waveguide characterized by indices  $n_1$ ,  $n_2$ , and  $n_3$  in the regions above the guide, in the guide and below the guide. This analysis was performed for diffraction from the guide to the direction normal to the guide. This work was published and a copy of the publication "Determination of Diffraction Efficiency for a Second-Order Corrugated Waveguide" is included in appendix A.

All of the published work on waveguide diffraction has been for the process of diffraction of the guided wave into an unguided (leaky) wave propagating away from the guide. Of most interest from the point of view of the grating coupled VCSEL, is the diffraction of light from a normally propagating wave into a guided wave (here the wave is generated within the vertical cavity and propagates into the grating as shown in Fig.3 ).

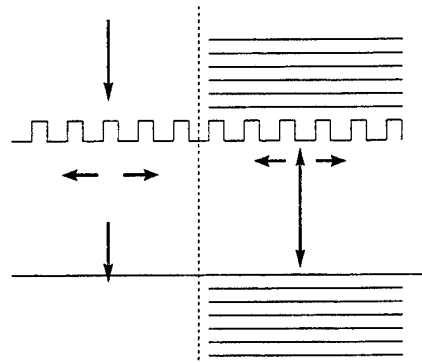


Fig.3 Topologies for the diffraction of light normal to a corrugated waveguide:  
left, light incident externally upon a corrugated waveguide  
right, light incident upon corrugation from within guide (w or w/o grating)

This is the reverse to the process described in the above paper but the efficiency of the process is not necessarily the same in spite of the fact that optical propagation of energy through a passive structure should be reversible. This is because of the transmission of energy straight through the guide which is not present in the out-of-guide case. Therefore this mechanism was also characterized using the same basic mathematical approach. This calculation was also performed for the generic three layer waveguide with a blazed grating. This work is summarized in the paper "Diffraction Into a Corrugated Waveguide From Normally Incident Radiation" which has been submitted for publication and forms appendix B. One further piece of necessary work was the determination of the optimum blaze angle to maximize the diffraction in one direction and to minimize it in the reverse. This design tool has also been developed and the results will be submitted for publication soon. Some typical results are shown in Fig.4 where we plot the diffraction efficiency into the guide for a corrugated waveguide as the blaze angle is varied. It shows the optimum angle for typical index parameters(  $n_1=n_3=3.4$  and  $n_2=3.6$ ) is about  $41^\circ$  and the ratio of the diffraction in the two directions is about 135.

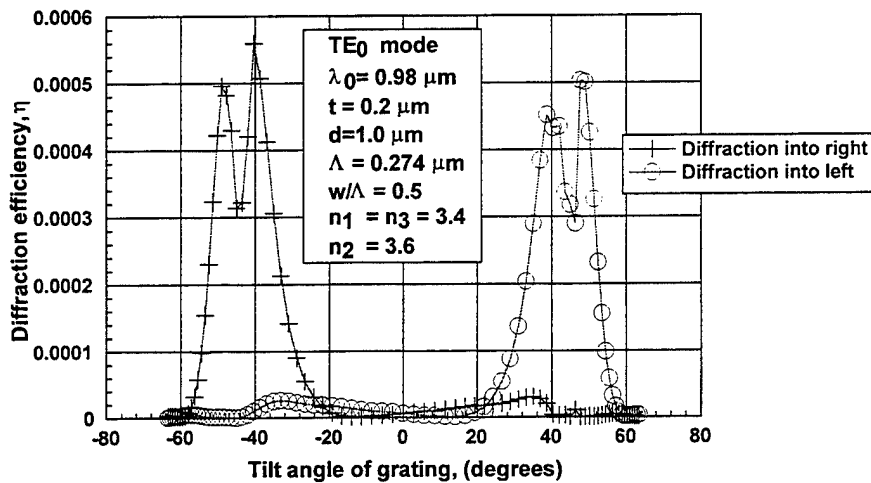


Fig. 4 Diffraction efficiency versus grating angle in a three-layer dielectric guide

The above two articles have produced the tools needed for the design of the GCVSEL. However, in the GCVSEL the waveguide cladding is formed by the Bragg mirrors and thus the structure forms a multilayer waveguide with very complicated propagation coefficients. In order to apply the diffraction model, it is necessary to represent the VCSEL waveguide by an equivalent three-layer guide. To do this it is necessary to represent the top(bottom) stack and its interface to air (substrate) by an infinite region with a single index. Since the material between the mirrors can be represented by a single index determined as the average over its layers, then the result will be a three-layer waveguide. The wave propagating in a vertical cavity laser is characterized by a penetration depth. This is normally used to determine the effective cavity length of the VCSEL as

$$L_{eff} = L_c + L_{pb} + L_{pt}$$

where  $L_{pb}$  and  $L_{pt}$  are the penetration depths of the bottom and top mirrors respectively which have been derived as

$$L_{ptb} = \frac{\tanh^2(|\kappa| \cdot L_{Mtb})}{2|\kappa|}$$

where  $L_{Mtb}$  is the total front and back mirror thicknesses, and  $\kappa$  is the coupling constant which is given by approximately

$$\kappa \cong 2i\Delta n/\lambda$$

Here,  $\Delta n$  is the index difference between the two layers in a pair of the mirror. In the standard description of the three-layer waveguide, the TE mode is normally described by a function within the guide (asymmetric or symmetric) and by evanescent decay into the cladding on either side of the guide. The evanescent decay away from the guide is determined by the refractive index in the region. To predict the behavior of the vertical cavity guide we assume that the penetration depth(s) of the vertical cavity mirror(s) correspond to the evanescent decay of a wave if it were propagating in the waveguide formed by the vertical cavity as the core of the guide, and the top and bottom mirrors as the claddings. Therefore, by using  $L_{pt,b}$  we can determine the effective index of the top and bottom mirror regions from the point of view of a three-layer waveguide. The formula given for  $L_{pt,b}$  corresponds to a vertically traveling wave which is a very high order mode in our vertical cavity (VC) waveguide, i.e. it is the maximum possible penetration. However in the fundamental mode the VC guide will propagate at some bounce angle and the penetration will be less. This penetration (and thus the more accurate indices) will be determined in general numerically by a TMM (transmission matrix method) solution of the multi-layer guide. Using these indices we can then use the model developed for the waveguide diffraction into a three layer waveguide to determine the efficiency of the second order diffraction from the vertically propagating light to the guided wave.

For the Vertical Cavity device we have designed, the mirror pairs on the top are  $\text{SiO}_2$  and GaAs corresponding to indices of 1.5 and 3.6. The bottom mirror is comprised of  $\text{Al}_x\text{O}_y$  and GaAs corresponding to indices of 1.6 and 3.6. The typical design will be 7 pairs on the bottom and 4-7 pairs on the top. Using these parameters we determine

$$L_{pt} = 0.16 \mu\text{m}$$

and therefore an effective index above the core of



$$n_{1eff} = 2.96$$

Similar calculations for the lower mirror yield  $n_{3eff} = 3.05$ . Then the diffraction efficiency is determined from our grating simulation by a three-layer waveguide with indices of  $n_1=2.96$ ,  $n_2=3.48$  and  $n_3=3.05$ . The index of the core region ( $n_2$ ) which is the vertical cavity itself, is determined by using a transmission matrix calculation for a slab waveguide. In Fig.5 we plot the efficiency of the diffraction process for a parallelogramic grating in the VCSEL waveguide such as the one portrayed in Fig.1. The results show that we can expect an efficiency of 0.0025 for a blaze angle of  $38^\circ$  and a grating etch depth of about  $0.2 \mu\text{m}$ . The simulation shows an efficiency of 0.0033 at an angle of  $46^\circ$ . Such large blaze angles may be difficult to achieve with ion beam etching and also, for a depth of  $0.2 \mu\text{m}$  the bottom of the parallelogram may penetrate back to undercut the top of the parallelogram which is not desirable. We thus choose an angle of about  $35^\circ$  which provides a value of diffraction efficiency of about 0.00178. For this calculation we determine that the ratio of the forward and backward diffracted waves is 600 or 28dB. This is an important consideration for rejection of reflected waves as discussed later.

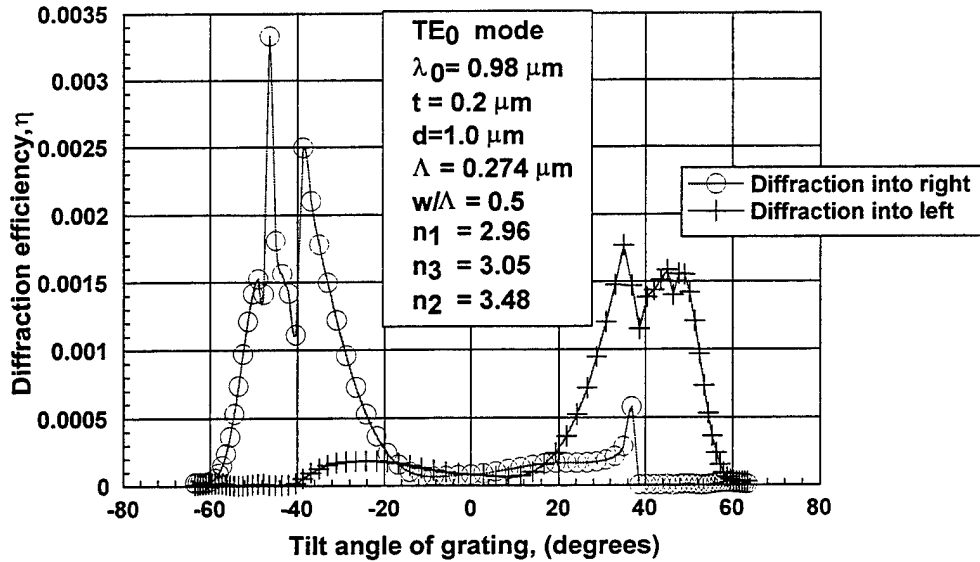


Fig. 5 Diffraction efficiency versus the grating angle in the vertical cavity waveguide.

It is noted that a sharp minimum exists in the efficiency curve at a certain blaze angle of about  $41^\circ$ . This effect is believed to result when the angle of the grating coincides with the Brewster angle for light incident normally upon the waveguide. It is currently under investigation. The above efficiencies are for electric fields. Corresponding power efficiencies will be a factor of 2 larger

## 6. DETAILED DC OPERATION OF THE GVCSEL

From the above description one can see that the light generated in the vertical cavity at  $z=0$  will be diffracted to the right continuously. The diffracted light propagates in the form of a guided wave. The guided wave will itself be diffracted back into the cavity at each position  $z$  and will be amplified. The amplification will continue until the gain is saturated. From that point onwards, the saturated vertical cavity output will continue to add to the waveguide power resulting in a maximum waveguide output power at the end of the device,  $z = L$ .

Consider the photon density at any position  $z$  in the cavity of thickness  $dz$  where the laser is above threshold. We have

$$F_{cav} = \frac{\tau_p'}{qL_x} \eta_e (J - J_{TH}) \quad (1)$$

where  $L_x$  is the quantum well width,  $\eta_e$  is the electrical confinement factor,  $J$  and  $J_{TH}$  are the current and current density and  $\tau_p'$  is the effective photon lifetime for the vertical cavity device given by

$$\tau_p'^{-1} = \frac{v_g}{\Gamma} \left[ \frac{1}{L} \ln\left(\frac{1}{R}\right) + \alpha_{vc} \right] \quad (2)$$

where  $\alpha_{vc}$  is the vertical cavity loss due to the diffraction grating. There will also be components of  $\alpha_{vc}$  which are due to free carrier absorption and parasitic diffraction but these will be ignored for the moment to focus on the desired effect. In the final formula we may simply replace  $\ln(1/R)$  by  $L_{cav} * \alpha_{par}$  to determine its effect since in all likelihood this term will dominate  $\ln(1/R)$ .

The power output from the laser is comprised of two components which are written as

$$P_{out} = h\nu W dz v_g t_f F_{cav} \quad (3)$$

where  $t_f$  is the power transmissivity of the output port. For the conventional transmission through the mirror (1) is substituted into (3) with  $t_f = \ln(1/R)$  to give the power increment

$$dP_{mir} = \frac{h\nu}{q} \frac{\eta_e}{1 + \frac{L_{cav} \alpha_{vc}}{\ln(1/R)}} (J - J_{TH}) W dz \quad (4)$$

There is another power component which is the power diffracted into the guide. The transmissivity for this mechanism is the diffraction efficiency  $t_f = \eta_{diff}$  so we have

$$dP_{wg} = \frac{h\nu}{q} \frac{\Gamma}{L_x} \frac{\eta_{diff} \eta_e}{\frac{1}{L_{cav}} \ln(1/R) + \alpha_{vc}} (J - J_{TH}) W dz \quad (5)$$

To determine  $\alpha_{vc}$  we note that the primary optical loss in the vertical cavity by design will be the second order diffraction by the grating of the vertically propagating wave. In the development of diffraction into the guide in this program [10] from a normally propagating wave we have determined the diffraction efficiency  $\eta_{diff}$  as

$$\eta_{diff} = 2\alpha_g d_{eff} \frac{\eta_1}{\eta_2} \frac{A_y A_y^*}{C_o C_o^*} \quad (6)$$

where  $\eta_1$  and  $\eta_2$  are the impedances of the guide and the incident medium (which in this case are the same),  $A_y$  is the field intensity at the edge of the guide of the  $z$  propagating wave and  $C_o$  is the field intensity of the incident wave. Also,  $\alpha_g$  is the growth of the guided wave due to diffraction and  $d_{eff}$  is the effective width of the guide which includes evanescent cladding penetration. Thus we can say that the power diffracted into the guide from the incident wave is  $\eta_{diff} C_o C_o^*$ . However we can also regard the grating as a loss in the  $x$  direction for the wave  $C_o$  and we can define a loss parameter  $\alpha_x$  by the statement

$$C_o C_o^* (1 - e^{-\alpha_x x}) = \eta_{diff} C_o C_o^* \quad (7)$$

so that for a grating thickness of  $x=t$  we have (for  $\alpha_x x \ll 1$ )

$$\alpha_x = \eta_{diff} / t \quad (8)$$

Since this loss occurs only over the grating thickness then we multiply by the confinement factor  $\Gamma = t / L_{cav}$  to obtain an effective value for the total cavity of

$$\alpha_{vc} = \eta_{diff} / L_{cav} \quad (9)$$

for use in (5) and (2). Therefore the waveguide power component (5) becomes

$$dP_{wg} = \frac{h\nu}{q} \frac{\eta_e}{1 + \frac{\ln(1/R)}{\eta_{diff}}} (J - J_{TH}) W dz \quad (10)$$

Since the concept of the GC VCSEL is to maximize the waveguide power then the design of the laser should be such that  $\alpha_{vc}$  is the dominant loss in the cavity and that negligible power escapes through the two mirrors which may be stated, by using (9) in (4), as

$$\eta_{diff} \gg \ln(1/R) \quad (11)$$

From (5) it is seen that the incremental power output into the guide is just the total output of the vertical cavity device with the efficiency of the diffraction as opposed to mirror transmission as in (4). According to (10) the power in the guide will be proportional to the guide length. As the wave propagates in the guide, there is also diffraction of power into the guide. Basically this power diffracts from the wave into the cavity and then back into the guide with the same efficiency as the cavity flux. However, this photon flux can amplify the cavity flux through an adjustment of  $F_{cav}$  and therefore of (10). In general, the amplification of waveguide power depends on the relative size of the mirror and diffractive loss. If the diffractive loss is very large, then the light realizes single pass gain, i.e. it passes through the cavity essentially once before it is diffracted back into the wave. This is equivalent to the linear optical amplifier with very low reflectivity in which case the majority of the light passes through the amplifier only once as a traveling wave. In these cases the amplifier always works below the threshold of the laser. If the diffractive losses are not too high, then the light may make many oscillations in the cavity before diffraction back into the guide and this situation is referred to as the multipass gain case. In this case, the laser is above threshold along most, if not all of the length of the laser. To obtain maximum laser output, this is the situation we are interested in here. For this kind of operation (as we describe elsewhere) the threshold current of the laser is modified. We can therefore write an equation for the guide power which is

$$\frac{dP_{wg}}{dz} = -\alpha_g \left( 1 - \frac{1}{1 + \frac{\ln(1/R)}{\eta_{diff}}} \right) P_{wg} + \frac{h\nu}{q} \frac{\eta_e}{1 + \frac{\ln(1/R)}{\eta_{diff}}} \left( J - J_{TH} \left( \frac{\alpha_g F_g}{F_{cav}} \right) \right) W \quad (12)$$

where in this case (6) is modified to

$$F_{cav} = \frac{\tau_p'}{qL_z} \eta_e \left( J - J_{th} \left( \frac{\alpha F_g}{F_{cav}} \right) \right) \quad (13)$$

and the threshold current has now become a function of the flux injected into the cavity. Here  $F_g$  is the waveguide photon density given by  $F_g = P_{wg}/A v_g h\nu$ . In (12) the second term is essentially (10) and the first term is the net diffraction of power into the cavity. It is comprised of two parts which are first the diffraction of power into the cavity with efficiency  $\alpha_g$  per unit length and second the diffraction of those same photons back into the guide with the efficiency we derived in arriving at (10). The determination of the function  $J_{th}(\alpha F_g/F_{cav})$  requires a modification of the photon rate equation from

$$\frac{F_{cav}}{\tau_{st}} + \frac{F_{cavT}}{\tau_{st}} = \frac{F_{cav}}{\tau_p'} \quad \text{to} \quad \frac{F_{cav}}{\tau_{st}} + \frac{F_{cavT}}{\tau_{st}} = \frac{F_{cav}}{\tau_p'} - \frac{\alpha F_g v_g}{L_{cav}} \quad (14)$$

The equation on the right is the conventional photon loss equation where the right hand side represents photon loss from the system. The equation on the right is the photon loss equation when an optical input is fed to the device. It is clear that the input photon term reduces the loss and therefore reduces the condition for threshold and therefore the threshold current. Specifically, the K parameter [9] which is used to determine threshold, contains  $\tau_p'$  and from (14), the photon lifetime is modified to

$$\tau_{peff}^{-1} = \tau_p'^{-1} \left( 1 - \frac{\alpha F_g v_g \tau_p'}{F_{cav}} \right) \quad (15)$$

i.e., the effective photon lifetime in the cavity increases with the input signal but decreases with the cavity flux itself.

The power output of the laser is determined by integration of (12) and is shown as a function of laser length  $L$  in Fig.6. If the effect of optical gain in the cavity were absent so that  $J_{TH}$  in (12) is a constant then the solution to (12) is

$$P_{wg}(L) = P = \frac{h\nu}{q} \frac{W \eta_{diff} \eta_e}{\alpha_g \ln(1/R)} [J - J_{TH}] \left( 1 - \exp \left( -\alpha_g \frac{\ln(1/R)}{\eta_{diff} + \ln(1/R)} L \right) \right) \quad (16)$$

which is equivalent to the output of a vertical cavity device with a width of  $W$ , a length of  $L = 1/\alpha_g$  and an efficiency of  $\eta = \eta_{diff} \eta_e / \{\ln(1/R) + L_{cav} * \alpha_{par}\}$ . Equivalently, we could say the efficiency was  $\eta_e$  and the effective length was  $\eta_{diff} / \alpha_g \{\ln(1/R) + L_{cav} * \alpha_{par}\}$ . In the figure, the parameters are taken from a typical grating efficiency analysis and the parameters of  $\eta_{diff} = 0.001$  and  $\alpha_g = 50$  are used with a cavity designed for  $R = 0.9999$ . Then the effective length is 0.7 cm. This may be stated alternatively by saying the device has an efficiency of 63% for a length of  $L = 0.7$  cm. Desirable parameters are therefore  $\eta = 0.001$  and  $\alpha_g = 50$  which can be achieved with the dielectric combination  $\text{SiO}_2/\text{GaAs}$

and a grating etch depth (thickness) of 1000 angstrom. From our calculations for an asymmetrical grating the optimum blaze angle is about 30°. With these numbers, the laser output power for  $J-J_{th} = 834 \text{ A/cm}^2$  and a waveguide width of  $10 \mu\text{m}$  is about  $0.24 \text{ W}$ .

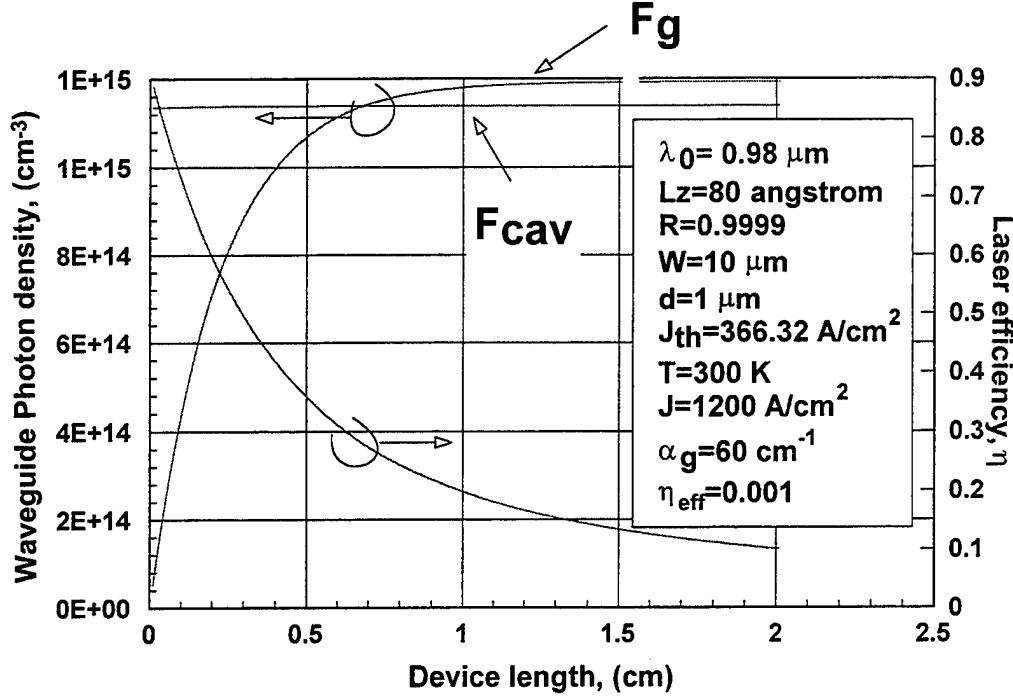


Fig. 6 Waveguide photon density versus device length

Also shown on the plot is the output power versus  $z$  when the dependence of  $J_{th}$  on input power is included in (12). It is evident that the gain internal to the device increases the output power by a factor of. The overall efficiency of the laser is a function of  $z$  and therefore of the actual device length and from (16) we obtain

$$\eta = \frac{\eta_{diff}\eta_e}{\alpha_g L \ln(1/R)} \left\{ 1 - \exp \left[ -\alpha_g \frac{\ln(1/R)}{\eta_{diff} + \ln(1/R)} L \right] \right\}$$

One interesting feature is the tradeoff between length and overall efficiency. For small  $z=L$ , the efficiency is close to 100%. As the length is increased the efficiency drops so that at  $L \approx 0.7 \text{ cm}$  the efficiency has dropped to about 45%. Note however that we cannot use the prefactor of  $J-J_{th}$  in (16) as the efficiency since this result implies that the power is independent of  $z$  (i.e. as the length is reduced to zero, the exponential term reduces the output power to zero). This is clearly a design tradeoff in which the total power and efficiency must be traded off by the appropriate choice of length.

The operation of the device as an optical amplifier will not be considered in detail here because the laser is our main objective. However, it is interesting to note that as long as the  $\eta_{diff}$  is large enough to prevent lasing it may still be quite small, i.e. it may easily be around  $10^{-3}$ . The gain is obtained because for every increment of propagation distance in the  $z$  direction the wave traverses the vertical cavity  $Q$  times where  $Q$  is the quality factor. Since  $Q = (\nu_0/\nu_F)\mathfrak{F}$  where  $\mathfrak{F}$  is the finesse given by approximately  $\mathfrak{F} = \pi/\alpha t = \pi/\eta_{diff}$  and  $\nu_0$  and  $\nu_F$  are the resonator frequency and free spectral range respectively then the

light may traverse a distance of  $QL_{cav}$  vertically in a propagation distance of  $dz$  in the guide. Estimating that  $1-1/e$  of the wave is diffracted into the cavity in the distance  $1/\alpha_g$  then the effective distance traveled by the wave is about  $(v_o/v_F) \pi/\eta_{diff} \cdot L_{cav} \cdot \alpha_g L_{guide}$  during which it receives optical gain. Using typical numbers this is a distance of 15cm.. This indicates the feasibility of implementing an optical amplifier on a chip with monolithic integration which has all the benefits of the fiber amplifier. This points to the direction of implementing an integrated transmission system.

There are other benefits to be realized from this grating coupled arrangement which are:

- 1) the polarization of the vertical cavity wave is forced to coincide with that of the waveguide. The locking of the polarization occurs because the waveguide mode is injected into the cavity at each point and creates some level of stimulated emission. The emission in the cavity reproduces the same polarization. The random nature of the polarization of the vertical cavity laser output has now been eliminated. The output of the waveguide will be  $TE_0$  normally because it is most easily excited in the guide. Earlier simulations of Lee and Streifer [11] have shown in general that the diffraction efficiency of the  $TM_0$  mode is at least 10 times smaller than the  $TE_0$  mode, which thus becomes the principle supported mode. Because of the diffraction of the light from the guide into the cavity there will be a stabilizing effect and an extended range of single mode output power. For a conventional VCSEL, the output is single mode until a certain level of power is achieved and then multimode behavior is observed. In the grating coupled laser the onset of higher order VCSEL modes will require a much higher level of laser power to occur because of the stabilizing effect of the waveguide injected energy. In fact, the GCVCSEL will remain single mode until a higher order mode in the waveguide matches to a higher order mode in the VCSEL.
- 2) The mode suppression ratio will be characteristic of the vertical cavity laser. Because of the single mode nature of the VCSEL, the tendency for mode partition noise will be much reduced. The RIN noise should be typical of the VCSEL
- 3) One of the problems of edge emitting and vertical cavity lasers is the effect of back reflections into the laser when coupling to a fiber. In the grating coupled VCSEL, this problem is addressed in a unique way as shown in Fig.2. Light is coupled from the laser to the waveguide and is transported to the chip edge. Reflections travel back to the laser and a standing wave will be set up which may be at a different frequency. Normally this energy will re-enter the cavity and may destabilize the laser. In the grating coupled laser, which we have modeled as an equivalent three-level waveguide, the asymmetry of the grating causes a dominant fraction of the power to be diffracted into the guide for light traveling towards the chip edge (direction of laser emission) and it also causes a dominant fraction of the light to be diffracted out of the waveguide for light approaching the laser from the edge of the chip. In essence then, the grating asymmetry acts to reject the light re-entering the laser with a ratio of diffraction up to diffraction down which can be up to 28dB according to the simulation. The grating thus acts as an optical isolator.
- 4) The GCVCSEL output is into a waveguide on the chip. The waveguide transports the light to the chip edge. Output coupling of the laser light to a fiber occurs from the waveguide to the fiber. One of the major problems in manufacturing involves attaching fiber to the chip and much effort has gone into the development of spot size

transformers which are ways to match the waveguide mode size to the fiber aperture. The waveguide output is easily tapered in the lateral dimension to achieve this matching. In the vertical dimension the mode size can be enlarged considerably by the use of the ion implant to disorder the waveguide. As we point out in the process flow sequence (section 8) the waveguide core is implanted with Si during the formation of the source-drain regions. This implant after RTA serves to disorder the bandgap of the quantum well layers which reduces the index. The net effect is to move the core index closer to the effective index of the upper and lower quantum well regions which causes the expansion of the mode into these regions. Judicious use of this implant and anneal step can be used to optimize the mode shape to increase the tolerances for the mode to fiber coupling problem.

Another way to widen the mode shape vertically is to remove layers of cladding from the waveguide as the chip edge is approached. In the device area there are many dielectric pairs to eliminate emission through the upper mirror. This maintains tight mode confinement. Along the waveguide these layers can be selectively removed to widen the mode shape.

## 7. HIGH SPEED OPERATION OF THE GCVSEL

A primary motivation for this design of laser is to achieve very high speed performance. Within the inversion channel technology the HFET laser is ideally suited to achieve the necessary bandwidths. The HFET laser is a laterally injected laser in which the gate/emitter and source injecting terminals lay next to each other along the surface and are therefore configured as adjacent electrodes as illustrated in Fig.2. Also, in the vertical cavity arrangement as illustrated in Fig. 1 or 2, the distance from the quantum wells to the semiconductor surface can be  $\frac{1}{2}$  wavelength as in most VCSEL designs and since the source drain implant is performed from approximately 1000 Å above the quantum well to achieve minimum channel access resistance, then the positive and negative electrodes form an almost perfect coplanar transmission line. The vertical cavity of the HFET laser structure is formed by the deposition of the dielectric stack over the electrode structure. These dielectric layers form the top dielectric cover for the coplanar line and are therefore important in determining  $Z_0$ . When implemented in this form the HFET laser implements almost perfectly a traveling wave laser. This traveling wave property extends the bandwidth of the laser to the limit imposed by the internal parasitic resistance and time constant because the coplanar electrical transmission line can be terminated on the chip by a transistor adjusted in impedance to match the  $Z_0$  of the line. Then if the transmission line phase velocity and the waveguide group velocity are matched, one could introduce a signal on the coplanar line which would propagate at the same speed as the photon pulse which was being produced by the continuous injection of charge into the channel from the pulse propagating on the line. Suppose there was no dispersion of the electrical pulse and no dispersion of the optical pulse. If there was negligible delay in producing the photon (i.e. negligible transit time into the channel) and negligible delay in converting the electron to a photon (very fast laser internal response) then the laser would have an infinite bandwidth since then a delta function of charge introduced to the line would produce (after the transit time of the waveguide) a delta function of photons. The extent to which these conditions are not met determines the maximum laser speed and generally it is the internal parasitic RC constant which becomes the limiting factor (as we show in the detector section 7 this parasitic bandwidth is about 100GHz).

To determine further the dynamic operation consider a pulse introduced on to the coplanar line at  $x=0$ . Because of the almost identical structure of the optical waveguide and the transmission line in terms of the materials both above and below the semiconductor surface, the optical group velocity and the electrical phase velocity will be almost matched. As the pulse propagates on the line, it will continuously decrease in value as charge is injected laterally at each position  $x$  into the laser active section. Now the effect of the injected charge will be a maximum if the charge is injected at precisely the point of the maximum photon density. Also the charge impulse initially begins to create a photon impulse starting at  $x=0$ . Then if the photon pulse and the charge pulse move at the same velocity (i.e. the matched condition), it follows that as the charge impulse travels on the transmission line it will always be injecting its incremental charge into the laser at the position which corresponds to the maximum photon density in the



waveguide. If this is the case, the photon pulse will grow the most efficiently because the number of photons produced by the injecting charge is proportional to the injected charge and the photon density, i.e. the product of the electron and photon densities. This behavior is illustrated schematically in Fig.7 which shows the case at some position  $x$  along the waveguide the situations when the electrical pulse travels slower, faster and at exactly the same speed as the optical pulse.

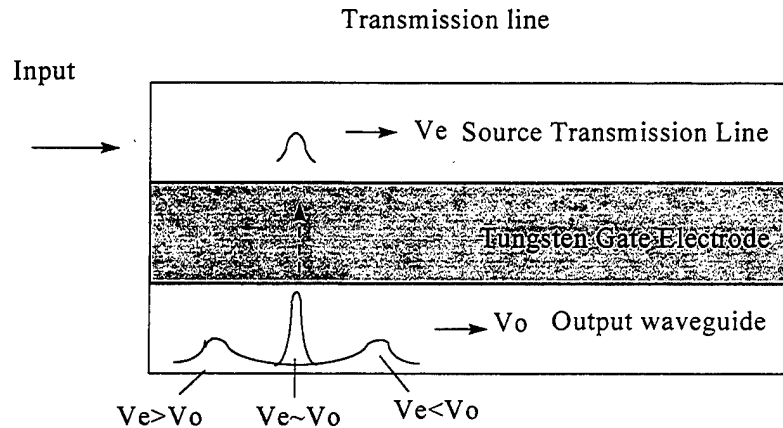


Fig. 7 Effective velocity matching on the optical output response

Ideally when they travel at the same speed, the photon pulse is a maximum height because the injected charge  $\times$  photon density product has been a maximum at all points during the propagation. Also, the pulse width will be the narrowest because, assuming that the internal laser dynamics are sufficiently fast, the pulse width of the photons will be as narrow as the charge pulse. If there is negligible dispersion on the transmission line then the charge pulse and thus the photon pulse will retain its original delta function form, i.e. the photon pulse will remain essentially as fast as the input electrical pulse.

A complete analysis of the laser dynamic performance is exceedingly complicated if one attempts to illustrate the effects of the velocity matching or lack thereof. This is because of several properties unique to the lasing mechanism which are

- the photon response is proportional to the product of the injected carriers and the injected photons. Therefore in the laser cavity, at any position along the guide we need to consider a mixture of the dispersed pulse traveling on the transmission line and the dispersed pulse traveling in the waveguide and to represent their individual time dependencies.

- in the laser there is an amplifier effect which means photons produce additional photons without the need for additional electrons. This may be considered an optical to optical effect as opposed to the electrical to optical effect of the carriers injected from the transmission line. Therefore we need to consider the dynamics of the optical amplifier effect in the waveguide itself so that the photon pulse is growing not only due to the injection from the line but also due to the internal optical gain. And as we mentioned

earlier, this optical gain can be in one of two forms depending upon how far above or below threshold the laser is biased. This situation is to be contrasted with the detector in which electrons are produced (i.e. the reverse process) only by the conversion of the pulse photons.

- proper analysis requires use of the actual differential equations representing the electron and photon populations but represented in the form of traveling waves. These equations have not yet been solved self-consistently in the literature for the conventional diode laser without any traveling wave effects.

Therefore more work is needed to obtain a clear analysis. However, the physical picture described above is clear which is that if the waveguide and transmission dispersions can be minimized and the internal parasitic RC constant can be reduced to 5-10ps, then velocity matching of the HFET transmission line and the vertical cavity waveguide can enable speeds in excess of 100GHz.

The analysis of the traveling wave detector is much easier and reinforces all of the conclusions made here for the laser. It is presented in the next section.

## 8. THE HFET VERTICAL CAVITY TRAVELING WAVE DETECTOR

### 8.1 General Design

To meet the transmission requirements for detection requires innovation also in the detector. Traditional detector geometries available to the designer include the classical vertically illuminated PIN structure or the waveguide structure which is edge illuminated. The inherent bandwidth-efficiency trade-off in the vertical device between absorption efficiency in the active layer and carrier transit time through it have been addressed significantly by the implementation of resonant cavity enhanced (RCE) structures wherein multiple optical passes are used to obtain almost total absorption in a very narrow active layer, i.e. in a quantum well. The drawback of the RCE is the narrow optical bandwidth which results from the high finesse of the cavity. Nevertheless, for many of the emerging practical system architectures in which wavelength division multiplexing is employed, the wavelength selectivity offered by the cavity is exactly what is required to perform optical to electronic demultiplexing. The difficulty of course is to devise a means to inject the light into the cavity since the high reflectivity of the cavity will reject the optical input unless it is exactly positioned within the narrow bandwidth corresponding to the position of the cavity optical mode.

In the waveguide configuration, it is typical to use a double heterostructure semiconductor structure with a quantum well active region. The thickness of the active layer can also be minimal since the absorption occurs along the length of the guide which can be designed for complete absorption. The transit time limitation and the RC limitation can be essentially the same as that of the vertically illuminated RCE device. The efficiency of the device does suffer, however, from the problem of poor input coupling since the numerical aperture of the typical semiconductor waveguide is small and the mode is not well matched to the typical mode of the optical fiber. These devices have been reported with 50 GHz bandwidth and 40% external quantum efficiency and also 68% external quantum efficiency with >50GHz bandwidth.

Both of the above approaches behave as lumped element devices electrically and consequently, the reported bandwidths are approximately limited by the load resistance and the device capacitance. To alleviate the lumped element limitation and thereby improve bandwidth, traveling wave structures have been proposed. These devices basically combine the optical waveguide configuration with an electrical transmission line. This approach, which was introduced initially to enhance the speed of lithium niobate waveguide modulators has the potential to substantially reduce the effect of the RC time constants imposed by external circuits. The advantage is obtained because the load impedance presented to the detector does not combine with the internal impedance of the detector to establish a time constant if the load is matched to the characteristic impedance of the line. The temporal response is further improved if the transmission line energy velocity and the waveguide optical group velocity are matched, i.e. the condition of zero velocity dispersion.

In practice, impedance matching and velocity matching are very difficult. Furthermore, the TWPD still suffers from the problem of poor input coupling since the

basic semiconductor waveguide structure has remained unchanged. In fact the waveguide must be  $1\mu\text{m}$  or less in width to realize reasonable transmission line parameters and this exacerbates the coupling problem.

Another limitation with the existing traveling wave, waveguide or RCE designs is the problem of integration with electronic devices. A traveling wave device intended for 100 GHz operation must feed photocurrent to an FET or bipolar front end in a matched configuration to avoid reflections. It is not practical or cost effective to do this with hybrid connections except for specialized applications and it thus becomes essential to have an integrated approach. Ideally, the integration should encompass the detector, the laser, and the electronic amplifier.

Since we intend to use the Inversion channel technology approach we then propose the HFET resonant cavity enhanced detector as a novel means to address these problems since it combines the virtues of the vertical cavity RCE structure and the TW concept into a single device. This approach has several advantages which include 1) optimized mode matching to an optical fiber to achieve improved input coupling, 2) optimized impedance matching to reduce reflections, 3) optimized velocity matching to reduce pulse dispersion, and 4) integrated circuit compatibility to achieve a low cost high performance package.

In the ICT the laser and detector are physically the same structure. Therefore the Figs. 1 and 2 also apply here. These figures show the traveling wave version of the HFET laser or detector since physically these are the same structure. To differentiate between the laser and the detector operation requires the device cross-section in Fig. 8. which shows the appropriate current flows.

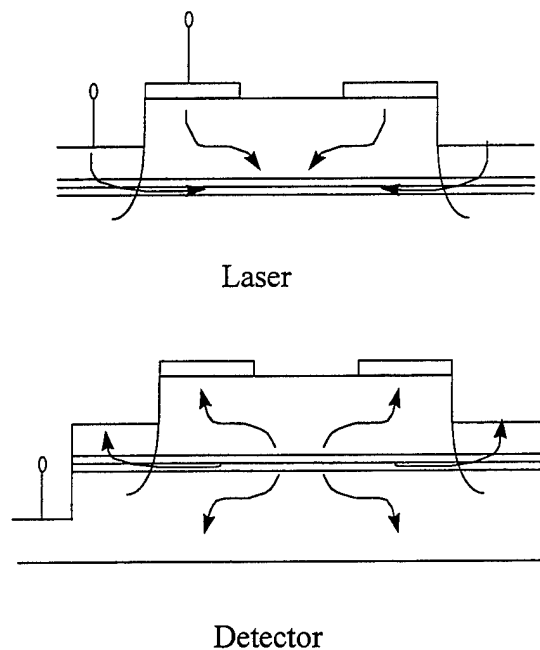


Fig. 8 Current flow diagram for laser and detector

This figure indicates that the collection of carriers in the devices is lateral for the electrons and vertical for the holes. If the collector is contacted with a negative bias then the holes are removed downward to the collector. On the other hand if the gate is contacted with a negative bias, the hole current flows upward to the gate electrode. It is noted that the collector operation can be achieved with zero collector to source bias since the barrier at zero bias is low whereas the gate operation requires a bias to lower the channel to gate barrier for holes preferentially relative to the collector. The electrons flow within the inversion channel and are collected at the source nodes. The electrons flow to both source nodes so that the worst case transit time corresponds to  $1/2$  of the channel length and the average effective delay corresponds to a transit distance of  $L/4$ . Note that the vertical cavity geometry in Fig.2 will typically admit light through an opening in the gate electrode so that the conduction of holes to the gate is by the 2D funneling mechanism which is typically used in the VCSEL structure to provide current injection into the same region as the optical emission. No conduction is required through the mirror structure however since the mirror is applied in the form of a dielectric stack at the end of the fabrication sequence.. For the case of the waveguide configuration in Fig.2, the gate electrode is continuous since the wave is guided under the top contact and sufficiently removed to avoid excessive loss.

The description of the technology changes to accommodate the detector are essentially the same as those of the laser above. The metal contact is opened, as in the conventional vertical cavity device , to allow the passage of the light in the vertical direction. However here the light is propagating both horizontally and vertically. The dielectric mirror of the vertical cavity device is used here in a multi-functional role. First, the semiconductor growth between the quantum well active region and the dielectric stack is very thin, i.e. approximately  $\lambda/2n$  , where  $n$  is the average material index, in order to move the gate contact as close as possible to the inversion channel. This is necessary to form a high frequency transistor structure . However the optical mode is still efficiently guided because the dielectric stack provides efficient guiding of the mode. The mode is centered in the quantum wells but extends well above the gate metal contact. Second, the dielectric stack also forms a high finesse cavity in the vertical direction. Therefore the number of pairs in the stack and the index difference are selected to achieve the desired finesse for the resonant cavity. Third, the multiple layer structure of the cavity mirror allows a large optical mode to be supported for propagation in the horizontal direction. The enlarged mode size increases the mode near-field pattern and decreases the far-field angles which facilitates easier coupling to a fiber. The input light is edge coupled to a waveguide at the chip edge with a cross-section designed for optimum coupling. The waveguide guides the light to the detector where it propagates along the device waveguide as shown in Fig.1.

As for the laser the key element to enable the combined waveguide, vertical cavity operation is a grating which is created in the first layer of the dielectric stack. This is a second order grating which diffracts a portion of the input wave into the vertical cavity at each position along the guide. Since the light propagating vertically in the cavity is absorbed essentially completely due to the resonant enhancement effect then the limitation on the detector efficiency, i.e. the length of detector required, is determined by the grating parameter  $\alpha_g$  . Because the grating index change can be made fairly large by

suitable design of the dielectric stack then  $\alpha_g$  can be large and the waveguide length can be optimized for high speed operation.

One of the obvious features of this design is that since the light is transferred to the resonant enhanced structure via the grating which passes below the dielectric stack then the problem of injecting light into the cavity through a dielectric mirror with a very narrow modal bandwidth has been eliminated. Clearly, the light will not be absorbed if its frequency does not align with that of the mode. However, this is a desirable property, since it allows the cavity to select any particular frequency as would be required in a WDM application, i.e. the light is always coupled into the cavity with the cavity mode providing the filtering or demultiplexing operation. Those frequencies which are not selected are simply coupled back into the waveguide by the grating and are propagated out of the device.

The HFET TW detector illustrated in Fig.2 uses the gate contact to collect the hole current in order that it may form the signal line for the transmission line. The other side of the line, i.e. the ground line, is formed by the metal electrodes on the source junctions. Due to the aspect ratio as indicated in Fig.3, which shows the two metal electrodes at approximately the same elevation, (within 1500-2000 Å), the source and gate electrodes behave as a coplanar transmission line. Therefore, as photo-charge is injected into the source and gate electrodes, these perturbations form a traveling wave on the coplanar line which propagates to the far end of the device ( $x = L$  in Fig.3). If the group velocity of the transmission line wave and the group velocity of the optical wave are matched then the photo-charge is added synchronously to the electrical wave and there will be no distortion of the pulse due to velocity mismatch. If the transit time of holes to the gate from the channel and of electrons to the source contact from the channel are equal and if there is no dispersion on the transmission line or the waveguide then the input pulse shape will be preserved. Finally if the transmission line is exactly matched in its characteristic impedance, there will be no reflection and the pulse will be perfectly replicated, i.e. the impulse response of the detector would be infinite. These conditions can never be realized perfectly and it is the deviation of these criteria from the ideal which determines the actual detector bandwidth.

The virtue of the traveling wave concept is that the impedance of the circuit following the detector does not combine with the detector impedance to produce delay if ideal line matching is achieved. However parasitic RC delays which are intrinsic to the device are still an issue. These are (Fig.2) the time constant associated with transferring the electron and hole from the absorption region to the source metal and gate metal respectively. To minimize these parasitic effects, the transmission line metal to metal spacing should be reduced and the channel doping increased as much as possible by aggressive technology scaling. The other fundamental delay is the transit time of electrons in the absorbing FET channel. For a channel length of  $L = 1 \mu\text{m}$ , this time corresponds to an average of  $L/4v_s$ . For a  $v_s \approx 2 \times 10^7 \text{ cm/sec}$  at low fields, this corresponds to a delay of about 0.15 ps. From the point of view of efficiency, the attenuation of the transmission line  $\alpha_e$  must now be added to the losses in the resonant cavity enhanced detection process. This attenuation increases with frequency with dependencies on the source and gate metal skin effect depths and the frequency dependent propagation constant. In this respect, the bandwidth limitation of the lumped element configuration has been exchanged for a

conversion efficiency limitation resulting from the attenuation or loss of the traveling photo-induced current.

## 8.2 Dynamic Response

The electrical model of the transmission line within the detector is shown in Fig.9.

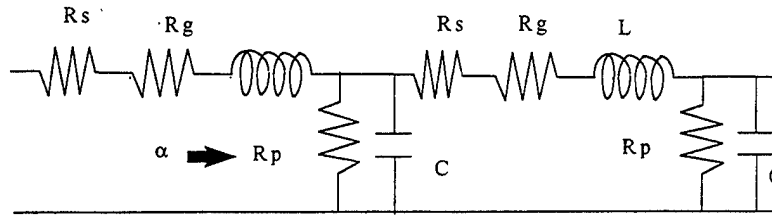


Fig. 9 Circuit model of transmission line for traveling wave optoelectronic devices

The electrical losses in the transmission are represented by R and G. The series R of the transmission line is determined by the combined skin effect resistance of the source and gate conductors which may be expressed

$$R = R_s + R_g = \frac{2\rho_s}{\omega_s} \sqrt{\pi f \mu \sigma_s} + \frac{2\rho_g}{\omega_g} \sqrt{\pi f \mu \sigma_g} = \sqrt{\frac{2\omega\mu}{\sigma_s w_s^2}} + \sqrt{\frac{2\omega\mu}{\sigma_g w_g^2}} \quad (17)$$

where  $\omega = 2\pi f$  is the frequency,  $w_s$  and  $w_g$  are the source and gate widths,  $\mu$  is the permittivity and  $\sigma_s$ ,  $\sigma_g$  are the metal conductivities. The parallel conductance represents essentially dielectric loss mechanisms in addition to dark current leakage. These parasitics combine to give a total loss parameter  $\alpha$  such that the wave on the transmission line propagates as

$$E(x) = E_0 e^{-\alpha x} e^{-j\beta x} \quad (18)$$

where both  $\alpha$  and  $\beta$  are frequency dependent, as outlined in standard textbooks. The loss may be written as the sum of the series and parallel contributions as

$$\alpha_e = \alpha_c + \alpha_d \quad (19)$$

and for the unbalanced coplanar line, these are expressed [12] as

$$\alpha_c = \frac{8.68 \times R_s(f) \sqrt{\epsilon_{eff}}}{480\pi \cdot K(k') \cdot (1-k^2)} \left\{ \frac{1}{a} \left[ \pi + \log \frac{8\pi a(1-k)}{t(1+k)} \right] + \frac{1}{b} \left[ \pi + \log \frac{8\pi b(1-k)}{t(1+k)} \right] \right\} \quad (20)$$

and

$$\alpha_d = 27.83 \times \frac{\tan \delta}{\lambda_0} \cdot \frac{\epsilon_r}{2\sqrt{\epsilon_{eff}}} \cdot \frac{K(k_1) \cdot K(k')}{K(k'_1) \cdot K(k)}$$

where  $K(k_1), K(k'_1), K(k), K(k')$  are the complete elliptic integrals of the first kind, and  $k'_1 = \sqrt{1 - k^2}$ . The effective index is also frequency dependent and is expressed [12] as

$$\sqrt{\epsilon_{eff}} = \sqrt{\epsilon_{eff}(0)} + \frac{\sqrt{\epsilon_r} - \sqrt{\epsilon_{eff}(0)}}{1 + A(f / f_{TE})^{-1.8}} \quad (21)$$

where

$$A = \exp \left\{ \left[ 0.54 - 0.64 \log \left( \frac{2a}{h} \right) + 0.015 \left( \log \left( \frac{2a}{h} \right) \right)^2 \right] \cdot \log \left( \frac{2a}{b-a} \right) + 0.43 \right. \\ \left. - 0.86 \log \left( \frac{2a}{h} \right) + 0.54 \left( \log \left( \frac{2a}{h} \right) \right)^2 \right\}$$

$$f_{TE} = \frac{c_0}{4h \cdot \sqrt{\epsilon_r - 1}}$$

The impulse response of the TW detector has been stated as

$$i(l, t) = \frac{\eta_i q}{h\nu} E_0 \left\{ \frac{\Gamma \alpha}{2} \frac{v_0 v_e}{v_0 - v_e} \exp \left[ \Gamma \alpha \frac{v_0 v_e}{v_0 - v_e} \left( t - \frac{l}{v_e} \right) \right] \cdot u \left( \frac{l}{v_e} - t \right) \right\} \quad (22)$$

which represents both forward and backward traveling waves, where  $E_0$  is the delta function input impulse of energy,  $\alpha$  is the absorption coefficient of the active layer,  $\Gamma$  is the optical confinement factor,  $v_0$  is the optical velocity,  $v_e$  is the electrical energy ( or group ) velocity,  $l$  is the detector length, and  $t$  is the time as measured from the time of incidence of energy to the detector,  $\eta_i$  is the internal quantum efficiency,  $q$  is the electronic charge,  $h\nu$  is the photon energy. In this section we will extend this result to demonstrate the importance of the electrical loss on both the detector efficiency and velocity mismatch which then establishes the bandwidth limit. We then utilize the result to determine the frequency dependent response to a realistic pulse input.

### 8.2.1 Impulse Response and Small Signal Transfer Function

The optical pulse enters the waveguide as shown in Fig. 10 at  $x = 0$  and continuously transfers electrons to the transmission line as it propagates.



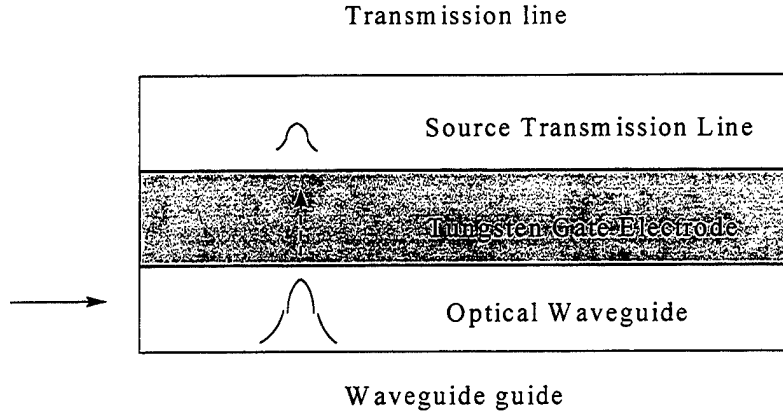


Fig. 10 Effective velocity matching on the optical input response

At any  $x$ , the photon density ( per unit area ) remaining in the light wave is

$$F(x) = F_0 \cdot e^{-\Gamma \alpha x} \quad (23)$$

where

$$F_0 = \frac{E_0}{h\nu}$$

and is moving with velocity  $v_0$ . Then the total charge per unit area on the transmission line is

$$Q(x) = Q_0 (1 - e^{-\Gamma \alpha x}) \quad (24)$$

where

$$Q_0 = \eta_i q F_0$$

and is moving with velocity  $v_e$ . The current produced by the moving charge is

$$I(x) = \frac{dQ(x)}{dx} e^{-\alpha_e(x) v_e} \quad (25)$$

where  $\alpha_e$  represents the attenuation of the electrical wave on the transmission line. From the relationship

$$\frac{x}{v_0} + \frac{l-x}{v_e} = t \quad (26)$$

we obtain

$$x = \frac{v_0 v_e}{v_e - v_0} t - \frac{v_0}{v_e - v_0} l \quad (27)$$

and then the current is

$$I(x) = Q_0 \Gamma \alpha \cdot e^{(\Gamma \alpha - \alpha_e) \frac{v_o v_e}{v_e - v_o} \left( t - \frac{l}{v_e} \right)} \cdot v_e, \quad \frac{l}{v_o} < t < \frac{l}{v_e} \quad (28)$$

By using the Fourier transform, we can convert time domain into frequency domain, then

$$\begin{aligned} I(l, f) &= \frac{1}{\tau} \int_{-\infty}^{\infty} I(l, t) \cdot e^{-j2\pi f t} dt = \frac{1}{\tau} \int_{\frac{1}{v_o}}^{\frac{1}{v_e}} I(l, t) \cdot e^{-j2\pi f t} dt \\ &= \frac{Q_0 \Gamma \alpha \cdot v_e \cdot e^{-\alpha_e l}}{\tau} \int_{\frac{1}{v_o}}^{\frac{1}{v_e}} e^{-(\Gamma \alpha - \alpha_e) \frac{v_o v_e}{v_e - v_o} \left( t - \frac{l}{v_e} \right)} \cdot e^{-j2\pi f t} dt \\ &= \frac{Q_0 \Gamma \alpha \cdot v_e \cdot e^{-\alpha_e l} e^{-j2\pi f \frac{1}{v_e}}}{\tau} \int_{\frac{1}{v_o} - \frac{1}{v_e}}^0 e^{-\left[ (\Gamma \alpha - \alpha_e) \frac{v_o v_e}{v_e - v_o} + j2\pi f \right] t} \cdot dt \\ &= \frac{1}{\tau} \frac{Q_0 \Gamma \alpha \cdot v_e \cdot e^{-\alpha_e l} e^{-j2\pi f \frac{1}{v_e}}}{-\left[ (\Gamma \alpha - \alpha_e) \frac{v_o v_e}{v_e - v_o} + j2\pi f \right]} e^{-\left[ (\Gamma \alpha - \alpha_e) \frac{v_o v_e}{v_e - v_o} + j2\pi f \right] t} \Bigg|_{\frac{1}{v_o} - \frac{1}{v_e}}^0 \\ &= \frac{1}{\tau} \frac{Q_0 \Gamma \alpha \cdot v_e \cdot e^{-\alpha_e l} e^{-j2\pi f \frac{1}{v_e}}}{-\left[ (\Gamma \alpha - \alpha_e) \frac{v_o v_e}{v_e - v_o} + j2\pi f \right]} \cdot \left[ 1 - e^{-(\Gamma \alpha - \alpha_e) l} \cdot e^{-j2\pi f l \cdot \frac{v_o v_e}{v_e - v_o}} \right] \quad (29) \end{aligned}$$

where  $\tau = \frac{1}{v_e} - \frac{1}{v_o}$ .

Then

$$I(l, f) = \frac{Q_0 \Gamma \alpha \cdot v_e \cdot e^{-\alpha_e l} e^{-j2\pi f \frac{1}{v_e}}}{(\Gamma \alpha - \alpha_e) - j2\pi f \frac{v_o - v_e}{v_o v_e} l} \cdot \left[ 1 - e^{-(\Gamma \alpha - \alpha_e) l} \cdot e^{-j2\pi f l \cdot \frac{v_o v_e}{v_e - v_o}} \right] \quad (30)$$

We can assume the input current is

$$I(0, f) = \frac{Q_0 v_o}{l} \quad (31)$$

Then, the modulation transfer function is expressed

$$\begin{aligned} H(f) &= \frac{I(l, f)}{I(0, f)} \\ &= \frac{\Gamma \alpha \cdot e^{-\alpha_e l} e^{-j2\pi f \frac{1}{v_e}}}{\left[ (\Gamma \alpha - \alpha_e) - j2\pi f \frac{v_o - v_e}{v_o v_e} l \right] \frac{v_o}{v_e}} \cdot \left[ 1 - e^{-(\Gamma \alpha - \alpha_e) l} \cdot e^{-j2\pi f l \cdot \frac{v_o v_e}{v_e - v_o}} \right] \end{aligned}$$

so that

$$|H(f)|^2 = \frac{(\Gamma \alpha \cdot e^{-\alpha_e l})^2}{\left[ (\Gamma \alpha - \alpha_e)^2 - \left( 2\pi f \frac{v_o - v_e}{v_o v_e} \right)^2 \right] \left( \frac{v_o}{v_e} \right)^2} \cdot \left[ 1 + e^{-2(\Gamma \alpha - \alpha_e)l} \right] \quad (32)$$

It is noted that  $x$  is introduced as a measure of velocity mismatch and if there is no mismatch ( $v_o = v_e$ ), then  $x$  is undefined. In that case (16) is no longer applicable and the current can no longer be defined, i.e. if an ideal delta function of shape is introduced and there is no pulse spreading, the current response is infinite which is the limit approached by (17). Equation (18) defines the impulse response of the system as

$$h(t) = \frac{I(t)}{I(0)} = e^{(\Gamma \alpha - \alpha_e) \frac{v_e v_o}{v_e - v_o} \left( t - \frac{l}{v_e} \right)}, \frac{l}{v_o} < t < \frac{l}{v_e}$$

It is noted that  $\alpha_e$  and  $v_e$  are frequency dependent and therefore the pulse response will degrade as inputs with higher and higher frequency content are considered. To show these effects more clearly, it is more appropriate to consider the transfer function

$$H(f) = \int_0^{+\infty} e^{(\Gamma \alpha - \alpha_e) v_x \left( t - \frac{l}{v_e} \right)} \cdot e^{-j2\pi f t} dt$$

and obtain

$$H(f) = \frac{1 - e^{-(\Gamma \alpha - \alpha_e)l}}{(\Gamma \alpha - \alpha_e) \frac{v_o v_e}{v_o - v_e} - j2\pi f}$$

Therefore the bandwidth of the detector is determined by the amplitude and phase of  $H(f)$  given by

$$|H(f)|^2 = \frac{\left\{ \frac{[v_o - v_e(\omega)] [1 - e^{-(\Gamma \alpha - \alpha_e(\omega))l}]}{v_o v_e (\Gamma \alpha - \alpha_e(\omega))} \right\}^2}{1 + \left[ \frac{\omega}{\Gamma \alpha - \alpha_e(\omega)} \frac{v_o - v_e(\omega)}{v_o v_e(\omega)} \right]^2}$$

$$\varphi = \tan^{-1} \left[ - \frac{\omega}{v_x(\omega) \cdot (\Gamma \alpha - \alpha_e(\omega))} \right]$$

where

$$v_x = \frac{v_o v_e}{v_o - v_e}$$

The frequency dependence of  $H(f)$  is established through that of  $\alpha_e$  which is decided by (4), (5), and (6), using (7) and (8). The frequency dependence of the group velocity ( or energy velocity )  $v_e$  is given by

$$v_e = \frac{1}{\sqrt{\mu \cdot \epsilon_{eff}(\omega)}}$$

with  $\epsilon_{eff}(\omega)$  as determined by (6)

$$\sqrt{\epsilon_{eff}} = \sqrt{\epsilon_{eff}(0)} + \frac{\sqrt{\epsilon_r} - \sqrt{\epsilon_{eff}(0)}}{1 + A(f / f_{TE})^{-1.8}}$$

The detector transfer function is plotted in Fig.11. the 3 dB frequency of the detector is given by

$$\omega_{3dB} = \frac{1}{2\pi} \left| \Gamma \alpha - \alpha_e(\omega_{3dB}) \right| \cdot \frac{v_o v_e(\omega_{3dB})}{v_o - v_e(\omega_{3dB})} \quad (33)$$

and is clearly reduced by the frequency dependence of both  $\alpha_e$  and  $\alpha_o$ . It is interesting to note that the bandwidth is independent of the length of the detector which results because of the matched load configuration.

#### TRAVELING WAVE DETECTOR DYNAMIC RESPONSE

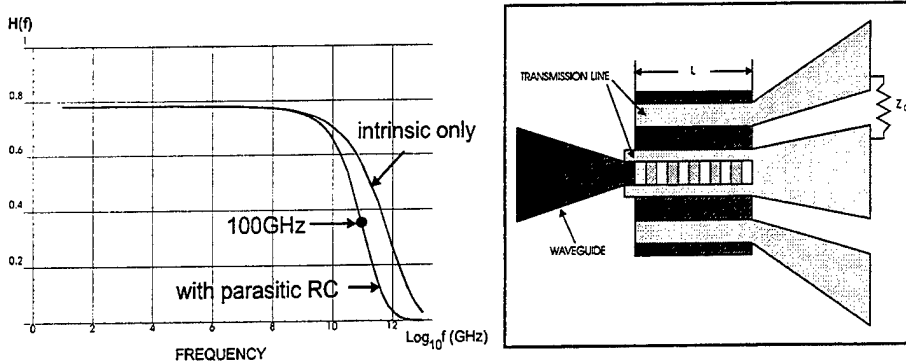


Fig.11 Traveling Wave Detector Dynamic Response

#### 8.2.2 Parasitic Time Constant

In the TW HFET detector, the resistance from the absorbing channel to the contact ( which includes the doped channel resistance, the n+ channel resistance and the metal contact resistance ) combine with the capacitance of the doped channel to gate contact to produce a parasitic RC time constant. This time constant constitutes delay in adding charge to the transmission line which results in an effective velocity mismatch

imposed before the onset of transmission line propagation. The 3dB response which is also shown in Fig.10 would be modified to

$$\frac{1}{\omega_{3dB}} = \frac{1}{\omega_{VM}} + \frac{1}{\omega_{RC}}$$

where  $\omega_{VM}$  is given by (33) and

$$\omega_{RC} = \frac{1}{2\pi R_p C_p}$$

## 9. FABRICATION AND PHOTOMASK DESIGN AND GENERATION

The fabrication sequence was redesigned to implement traveling wave devices. Several changes were made as follows

- The Si implant will be used for the laser and detector current steering function.

It will also be used to create the proper threshold voltage for depletion transistors. This is a light field mask.

- Waveguides must be formed and the waveguide core must be disordered to shift its bandgap to higher energy to produce low loss. To achieve this, the Si implant that forms the source and drain regions is now performed as a blanket implant over the entire wafer. Where the Si is required in the waveguide for disorder, it remains and where it is required as the source and drain of active devices it remains. Everywhere else it is removed after the RTA step. The RTA step is performed both to activate source/drain regions and to disorder the waveguide. The implant is performed everywhere except where blocked by W or resist.

- $\text{Al}_x\text{O}_y$  is used for isolation, passivation and to form the lower bragg reflector for the optical devices. However it is not used to form the current funneling layer as in most approaches today. Placing AlAs that close to the interface would compromise the operation of the FET. We see no possibility to use the oxide to form a high performance FET. The HFET or PHEMT is already the ideal FET. Further, the concept of oxidizing large lateral distances to produce a small aperture is not manufacturable. That is why the Si implant step is chosen above. Since we are using oxidation of the bottom mirror, then an etch step referred to as trench etch is added which etches through the back mirror prior to oxidation. Thus all devices are isolated by the trench etch and after oxidation all the etched vertical surfaces are passivated by oxide.

It is noted that the oxide is used primarily to produce the lower mirror. Since the oxide rate is quite sensitive to the Al concentration then the  $\text{Al}_{0.7}$  layers will oxidize much more slowly than the Al layers. Therefore when 20-30  $\mu\text{m}$  of AlAs is oxidized in the bragg mirror, there may be only 2  $\mu\text{m}$  of oxidation of  $\text{Al}_{0.7}$ . Since this oxidation occurs under the source and drain regions and along the waveguide walls then it serves additional purposes which are 1) it reduces the capacitances of the sources and drain regions to produce higher speed FETs 2) it provides a low index lateral cladding on the waveguide to allow very tight waveguide bends. Just how far we can push this concept of lateral oxidation remains to be determined experimentally.

We have devised a unique approach to use the selective oxidation of Al containing compounds over GaAs to produce our structures which follows the same principles as the Si LOCOS technology. The oxidation is done with GaAs as a mask, with W as a mask and with  $\text{SiO}_2$  as a mask.

With these modifications the process flow and masking steps are as follows:

1. Pattern mask 1 to etch alignment marks. Deposit protective oxide over apertures
2. Pattern mask 2 for first Si implant and perform implant

3. Pattern for lift off of W. Etch SiO<sub>2</sub>. Sputter W and lift-off
4. Pattern W gates, etch in SF<sub>6</sub>
5. Blanket ion implant. RTA for disorder and activation.
6. Pattern Source/Drain implants to protect N<sup>+</sup> junctions and waveguides. Etch to top of Al<sub>0.7</sub> layers.
7. Pattern for trench etch. Etch trench and then oxidize
8. Pattern to protect waveguide, etch to etch stop in S/D areas
9. Pattern for subcollector etch, etch oxide and semiconductor with RIE
10. Pattern for N lift-off, evaporate and lift-off
11. Pattern for collector etch, etch oxide and semiconductor with RIE
12. Pattern for P lift-off, evaporate and lift-off
13. Apply polyimide isolation
14. Pattern for polyimide holes
15. Lift-off of final Au bond pads
16. Deposit first stack layer. Pattern grating, and RIE etch grating pattern. Finish stack deposition
17. Etch stack for final Au bond pads

The total mask count is 15 or 14 if we choose to delete the pattern in step 8. This becomes a question of how the waveguide losses are affected by forcing the mode close to the top mirror. It probably can be deleted.

The mask set was designed for maximum debugging capability. Several chip sites were developed. One of these was shortened to 7 levels to produce only FET devices. Another chip site was shortened to only 8 levels to produce only VCSELs. These are top emitting rectangular devices of various sizes and aspect ratios. Another chip site was devoted to process diagnostics including mirror testing areas and also etch depth testers for all of the various etches involved in the process. The purpose of the shortened fabrication chip sites was to provide a means to obtain feedback on laser or FET devices independently with fewer man hours than required for the grating laser. These modules need to work first to verify the integrity of the approach. When these have proven themselves we will implement the full process to make the grating laser.

The laser/detector requires the grating level which is a non-standard item. We have chosen the phase mask approach to achieve this. The phase mask can be made by holography or by e-beam printing of each desired feature and then transferring these patterns to a quartz plate. The plate is used as a photomask and exposed with 248 nm light. We worked with two companies to make the phase mask, one using e-beam charged \$10.5K and the other using holography (Denmark) charged \$5.5K. It seems the holography approach is correct for initial testing because the grating pitches on all devices are the same and the devices have been arranged to be in parallel.

A major activity was invested in the development of the photomask set involving more than 12 man months of effort. We were bridging the gap between the earlier vertical cavity process flow that only begun to yield results at AT&T. Completely reworking this procedure to incorporate waveguides, traveling wave structures, a new oxidation technique, disorder etc. turned out to be an enormous task. The masks were produced with the best simulation support we could provide. These masks contain a very wide variety of circuits and devices. The list of circuits and devices includes among others

ring oscillators to determine transistor speed  
ring oscillators to determine switch laser speed  
12 traveling wave detectors (geometry and output variations)  
12 traveling wave lasers (geometry and output variations)  
a traveling wave DOES detector receiver  
temperature tuned lasers and detectors using FET control  
waveguide combined lasers with temp. tuning to produce 100GHz optical RF  
a directional coupler using the HFET modulator with dual waveguide I/O  
optical waveguide amplifiers  
HFET CCD arrays with optical outputs  
numerous test devices for the DOES, HFET laser and HFET transistors



## 10. GROWTH AND TESTING

The program required that no more than 20% of the effort be devoted to simulation but in our case this turned out to be impossible. In April 1994 the PI launched an effort at UConn to install a state of the art clean room and growth facility which included acquisition of space and funds and the design and implementation. Due to the bidding process and uncountable unforeseen delays, construction did not finally get under way until June 1996 and the facility was occupied in Nov. 1996. With the equipment installation and required qualification procedures we ran out of time to produce working devices. Another major problem was the supply of MBE material. A Varian GEN II system has been installed in the new growth facility at UConn but it was not on line at that time to produce the wafers for this program. Thus an arrangement was made with Penn State (PSU) to supply wafers. The PI had been awarded an SBIR (Rome Labs) contract with a company in MD to implement neurodes for an optoelectronic processor and PSU was to receive \$28K per year for wafers. The PI was also trying to raise venture capital to continue this work. At the time of the Phase II award (Sept 1996), a conflict arose as to the ownership of IP between the small company and the venture people. Due to an unfortunate turn of events the small company took the money elsewhere and this source of funding disappeared. Thus PSU was unwilling to supply wafers without funds. By the end of the contract (March 1997) we were still trying to obtain wafers. The MBE reactor at UConn is still being qualified but will require an infusion of funds before serious MBE growth can begin. In order to perform the testing the PI acquired an HP design and test station at a total cost of \$250K that will perform on wafer measurements up to 50GHz. About \$25K of contract money was used to start the lease for this equipment and the PI is now trying to raise the funds to continue this lease within the university and by finding new funding sources. Therefore during this one year program, the PI did all of the fundamental design work to support this new concept, and he assembled all of the necessary tools and laboratories to continue this work.

At the present time, funding is a major problem. A new SBIR has been started (Phase I) to demonstrate true time delay circuits for phased array systems. This contract is with the NavAir department of the DoD. Any results arising from this SBIR will be made available to the airforce electro-optics directorate on a continuous and timely basis. The Phase I work will result in a small fabrication activity to build a directional coupler. Hopefully the Phase II will enable a substantial effort. Also recently an STTR was awarded to demonstrate a CCD with infra red detection using the QWIP from the BMDO. This may provide another source if it can go to a Phase II.

The attempt to raise venture capital was not really successful. They agreed to supply \$360K but they wanted another investor. We could not find another investor. An ATP was applied for but the outcome is unknown. NSF proposals have been submitted. More SBIR proposals will be submitted. Visits have been made to DARPA to seek support but requests for funding have not been successful. There is some potential interest from Celeritek, a small company in Ca. which manufactures GaAs circuits for wireless and DBS systems (this company was founded with help from Sutter Hill Ventures and were briefed on the ICT). They have determined that an optical link from the satellite

receiver to the set top would be an exciting product and may be interested in funding (such a link would allow an IF frequency of 4GHz instead of 70MHz currently and could dramatically increase data flow). Only a monolithic chip could achieve a low enough cost to make this concept viable. There is a possibility that Celeritek may provide the funds for a prototype if they can accept the risk. Their decision should be known within two months.

## 11. REFERENCES

1. Integrated Inversion Channel Optoelectronic Devices and Circuit Elements for Multi-Functional Array Application, G. W. Taylor, P. A. Evaldsson, P. A. Kiely, T. Vang, D. P. Doctor, IEEE Journal of Quantum Electronics, Vol. 29, No. 2, pp. 785-800, February, 1993
2. Inversion Channel HFET with Unit Current Gain Frequency of 14ghz and Surface Emitting Laser from a Single Epitaxial Growth, P. A. Kiely, P. A. Evaldsson and P. Cooke, Electronics Letters, Vol. 29, No. 17, Aug. 19, 1993, p. 1521.
3. Submicrometre Gate Length Scaling of Inversion Channel Heterojunction Field Effect Transistor, P. A. Kiely, T. A. Vang, M. Micovic, A. Lepore, G. W. Taylor, R. Malik, Electronics Letters, 17 March, 1994, Vol. 30, No. 6, pp. 529-531.
4. Inversion Channel vertical cavity double heterostructure optoelectronic switchg lasers, P.A.Evaldsson, G.W.Taylor, P.Cooke, and S. Jiang, Electronics Letters, 25 May, 1995, Vol. 31, No. 11, p.920
5. W. Streifer, D.R. Scifres, and R. Burnham, "Analysis of grating-coupled radiation in GaAs:GaAlAs lasers and waveguides", IEEE J. Quantum Electronics, Vol. QE-12, pp422-428, July 1976.
6. R.F.Kazarinov and C.H.Henry, "Second-Order distributed feedback lasers with mode selection provided by first-order radiation losses", IEEE J. of Quantum Electronics, Vol. QE-21, pp.144-150, May 1985.
7. G.W.Taylor and C. Kwan, "Determination of Diffraction Efficiency for a Second-Order Corrugated Waveguide", IEEE J. of Quantum Electronics, Vol. QE-33, pp. 176-187, Feb. 1997.
8. A.Yariv, Optical Electronics in Modern Communications, Oxford Press, 1996.
9. G.W.Taylor, "Theory of Operation of the quantum well injection laser without k selection", J. of Appl Phys., Vol. 70, No.5, pp2508-2534, Sept. 1991.
10. G.W.Taylor, "Diffraction into a Corrugated Waveguide From Nomally Incident Radiation", IEEE JQE, submitted for publication.
11. W.H. Lee and W. Streifer, "Radiation loss calculation for corrugated dielectric waveguides. II TM polarization", J. Opt. Soc. Am. , Vol 69, No.12, p.1671, Dec. 1979
12. R. Goyal, "Monolithic Microwave Integrated Circuits", Artech House, 1989

## ACRONYMS

E/O, O/E	Optical to Electrical, Electrical to Optical
BER	Bit Error Rate
ATM	Asynchronous Transfer Mode
ICT	Inversion Channel Technology
MBE	Molecule Beam Epitaxy
PHEMT	Pseudomorphic High Electron Mobility Transistor
III-V	Semiconductor compounds using group III and Group V elements
SI GaAs	Semi-Insulating GaAs
IC's	Integrated Circuits
FET	Field Effect Transistor
DOES	Double Heterostructure Optoelectronic Switch
HFET	Heterostructure Field Effect Transistor
CAD	Computer Aid Design
UConn	University of Connecticut
SCH	Separate Confinement Heterostructure
Q factor	Quality factor
GC VCSEL	Grating Coupled Vertical Cavity Surface Emitting Laser
VCSEL	Vertical Cavity Surface Emitting Laser
DFB	Distributed Feedback
DBR	Distributed Bragg Reflection
PC	Personal Computer
VC	Vertical Cavity

TMM	Transmission Matrix Method
DC/AC	Direct Current/Alternating Current
RIN	Relative Intensity Noise
RTA	Rapid Thermal Anneal
RC	Resistance Capacity
RCE	Resonant Cavity Enhanced
TWPD	Traveling Wave Photon Detector
WDM	Wavelength Division Multiplexing
TW	Traveling Wave
R	series Resistance per unit length
G	shunt conductance per unit length
LOCOS	Local Oxidation of Silicon
S/D	Source/Drain
RIE	Reactive Ion Etching
PSU	Penn State University
SBIR	Small Business Innovation Research
CCD	Charge Coupled Device
QWIP	Quantum Well Infrared Detector
DBS	Direct Broadcast System
IF	Intermediate Frequency

## LIST OF SYMBOLS

$\text{Gb/s}$	Giga bit per second
$n_1, n_3$	the index of the cladding region
$n_2$	the index of the core region
$L_{pb}, L_{pt}$	the penetration depths of the bottom and top mirrors
$\Delta n$	the index difference between the two layers in a pair of the mirror
$L_{Mt,b}$	is the total front and back mirror thicknesses
$\kappa$	the coupling constant
$L_x$	the quantum well width
$\eta_e$	the electrical confinement factor
$J, J_{TH}$	the current and theoreld current density
$\tau_p'$	the effective photon lifetime for the vertical cavity device
$\alpha_{vc}$	the vertical cavity loss due to the diffraction grating
$P_{out}$	power output from the laser
$t_f$	the power transmissivity of the output port
$\alpha_{vc}$	the primary optical loss in the vertical cavity
$\eta_{diff}$	the diffraction efficiency due to grating
$\eta_1, \eta_2$	the impedances of the guide and the incident medium
$A_y$	the field intensity at the edge of the guide of the z propagating wave
$C_0$	the field intensity of the incident wave
$\alpha_g$	the growth of the guided wave due to diffraction
$d_{eff}$	the effective width of the guide which includes evanescent cladding penetration.
$\alpha_x$	the loss of wave propagating along x direction (vertical)
$\Gamma$	the confinement factor
$F_g$	the waveguide photon density
$\tau_p'$	the effective photon lifetime in the cavity
$W$	the width of waveguide,
$L$	the length of waveguide

$\eta_e$	the electrical efficiency of laser
$Z_0$	the characteristic impedance
$\lambda$	the wavelength
$\omega$	the frequency
$w_s, w_g$	the source and gate widths,
$\mu$	the permittivity
$\sigma_s, \sigma_g$	the metal conductivities
$K(k_1), K(k_1'), K(k), K(k')$	the complete elliptic integrals of the first kind
$\sqrt{\epsilon_{eff}}$	the effective index
$E_0$	the delta function input impulse of energy
$\alpha$	the absorption coefficient of the active layer
$\Gamma$	the optical confinement factor
$v_0$	the optical velocity
$v_e$	the electrical energy (or group) velocity,
$l$	the detector length
$t$	the time as measured from the time of incidence of energy to the detector
$\eta_i$	the internal quantum efficiency
$q$	the electronic charge
$h\nu$	the photon energy
$\alpha_e$	the attenuation of the electrical wave on the transmission line.
$H(f)$	the transfer function

## 12. Appendices

### Appendix A. Determination of Diffraction Efficiency for a second order Corrugated Waveguide

## Determination of Diffraction Efficiency for a Second Order Corrugated Waveguide

G. W. Taylor and C. Kwan  
Electrical and Systems Engineering  
University of Connecticut  
Storrs, CT 06269

### Abstract

The diffraction from a second order corrugated waveguide is analyzed to determine its efficiency as an element to redirect a guided wave. Using a rectangular grating, the efficiency is evaluated in an approximate closed form. The dependence upon grating thickness, waveguide thickness and wavelength are investigated and the results indicate usefulness as a simulation tool for photonic integrated circuits.



# 1 Introduction

Gratings combined with waveguides have been important structures for realizing many useful components for integrated optics [1] [2]. These include co-directional and contra-directional waveguide couplers for optical switches [3] and DFB (Distributed feedback) or DBR (Distributed Bragg Reflector) laser structures [4]. In the application to lasers, first and third order gratings are normally applied to make classic DFB or DBR devices since these gratings produce diffracted components only in the plane of the guide. However second order gratings have been considered as a means to discriminate between the two symmetrical modes produced by a DFB laser, i.e. the second order grating produces components in forward, backward and surface normal directions and the lasing action will naturally select the mode which favors the least surface normal radiation loss [5] [6]. Thus the wavelength is selected and stabilized. In the past few years, second order gratings have been used as the output coupling device for DBR lasers to produce surface-emitting devices either individually (as a broad area laser) or as arrays to generate significant power [7] [8]. Another use of the second order grating [9] is to couple from a passive waveguide into an active optoelectronic component such as a detector or a modulator or of coupling the light into a passive waveguide from a laser. The most significant parameter characterizing such grating structures is the loss parameter  $\alpha$  which describes the fraction of power propagating in the guide which can be coupled to the surface normal direction. In general, this parameter has been determined from numerical simulations. It is the purpose of this paper to investigate the calculation of  $\alpha$  and its dependence on the waveguide and grating parameters using quasi-analytical techniques.

## 2 Second order grating calculation

The original calculations which formalized Maxwell's equations to address this problem were published by Streifer *et al.* [10]. The approach was generalized to any order and to any shape of grating. A significant result of their work was a numerical algorithm which could be used to determine the behavior of the grating. Subsequent calculations by Streifer [11] and others [5] have focussed on the analysis of the second order grating in the context of the DFB laser in which coupled mode analysis was employed to determine the behavior of the grating in the presence of symmetrical forward and backward travelling coupled modes. Here also the analysis yields numerical solutions. Our interest here is to re-examine the basic diffraction for a wave incident upon a second order grating and to determine an analytic form for the grating coupling coefficient in terms of the structural parameters. By representing, the first

order backward travelling wave as a reduced version of the forward wave, we are able to consider both weak and strong coupling situations. This enables a simplification and thus an analytic result is possible. The result we obtain will be useful in evaluating and designing waveguide couplers as inputs or outputs for lasers and detectors into waveguides without resorting to extensive numerical methods. These simulated results are ideally suited as the basis of CAD tools for integrated optic design.

The problem we address is illustrated in Fig. 1. A slab waveguide of thickness  $d$  is corrugated with a grating of thickness  $t$ . The grating begins at  $z = 0$  and extends continuously in the positive  $z$  direction. The  $x$  direction is taken as positive downwards. The slab waveguide is characterized by the indices  $n_1$  above,  $n_2$  within, and  $n_3$  below the waveguide respectively. The grating section has a refractive index with a periodic variation and is described by the Fourier series

$$n_g^2(x, z) = \bar{n}^2(x) + \sum_{q=-\infty \text{ \& } q \neq 0}^{\infty} B_q(x) e^{i2\pi qz/\Lambda} \quad (1)$$

where  $\bar{n}$  is the average index over one grating period,  $B_q$  are the Fourier coefficients, and  $\Lambda$  is the grating period as illustrated in Fig. 1.

The  $TE$  modes in the waveguide are described by the two dimensional wave equation

$$\frac{\partial^2 E_y}{\partial x^2} + \frac{\partial^2 E_y}{\partial z^2} + k_0^2 n^2(x, z) E_y = 0 \quad (2)$$

where  $k_0 = 2\pi/\lambda_0$  is the wave number, and  $\lambda_0$  is the free space wavelength. The index is expressed by region as

$$n^2(x, z) = \begin{cases} n_1^2 & x < 0 \\ n_g^2(x, z) & 0 < x < t \\ n_2^2 & t < x < d \\ n_3^2 & d < x \end{cases} \quad (3)$$

In the standard approach to this problem the mode field  $E_y$  is represented as shown by Streifer [10], by an infinite sum of partial waves in the form

$$E_y(x, z) = \sum_{m=-\infty}^{\infty} E_m(x, z) \exp(i\beta_m z) \quad (4)$$

where the propagation constants  $\beta_m$  are expressed

$$\beta_m = \beta_0 - \frac{2\pi m}{\Lambda} \quad (5)$$

and we note that (5) implies (as shown later) that  $m$  takes positive values for diffracted waves. If no grating were present then all  $E_m(x, z)$  with  $m \neq 0$  would be zero, and

we would have  $E_0(x)$  and  $\beta_0$  as the mode pattern and propagation constant of the unperturbed waveguide. Therefore in our analysis we assume that a wave  $E_{in}$

$$E_{in} = A_0(x)e^{-i\beta_0 z} \quad (6)$$

is propagating in the waveguide for  $z < 0$  where  $A_0(x)$  is an arbitrary amplitude. We assume a  $TE$  mode in the guide and therefore  $A_0(x)$  is determined by

$$A_0(x) = \begin{cases} A_y e^{\delta x} & x \leq 0 \\ A_y \cos \kappa x + B_y \sin \kappa x & 0 \leq x \leq d \\ (A_y \cos \kappa d + B_y \sin \kappa d) e^{-\gamma(x-d)} & d \leq x \end{cases} \quad (7)$$

where

$$\begin{aligned} \kappa &= n_2 k_0 \sin \theta_b, \\ \delta &= \left[ (n_2^2 - n_1^2) k_0^2 - n_2^2 k_0^2 \sin^2 \theta_b \right]^{1/2}, \\ \gamma &= \left[ (n_2^2 - n_3^2) k_0^2 - n_2^2 k_0^2 \sin^2 \theta_b \right]^{1/2}, \\ A_y &\text{ is the value of } A_0(0), \end{aligned}$$

and  $\theta_b$  is the bounce angle.

From continuity of  $H_z$  at  $x = 0$ , we also obtain

$$\frac{A_y}{B_y} = \frac{\kappa}{\delta} \quad (8)$$

For the  $TE$  mode, the graphical solution of the eigenvalue equation,  $\tan \kappa d = \frac{\kappa(\gamma+\delta)}{\kappa^2 - \gamma\delta}$ , yields the eigenvalue  $\kappa$ . From the eigenvalues we also obtain the bounce angles for  $TE$  modes as

$$\theta_b = \sin^{-1} \frac{n_2 \cdot k_0}{\kappa} \quad (9)$$

and from basic waveguide theory we know that the propagation constant  $\beta_0$  is related to the bounce angle  $\theta_b$  by

$$\beta_0 = n_2 k_0 \cos \theta_b \quad (10)$$

Our analysis will be confined to the problem of the second order grating imposed on the waveguide. This grating is of particular importance to applications which require the redirection of optical waves through  $90^\circ$  such as in coupling from a waveguide to a detector. Second order grating diffraction principles are outlined in many texts (e.g.[12]) and, as illustrated in Fig. 2a, the light is diffracted by an angle  $\psi$  according to the Bragg relation

$$-\cos \psi = \sin \theta = m - 1 \quad (11)$$

where  $\psi = \theta + \pi/2$  is the angle of propagation of the diffracted wave with respect to the direction of propagation of the incoming wave. For real  $\theta$ , only the values of  $m = 0, 1$ , and  $2$  are allowed corresponding to components in the forward direction ( $m = 0$ ), the reverse direction ( $m = 2$ ) and the direction approximately normal to the waveguide ( $m = 1$ ). For  $\theta = 0$ , the wave propagates normal to the guide and for small positive or negative values it propagates to the right or left of the normal respectively of the guide in Fig. 2a. The component approximately normal to the waveguide is comprised of upward and downward travelling waves since both will be allowed by the Bragg relation. Their relative magnitudes will be determined by the indices involved in a particular case as illustrated by example later. Therefore in consideration of (4) only three terms in the summation need to be considered. The diffraction orders can be shown with the vector diagram as illustrated in Fig. 2b.

We first consider the rectangular grating because of its mathematical simplicity. In the appendix, the sinusoidal grating is considered

### 3 Rectangular grating

The rectangular grating has been discussed in detail by Streifer [10]. For this case the coefficients in (1) are expressed

$$B_q = \begin{cases} -\frac{(n_2^2 - n_1^2)}{\pi q} \sin\left(\frac{\pi q w}{\Lambda}\right) & 0 < x < t \\ 0 & x < 0, \quad t < x, \quad q \neq 0 \end{cases} \quad (12)$$

where  $w$  is the grating tooth width (see Fig. 4). The index in the grating region corresponding to (3) is expressed

$$n_g^2(x, z, q) = \bar{n}^2 - \frac{(n_2^2 - n_1^2)}{q\pi} \sin\left(\frac{\pi q w}{\Lambda}\right) e^{\frac{i2\pi q}{\Lambda} z} \quad (13)$$

where the average  $\bar{n}$  is given by

$$\bar{n}^2 = \{wn_1^2 + (\Lambda - w)n_2^2\}/\Lambda, \quad 0 < x < t \quad (14)$$

The remaining indices are as in (3). The first step in the solution is to determine  $E_y(x, z)$  in the region of the grating itself. However, we first note that the coefficients  $q = -1$  and  $+1$  determine the coefficients for the waves with  $m = 0$  and  $2$  respectively. Separate wave equations are obtained for each value of  $m$  by substituting (4) into (2) and collecting the coefficients for each value of  $e^{i\beta_m z}$ . We obtain

$$\frac{\partial^2 E_0}{\partial x^2} - \beta_0^2 E_0 + k_0^2 \bar{n}^2 E_0 + 2i\beta_0 \frac{\partial E_0}{\partial z} + k_0^2 (\tilde{B}_1 E_1 + \tilde{B}_2 E_2) = 0, \quad m = 0 \quad (15)$$

$$\frac{\partial^2 E_1}{\partial x^2} - \beta_1^2 E_1 + k_0^2 \bar{n}^2 E_1 + 2i\beta_1 \frac{\partial E_1}{\partial z} + k_0^2 (\tilde{B}_{-1} E_0 + \tilde{B}_1 E_2) = 0, \quad m = 1 \quad (16)$$

$$\frac{\partial^2 E_2}{\partial x^2} - \beta_2^2 E_2 + k_0^2 \bar{n}^2 E_2 + 2i\beta_2 \frac{\partial E_2}{\partial z} + k_0^2 (\tilde{B}_{-1} E_1 + \tilde{B}_{-2} E_0) = 0, \quad m = 2 \quad (17)$$

where we represent  $\tilde{B}_{-1} = \tilde{B}_1 \equiv \tilde{B} = -\frac{(n_2^2 - n_1^2)}{\pi} \sin(\frac{\pi w}{\Lambda})$  as determined by (13) and, as is normally done, the terms in  $\frac{\partial^2 E}{\partial z^2}$  are neglected. It is noted that these equations more closely resemble those of Kazarinov and Henry [5] rather than Streifer [10] since  $E_m(x, z)$  in (4) has been given an explicit  $z$  dependence which results in the extra term of  $\partial E_1 / \partial z$  in (16). This term will be important in considering diffraction at angles of  $\psi$  other than  $\pi/2$  (i. e. for non-zero values of  $\theta$ ).

These are three coupled equations in the unknowns  $E_0$ ,  $E_1$  and  $E_2$  and it has been shown previously by Streifer and others that the only way of obtaining solutions is through a numerical perturbation. For the perturbation, the term in  $\tilde{B}$  in each equation is initially neglected to obtain a first attempt solution. These results are then used to determine the  $\tilde{B}$  terms and the procedure repeated until convergence is obtained. Boundary conditions are also applied. For each of the solutions  $E_0$ ,  $E_1$  and  $E_2$ , the continuity of  $E$  and  $dE/dx$  must be applied at the interfaces  $x = 0$ ,  $x = t$  and  $x = d$ . It is thus required to obtain the solution of 18 equations in 18 unknowns with one extra relation for input power conservation.

### 3.1 Ideal Second Order Grating

To circumvent this lengthy numerical procedure, a closed form result may be obtained with some reasonable approximations. In Fig. 3 we sketch the nature of the solution. The wave  $E_{in}$  enters the grating from the left and decays with the constant  $\alpha$  as it travels through the grating, giving rise to the two guided waves  $E_0 e^{-\alpha z}$  and  $E_2 e^{\alpha z}$  and a radiating wave  $E_1$ . It is clear that the wave  $E_1$  arises from the losses that are incurred by  $E_0$  as it propagates through the grating. Although  $E_1$  represents a wave propagating in the positive and negative  $x$  directions it will also, in general, have a  $z$  dependence resulting in a finite  $dE_1/dz$  in (16). However for the second order grating it is true in general that  $\beta_0 = -\beta_2$  and then it can be shown from (5) that

$$\beta_1 = 0 \quad \text{with} \quad \beta_o = 2\pi/\Lambda \quad (18)$$

Therefore the terms  $\beta_1^2 E_1$  and  $2i\beta_1 dE_1/dx$  disappear in (16). Equations (10) and (18) state that for a perfect second order grating the grating pitch is fairly close to the wavelength and is dependent on the bounce angle  $\theta_b$  and therefore on the thickness of the guide  $d$ , through (9). For a two dimensional or rib waveguide  $\beta_0$  will also depend

on the lateral geometries. Therefore it is necessary to know the exact waveguide shape before designing the grating for second order diffraction.

The grating produces a first order reflected wave  $E_2 e^{j\beta_0 z}$  travelling in the  $-z$  direction, as Figure 3 shows, which is a diminished version of  $E_0$  in amplitude. Since it is only the amplitude is required in (16), then  $E_2$  can be represented from transmission matrix theory as

$$E_2 = E_0 r_1 \tilde{m}_{eff}, \quad (r_g = r_1 \tilde{m}_{eff})$$

where  $r_1$  is the reflectivity of one grating period,  $r_g$  is the total reflectivity of the grating, and  $\tilde{m}_{eff} = \frac{\tanh \tilde{m} \xi}{\tanh \xi}$  is the effective number of mirror periods seen by the incident field. For a strictly first order grating it can be shown that  $r_g$  is a real number and approaches unity for an infinite grating, i.e.

$$r_g = \frac{1 - (n_1/n_2)^{2\tilde{m}}}{1 + (n_1/n_2)^{2\tilde{m}}}$$

where  $\tilde{m}$  is the number of grating periods. Due to the existence of the second order component,  $r_g$  will be less than unity but we can still express the  $z$  propagating grating field as

$$\tilde{E}_0(x, z) = E_0 e^{-\alpha z} + r_g E_0 e^{-\alpha z} = E_0 (1 + r_g) e^{-\alpha z} \quad (19a)$$

An important approximation we make regards  $E_0$  and  $E_2$ . Since  $E_0$  is a continuation of  $E_{in}$  and  $E_2$  is a reflection of  $E_0$ , then instead of finding  $E_0$  and  $E_2$  in the grating and matching it to the remainder of the guide (i.e. finding  $E_0$  and  $E_2$  solutions in all sections of the guide), we represent  $E_0 + E_2$  as one solution for the entire guide in the form of  $\tilde{E}_0$  as given by (19a). These two waves are assumed to continue to propagate in the grating with the constants  $\beta_0$  and  $-\beta_0$ , where  $\beta_0$  is the propagation constant of the input wave. Obviously, the actual propagation constant will be somewhere between that for a waveguide of thickness  $d$  and thickness  $d - t$  and as the depth of the grating  $t$  increases and begins to approach the waveguide thickness  $d$ , this assumption no longer becomes tenable. This issue is discussed in the context of the results. The  $x$  dependence of the  $\tilde{E}_0$  wave given by (19a) is contained in the waveguide mode profile given by (7). It will be noted therefore that  $A_0(x)$  and thus  $A_y$  as it is used below represents the net amplitude of a wave travelling in the corrugated section of the guide which allows us to calculate the diffraction efficiency accurately without specifying the relative magnitude of  $E_0$  and  $E_2$ . Thus (19a) becomes

$$\tilde{E}_0(x, z) = A_0(x) e^{-\alpha z} \quad (19b)$$

With these assumptions we need to solve only (16) rewritten as

$$\frac{\partial^2 E_1}{\partial x^2} + k_0^2 \bar{n}^2 E_1 + k_0^2 \tilde{B} \tilde{E}_0(x, z) = 0 \quad (20)$$

together with (19). From the solution of (20) it is then possible to determine  $\alpha$ , which is a real constant and can be found from the application of boundary conditions. This is a major distinction from previous work in which  $\alpha$  was evaluated from numerical solutions of  $E_1$  and  $E_0$ . Since  $E_1(x, z)$  is the solution of interest we refer to it henceforth as  $E$  and determine its solutions  $E_{1x}$ ,  $E_g$ ,  $E_{2x}$ ,  $E_{3x}$  in the various regions of the guide. This approximation may be summarized by stating that outside the grating, the waveguide is a three layer waveguide and that within the grating we maintain a three-layer description. Equation (20) then yields the complementary solution

$$E_{gc}(x) = C_2 e^{ik_g x} + C_3 e^{-ik_g x}, \quad k_g = k_0 \bar{n} \quad (21)$$

and the particular solution (see Appendix A),

$$E_{gp} = \frac{k_0^2}{\kappa^2 - k_g^2} \tilde{B} A_y e^{-\alpha z} (\cos \kappa x + \frac{\delta}{\kappa} \sin \kappa x) \equiv b(z) (\cos \kappa x + \frac{\delta}{\kappa} \sin \kappa x) \quad (22)$$

which defines  $b(z) = \frac{k_0^2}{\kappa^2 - k_g^2} \tilde{B} A_y e^{-\alpha z} \equiv b$ . Then the total solution for  $E_g$  is

$$E_g(x, z) = C_2 e^{ik_g x} + C_3 e^{-ik_g x} + b(\cos \kappa x + \frac{\delta}{\kappa} \sin \kappa x) \quad (23)$$

The solutions in the non-grating sections of the waveguide are determined from (16) and (3) to be (note that  $\beta_1 = 0$ )

$$E_{1x}(x, z) = C_1 e^{ik_1 x}, \quad k_1 = (k_0^2 n_1^2 - \beta_1^2)^{1/2} = k_0 n_1 \quad (24)$$

$$E_{2x}(x, z) = C_4 e^{ik_2(d-x)} + C_5 e^{-ik_2(d-x)}, \quad k_2 = (k_0^2 n_2^2 - \beta_1^2)^{1/2} = k_0 n_2 \quad (25)$$

$$E_{3x}(x, z) = C_6 e^{-ik_3(x-d)}, \quad k_3 = (k_0^2 n_3^2 - \beta_1^2)^{1/2} = k_0 n_3 \quad (26)$$

The arbitrary constants in (23)-(26) are determined by the continuity of  $E(x)$  and  $dE/dx$  (continuity of  $H_z$ ) at the boundaries  $x = 0, x = t$  and  $x = d$ . Then the following relations are obtained

$$C_1 = C_2 + C_3 + b, \quad x = 0 \quad (27)$$

$$ik_1 C_1 = ik_g C_2 - ik_g C_3 + \delta \cdot b, \quad x = 0 \quad (28)$$

$$C_2 e^{ik_g t} + C_3 e^{-ik_g t} + b(\cos \kappa t + \frac{\delta}{\kappa} \sin \kappa t) = C_4 e^{ik_2(d-t)} + C_5 e^{-ik_2(d-t)}, \quad x = t \quad (29)$$

$$ik_g(C_2e^{ik_gt} - C_3e^{-ik_gt}) - b(\kappa \sin \kappa t - \delta \cos \kappa t) = -ik_2(C_4e^{ik_2(d-t)} - C_5e^{-ik_2(d-t)}) , \quad x = t \quad (30)$$

$$C_4 + C_5 = C_6 , \quad x = d \quad (31)$$

$$-ik_2C_4 + ik_2C_5 = -ik_3C_6 , \quad x = d \quad (32)$$

This set of linear equations is solved in a straight-forward way and some of the important results are

$$C_2 = \frac{1}{2}(1 + \frac{k_1}{k_g})C_1 - \frac{1}{2}(1 + \frac{\delta}{ik_g})b, \quad C_3 = \frac{1}{2}(1 - \frac{k_1}{k_g})C_1 - \frac{1}{2}(1 - \frac{\delta}{ik_g})b, \quad (33)$$

$$C_1 = 2b \frac{A + iB}{C + iD} \equiv 2bY(k_g), \quad (34)$$

and

$$C_6 = 2b \left\{ \frac{A + iB}{C + iD} Y_1 + Y_2 \right\} \quad (35)$$

where

$$\begin{aligned} A = & \cos(k_gt) + \frac{\delta}{k_g} \sin(k_gt) - [\cos(\kappa t) + \frac{\delta}{\kappa} \sin(\kappa t)] \\ & - \frac{1}{2} \left( \frac{k_2 + k_3}{k_2 - k_3} \right) \left( 1 + \frac{k_g}{k_2} \right) \{ \cos[2k_2(d-t) + k_gt] + \frac{\delta}{k_g} \sin[2k_2(d-t) + k_gt] \} \\ & - \frac{1}{2} \left( \frac{k_2 + k_3}{k_2 - k_3} \right) \left( 1 - \frac{k_g}{k_2} \right) \{ \cos[2k_2(d-t) - k_gt] - \frac{\delta}{k_g} \sin[2k_2(d-t) - k_gt] \} \\ & + (\cos \kappa t + \frac{\delta}{\kappa} \sin \kappa t) \left( \frac{k_2 + k_3}{k_2 - k_3} \right) \cos[2k_2(d-t)] \\ & + \left( \frac{\delta}{k_2} \cos \kappa t - \frac{\kappa}{k_2} \sin \kappa t \right) \left( \frac{k_2 + k_3}{k_2 - k_3} \right) \sin[2k_2(d-t)] \end{aligned}$$

$$\begin{aligned} B = & -\frac{k_g}{k_2} \sin(k_gt) + \frac{\delta}{k_g} \cos(k_gt) - \left[ \frac{\delta}{k_2} \cos(\kappa t) - \frac{\kappa}{k_2} \sin(\kappa t) \right] \\ & - \frac{1}{2} \left( \frac{k_2 + k_3}{k_2 - k_3} \right) \left( 1 + \frac{k_g}{k_2} \right) \{ \sin[2k_2(d-t) + k_gt] - \frac{\delta}{k_g} \cos[2k_2(d-t) + k_gt] \} \\ & - \frac{1}{2} \left( \frac{k_2 + k_3}{k_2 - k_3} \right) \left( 1 - \frac{k_g}{k_2} \right) \{ \sin[2k_2(d-t) - k_gt] + \frac{\delta}{k_g} \cos[2k_2(d-t) - k_gt] \} \\ & + (\cos \kappa t + \frac{\delta}{\kappa} \sin \kappa t) \left( \frac{k_2 + k_3}{k_2 - k_3} \right) \sin[2k_2(d-t)] \\ & - \left( \frac{\delta}{k_2} \cos \kappa t - \frac{\kappa}{k_2} \sin \kappa t \right) \left( \frac{k_2 + k_3}{k_2 - k_3} \right) \cos[2k_2(d-t)] \end{aligned}$$



$$C = 2(1 - \frac{k_1}{k_2}) \cos(k_g t) - (1 + \frac{k_1}{k_g})(1 + \frac{k_g}{k_2})(\frac{k_2 + k_3}{k_2 - k_3}) \cos[k_g t + 2k_2(d - t)] \\ - (1 - \frac{k_1}{k_g})(1 - \frac{k_g}{k_2})(\frac{k_2 + k_3}{k_2 - k_3}) \cos[k_g t - 2k_2(d - t)]$$

$$D = 2(\frac{k_1}{k_g} - \frac{k_g}{k_2}) \sin(k_g t) - (1 + \frac{k_1}{k_g})(1 + \frac{k_g}{k_2})(\frac{k_2 + k_3}{k_2 - k_3}) \sin[k_g t + 2k_2(d - t)] \\ + (1 - \frac{k_1}{k_g})(1 - \frac{k_g}{k_2})(\frac{k_2 + k_3}{k_2 - k_3}) \sin[k_g t - 2k_2(d - t)]$$

$$Y_1 = \{[\cos(k_g t) \cos k_2(d - t) - \frac{k_g}{k_2} \sin(k_g t) \sin k_2(d - t) \\ + i[\frac{k_1}{k_2} \cos(k_g t) \sin k_2(d - t) + \frac{k_1}{k_g} \sin(k_g t) \cos k_2(d - t)]]\} \\ = Y_{1\text{Re}} + iY_{1\text{Im}}$$

$$Y_2 = \frac{1}{2} \{ [\frac{k_g}{k_2} (\sin k_g t - \frac{\delta}{k_g} \cos k_g t) + \frac{\delta}{k_2} (\cos \kappa t - \frac{\kappa}{\delta} \sin \kappa t)] \sin k_2(d - t) \\ + [(\cos \kappa t + \frac{\delta}{\kappa} \sin \kappa t) - (\cos k_g t + \frac{\delta}{k_g} \sin k_g t)] \cos k_2(d - t) \}$$

Thus the field solution (23) within the grating may be expressed

$$E_g(x, z) = b(z) \{ [(1 + \frac{k_1}{k_g}) \frac{A + iB}{C + iD} - \frac{1}{2} (1 + \frac{\delta}{ik_g})] e^{ik_g x} \\ + [(1 - \frac{k_1}{k_g}) \frac{A + iB}{C + iD} - \frac{1}{2} (1 - \frac{\delta}{ik_g})] e^{-ik_g x} + (\cos \kappa x + \frac{\delta}{\kappa} \sin \kappa x) \} \quad (36) \\ \equiv b(z) X(x)$$

where

$$X(x) = [(1 + \frac{k_1}{k_g}) \frac{A + iB}{C + iD} - \frac{1}{2} (1 + \frac{\delta}{ik_g})] e^{ik_g x} \quad (37) \\ + [(1 - \frac{k_1}{k_g}) \frac{A + iB}{C + iD} - \frac{1}{2} (1 - \frac{\delta}{ik_g})] e^{-ik_g x} + (\cos \kappa x + \frac{\delta}{\kappa} \sin \kappa x)$$

One additional relation is required to relate the decrease in energy in the wave  $\tilde{E}_0$  given by (19b) to the energy radiated from the guide by the components  $E_{1x}(z)$  and  $E_{3x}(z)$ . Using the Poynting vector notation

$$\frac{1}{2\eta_3} C_6 \cdot C_6^* + \frac{1}{2\eta_1} C_1 \cdot C_1^* = \frac{d}{dz} (\frac{1}{2\eta_f} A_{0m}^2 e^{-2\alpha z} d') \quad (38)$$

where  $A_{0m}$  is the value of field related to the value  $A$  at  $x = 0$  as  $A_{0m} = A\sqrt{(\kappa^2 + \delta^2)/2\kappa^2}$ . Also,  $\eta_1$  is the characteristic impedance of the medium 1 ( $\eta_1 \propto \omega/n_1$ ),  $\eta_f$  is the characteristic impedance of the waveguide ( $\eta_f \propto \omega/n_2 \cos \theta_b$ ) and  $d'$  is the effective width of the guide from which the power in the input wave  $E_0$  can be extracted. This relation states that the gradient of the total guide power in  $z$  is equal to the vertically directed power. The effective width of the guide is

$$d' = (d + \frac{1}{\delta} + \frac{1}{\gamma}) \quad (39)$$

where the terms  $d, \delta, \gamma$  are due to the mode shape which comes from the conventional calculation of power inside and outside of the guide using (7). Equations (34), (35), (38), (39) are solved to give

$$2\alpha = \frac{k_0^4}{k_g^2(\kappa^2 - k_g^2)} \frac{\kappa^2}{\kappa^2 + \delta^2} \frac{\tilde{B}^2}{d'} \left\{ \frac{\eta_f}{\eta_1} \left[ \frac{A^2 + B^2}{C^2 + D^2} \right] + \frac{\eta_f}{\eta_3} \left[ \frac{A^2 + B^2}{C^2 + D^2} (Y_{1\text{Re}}^2 + Y_{1\text{Im}}^2) + Y_2^2 + \frac{2(AY_{1\text{Im}} + BY_{1\text{Re}})}{C^2 + D^2} Y_2 \right] \right\} \quad (40)$$

where the definitions of  $\gamma, \delta, \kappa$  are given by (7). Power loss is defined as  $2\alpha$ . It is evident from (38) that due to the exponential decay of input power with  $z$  then  $2\alpha$  also defines the diffraction efficiency as  $2\alpha = \alpha_T = \frac{P_{\text{out}}}{P_{\text{in}}}$  (including all radiation from the guide). Actually  $\alpha_T$  is proportional to the efficiency, since efficiency as a unitless quantity would be  $\alpha_T d'$  but we will refer to  $\alpha_T$  in general as the efficiency.

In general, one would be interested in the diffraction efficiency for power in either the upward ( $P_u$ ) or downward direction ( $P_d$ ). These are expressed respectively as

$$\alpha_u = \frac{k_0^4}{k_g^2(\kappa^2 - k_g^2)} \frac{\kappa^2}{\kappa^2 + \delta^2} \frac{(n_2^2 - n_1^2)^2 \sin^2(\frac{\pi w}{\Lambda})}{\pi^2 d'} \frac{\eta_f}{\eta_1} \left( \frac{A^2 + B^2}{C^2 + D^2} \right) \quad (41)$$

which is  $\frac{P_u}{P_{\text{in}}}$  and

$$\alpha_d = \frac{k_0^4}{k_g^2(\kappa^2 - k_g^2)} \frac{\kappa^2}{\kappa^2 + \delta^2} \frac{(n_2^2 - n_1^2)^2 \sin^2(\frac{\pi w}{\Lambda})}{\pi^2 d'} \frac{\eta_f}{\eta_3} \left[ \frac{A^2 + B^2}{C^2 + D^2} (Y_{1\text{Re}}^2 + Y_{1\text{Im}}^2) + Y_2^2 + \frac{2(AY_{1\text{Im}} + BY_{1\text{Re}})}{C^2 + D^2} Y_2 \right] \quad (42)$$

which is  $\frac{P_d}{P_{\text{in}}}$ . Thus  $\alpha_T = \alpha_u + \alpha_d$ .

### 3.2 Results and Discussion

In Fig. 4a we plot the dependence of  $\alpha$  upon  $t$ , the grating depth for both the  $TE_0$  and the  $TE_1$  mode. In Fig. 4b the  $TE_0$  result is shown for two different waveguide

thicknesses. The wavelength is chosen to be equal to the grating pitch (i.e.  $\lambda/n_2 = \Lambda$ ) so that ideal second order diffraction is obtained. The indices and other parameters used (indicated in the figure) are chosen to coincide with the calculations of Streifer and some of his data points are also shown in the Fig 4a for the  $TE_0$  calculation. (These indices are typical of a semiconductor laser waveguide in which the index differences  $n_2 - n_1$  and  $n_2 - n_3$  are small for a weakly guided wave). It is noted that the calculation agrees fairly well with Streifer's although his is slightly smaller because as he points out, he has not included the contribution of the  $E_2$  wave in his perturbation analysis. The main feature of the result is the resonance that occurs with  $t$ . At  $t = 0.14 \mu m$ , constructive interference occurs for the  $x$  directed wave in the grating and as  $t = 0.24 \mu m$  the interface is destructive. Therefore grating thickness is a key concern when optimizing the diffraction efficiency.

In Fig. 5 the variation with the tooth width,  $w$ , is shown and as expected a maximum is found for a slightly asymmetric tooth shape of  $w/\Lambda = 0.52$ . As shown this behavior also agrees fairly well with Streifer's. Streifer notes that the maximum occurs for  $w/\Lambda$  slightly less than 0.5 whereas we find the  $w/\Lambda$  slightly greater than 0.5. Inspection of (40) indicates that  $w/\Lambda > 0.5$  for the maximum.

In Fig. 6, the grating thickness is fixed and the waveguide thickness is varied. It is noted that the total diffraction efficiency is reduced for increasing thickness and Streifer's calculation is also indicated. The approximate region of validity is limited to a ratio of  $t/d = 0.7$  as discussed later. The undulations in the curve are due to the same resonance as observed in Fig. 4.

In Fig. 7 the index  $n_3$  is varied and the variation of diffracted power in the upward and downward direction is shown together with the total radiated power. Here also the result agrees well with Streifer's exact numerical procedure.

In Fig. 8 the variation of  $\alpha$  versus  $t$  shown in Fig. 4 cannot be valid as  $t$  approaches  $d$  as mentioned previously. To address this issue it is useful to define the effective index  $n_{eff}$  for the propagation of the wave  $E_0$  in the guide in the presence of the grating. We use the relations

$$\beta_0 = n_{eff} k_0 \cos \theta'_b \quad (43)$$

$$\beta_0 = n_2 k_0 \cos \theta_b \quad (44)$$

$$\beta_0 = \bar{n} k_0 \cos \theta_{b1} \quad (45)$$

to ensure a constant propagation constant in the all regions of the guide. This is illustrated in terms of a ray diagram shown in Fig. 8a which shows the ray  $\overline{AB}$  for the guide without a grating, the ray  $\overline{AFC}$  for a composite guide consisting of both  $n_2$  and  $\bar{n}$  regions and the ray  $\overline{AC}$  showing the final ray after the effects of propagation in the grating are included. To appreciate the effect of the grating in this diagram,

the vector  $\beta_0$  is indicated in the vector diagram of Fig. 8b. The grating vector subtracts from  $\beta_0$  to give a net vector of length  $\beta_1$  according to (5) as shown. From the diagram  $\theta_b$ ,  $\theta_{b1}$  can be found from geometrical relations in order to obtain the lateral displacements. Using (43)-(45) together with Fig. 8a, the effective index may be found as,

$$n_{eff} = \frac{n_2 \cos \theta_b}{\cos \theta'_b} = \frac{n_2 \cos \theta_b}{\cos \{ \tan^{-1} [ \frac{d}{(d-t) \cot \theta_b + t \cot \theta_{b1}} ] \}} = \frac{n_2 \cos \theta_b}{\frac{(d-t) \cot \theta_b + t \cot \theta_{b1}}{\sqrt{d^2 + [(d-t) \cot \theta_b + t \cot \theta_{b1}]^2}}} \quad (46)$$

where  $\cot \theta_b = \frac{\beta_0}{\sqrt{n_2^2 k_0^2 - \beta_0^2}}$  and  $\cot \theta_{b1} = \frac{\beta_1}{\sqrt{n_2^2 k_0^2 - \beta_1^2}}$  are determined from Fig. 8a.

In Fig. 9 we plot the variation of  $n_{eff}$  versus the grating thickness with different  $\beta_1$  values. The value of  $n_{eff}$  starts from  $n_2$  at  $t = 0$  and slowly increases with increasing  $t$ . The result shows the perturbation technique is still reasonable until the grating thickness is greater than about 0.7 of the waveguide thickness ( $\pm 4\%$  errors). This justifies in general the approximation using  $n_{eff} \simeq n_2$  as discussed earlier.

### 3.3 Approximate Second Order

Suppose the input wavelength does not coincide with the grating period, so that the diffraction is either somewhat greater or somewhat less than second order (non-zero values of  $\theta$ ). Then the differential equation is given by (compare with (16) and (20))

$$\frac{\partial^2 E_1}{\partial x^2} + (k_0^2 \bar{n}^2 - \beta_1^2) E_1 + 2i\beta_1 \frac{\partial E_1}{\partial z} + k_0^2 \tilde{B} E_0(z) = 0 \quad (47)$$

where now

$$\beta_1 = \frac{2\pi n_2}{\lambda_0} \cos \theta_b - \frac{2\pi}{\Lambda} \quad (48)$$

which now includes two additional terms by comparison with (20). To solve this equation, we will assume that  $E_1$  has a form similar to the ideal second order result given by (36), i.e. we assume

$$E_1 = b'(z) X'(x) \quad (49)$$

where  $b'(z)$  is an exponential function of  $z$  which is expected to be similar but not necessarily the same as  $b(z)$  as given by (22). Since we expect the same decay rate in the  $z$  direction, then (47) becomes

$$\frac{\partial^2 E_1}{\partial x^2} + (k_g'^2) E_1 + k_0^2 \tilde{B} E_0(x, z) = 0 \quad (50)$$

where

$$k_g' = k_{gr}' + i k_{gi}' \quad (51)$$

and the components  $k'_{gr}$ ,  $k'_{gi}$  are found by splitting  $k'_g = \sqrt{k_0^2 \bar{n}^2 - \beta_1^2 - 2i\alpha\beta_1}$  into real and imaginary parts to give

$$k'_{gr} = \left[ \frac{k_0^2 \bar{n}^2 - \beta_1^2}{2} + \frac{1}{2} \sqrt{(k_0^2 \bar{n}^2 - \beta_1^2)^2 + 4\alpha^2 \beta_1^2} \right]^{1/2} \simeq (k_0^2 \bar{n}^2 - \beta_1^2)^{1/2} \quad (52)$$

and

$$k'_{gi} = \frac{2\alpha\beta_1}{\left[ k_0^2 \bar{n}^2 - \beta_1^2 + \sqrt{(k_0^2 \bar{n}^2 - \beta_1^2)^2 + 4\alpha^2 \beta_1^2} \right]^{1/2}} \simeq \frac{\sqrt{2}\alpha\beta_1}{k'_{gr}} \quad (53)$$

since  $\alpha \ll \beta_1, k_0 \bar{n}$ . The solution procedure now follows that for the ideal second order and equations (27)-(32) are reproduced with the modification that  $k_g$  is replaced wherever it appears by  $k'_g$  and that  $b'(z)$  now has real and imaginary parts given by

$$\begin{aligned} b'(z) &= b_r - ib_i \\ &= \left[ \frac{k_0^2 \bar{n}^2 (\kappa^2 - k_0^2 \bar{n}^2 + \beta_1^2)}{(\kappa^2 - k_0^2 \bar{n}^2 + \beta_1^2)^2 + 4\alpha^2 \beta_1^2} - i \frac{2\alpha\beta_1}{(\kappa^2 - k_0^2 \bar{n}^2 + \beta_1^2)^2 + 4\alpha^2 \beta_1^2} \right] \tilde{B} A_y e^{-\alpha z} \end{aligned} \quad (54)$$

The results are similar to (34) and (35) with

$$C_1 = 2b' \frac{A' + iB'}{C' + iD'}, \quad C_6 = 2b' \left\{ \frac{A' + iB'}{C' + iD'} Y'_1 + Y'_2 \right\} \quad (55)$$

It will be appreciated that the solution of the linear equations (22)-(32) with these changes is tedious by hand but that a simple matrix solution is possible and readily solved by conventional programs to obtain relatively quick results. On the other hand, closed form solutions for  $A'$ ,  $B'$ ,  $C'$ ,  $D'$ ,  $b'$ ,  $Y'_1$  and  $Y'_2$  can be found straightforwardly and then results can be plotted in about 3 seconds on a PC platform. Some of these results are given in the appendix C.

In order to express the diffraction efficiency in a similar way to the ideal second order case, it is assumed that  $\alpha$  can be used for  $\alpha_0$  in (52)-(53). This expedient is justified as we show later. Then the expressions for  $\alpha_u$  and  $\alpha_d$  as given by (41) and (42) can be used with  $A$ ,  $B$ ,  $C$ ,  $D$ ,  $Y_1$  and  $Y_2$  replaced by their primed counterparts.

These results are illustrated in Fig. 10 which shows the variation in the diffraction efficiencies  $\alpha$  (total),  $\alpha_u$  (upwards) and  $\alpha_d$  (downwards) as a function of  $\Lambda$ . Also shown on this plot using the points is a comparison of  $\alpha$  calculated by using  $\alpha_0$  for  $\alpha$  in (52)-(53) versus a totally self-consistent calculation and there is no difference in these results. The value of  $\alpha$  is seen to go to a minimum at  $\Lambda = 2\pi/\beta_0$  which is the ideal second order condition and to rise for a smaller or larger values. This implies power escaping from the guide and propagating in both  $x$  and  $z$  directions with the  $z$  component increasing as we move away from the second order condition.

This is also explained by the presence of  $k'_{gi}$  which implies an  $x$  dependent decay in the wave  $C_1 e^{ik_1 x}$ . The decay in energy is accounted for by the  $z$  travelling wave with propagation constant  $\beta_1$ .

Now for the case that the diffraction is not perfectly second order, there is a component of diffracted power flow both in the  $x$  direction and in the  $z$  direction. If  $\Lambda < \lambda$ , the  $m = 1$  component of the field has  $z$  diffracted power primarily in the same direction as the incident wave and if  $\Lambda > \lambda$ , the component is primarily in the opposite direction to the incident wave. Therefore the direction of the  $m = 1$  diffracted wave makes an angle with the vertical direction of  $\theta_1$  where

$$\tan \theta_1 = \frac{\beta_1}{k_1} = \frac{n_2}{n_1} \cos \theta_b - \frac{\lambda_0}{n_1 \Lambda} \quad (56)$$

Consequently the  $x$  axis in Fig. 10 also represents the angular deviations of the total emitted energy with respect to the vertical direction (ideal second order) and this is indicated. The discussion here is limited to values of  $\theta_1$  which are actually limited by (24) or (26) since  $k_1$  and  $k_3$  must be real in order to propagate power out of the waveguide. Therefore using (24), (26) and (56) the limitations on  $\theta_1$  are given by

$$\theta_{1u} \leq \tan^{-1} \frac{n_1}{n_1}, \quad \theta_{1d} \leq \tan^{-1} \frac{n_3}{n_1} \quad (57)$$

These limiting values are about  $\pm 45^\circ$  using the parameters in Fig. 10a.

Since these values depend on the index difference in the grating then for weak gratings it may be the case that  $\theta_{1u} \geq \theta_{3rd}$  (see Fig. 2b). For these situations there is no distinct regime of grating pitch without diffraction. Rather there is a continuous coexistence and overlap of the approximate second and third order diffraction components.

## 4 Analogy to coupled mode theory

Coupled mode equations are used to determine the guided wave solutions to the first order waveguide diffraction which would be the  $E_0$  and  $E_2$  solutions in this paper. The coupled mode approach is to represent the grating diffracted waves as conventional  $TE$  or  $TM$  waves and then substitute into the perturbed Maxwell equation to determine the wave envelope shape (i.e. the growth or decay). The present approach to second order diffraction is analogous to the coupled mode approach in that the first order waves are represented in the same way in order to predict the radiating wave.

## 5 Summary

The diffraction efficiency of a second order grating has been calculated by considering first the ideal second order situation of emission at  $90^\circ$  to the guide and then arbitrary angles of emission as separate cases. A closed form result has been found based on the approximation of a single value of propagation constant ( $\beta_0$ ) for the guided wave. The approach maintains accuracy by including both forward and reverse first order diffracted waves as perturbation terms. The magnitude of the composite wave is not important since it cancels out in the determination of  $\alpha$ . The calculations are compared with the numerical results of earlier work and it is shown that the analytical or quasi-numerical simplified approach is a useful tool for iterative device design. An important aspect of this work is that the solutions are valid for strong or weak gratings because no approximations have been made which depend on a small index change.

## References

- [1] H. Nishihara, M. Haruna, and T. Suhara. *Optical integrated circuits*. McGraw-Hill, 1987.
- [2] A. Yariv and M. Nakamura. "Periodic structure for integrated optics". *IEEE J. Quantum Electronics*, vol. 13, no. 4, pp. 233-253, Apr. 1977.
- [3] J. M. Hommer, R. A. Bartolini, A. Miller, and C. C. Neil. "Optical grating coupling between low-index fibers and high-index film waveguides". *Appl. Phys. Lett.*, vol. 28, no. 4, pp. 192-194, Feb. 1976.
- [4] H. Kogelnik and C. V. Shank. "Coupled mode theory of distributed feedback lasers". *J. Appl. Phys.*, vol. 43, no. 5, pp. 2327-2335, May 1972.
- [5] R. F. Kazarinov and C. H. Henry. "Second-order distributed feedback lasers with mode selection provided by first-order radiation losses". *IEEE J. Quantum Electronics*, vol. 21, no. 2, pp. 144-150, May 1985.
- [6] A. Hardy, D. F. Welch, and W. Streifer. "Analysis of second-order gratings". *IEEE J. Quantum Electronics*, vol. 25, no. 10, pp. 2096-2105, Oct. 1989.
- [7] G. A. Evans, D. P. Bour, N. W. Carlson, R. Amantea, J. M. Hammer, H. Lee, M. Lurie, R. C. Lai, P. K. Pelka, R. E. Farkas, J. B. Kirk, S. K. Liew, W. F. Riechert, C. A. Wang, H. K. Choi, J. N. Walpole, J. K. Butler, W.F. Ferguson Jr., R. K. DeFreez, and M. Felisky. "Characteristics of coherent two-dimensional grating surface emitting diode laser arrays during CW operation". *Appl. Phys. Lett.*, vol. 27, no. 6, pp. 1594-1608, June 1991.
- [8] D. Botez, M. Jansem, L. J. Mawst, G. Peterson, and T. J. Roth. "Watt-range, coherent, uniphase powers from phase-locked arrays of antiguided diode lasers". *IEEE J. Quantum Electronics*, vol. 58, no. 19, pp. 2070-2072, May 1991.
- [9] T. Souara and H. Nishihara. "Integrated optics components and devices using periodic structure". *IEEE J. Quantum Electronics*, vol. 13, no. 4, pp. 62-95, Apr. 1986.
- [10] W. Streifer, D. R. Scifres, and R. Burnham. "Analysis of grating-coupled radiation in GaAs:GaAlAs lasers and waveguides". *IEEE J. Quantum Electronics*, vol. 12, no. 7, pp. 422-428, July 1976.
- [11] W. Streifer, D. R. Scifres, and R. Burnham. "Coupled wave analysis of DFB and DBR lasers". *IEEE J. Quantum Electronics*, vol. 13, no. 4, pp. 134-141, Apr. 1977.
- [12] H. C. Casey Jr. and M. B. Panish. *Heterostructure lasers*. Academic Press, 1978.



## Appendix A

### Particular Solution of Wave Equation

The  $x$  dependent differential wave equation in the grating is obtained from (19b) and (20) as

$$\frac{\partial^2 E_g}{\partial x^2} + k_g^2 E_g = -k_0^2 \tilde{B} A_0(x) e^{-\alpha z} \quad (\text{A1})$$

The complementary solution (RHS=0) is

$$E_{gc}(x) = C_2 e^{ik_g x} + C_3 e^{-ik_g x} \quad (\text{A2})$$

the particular solution is

$$\begin{aligned} E_{gp} &= k_0^2 \tilde{B} e^{ik_g x} \int \frac{A_0(x) e^{-\alpha z} e^{-ik_g x}}{-2ik_g} dx - k_0^2 \tilde{B} e^{-ik_g x} \int \frac{A_0(x) e^{-\alpha z} e^{ik_g x}}{-2ik_g} dx \\ &= \left( \frac{k_0^2}{\kappa^2 - k_g^2} \right) \tilde{B} A_y e^{-\alpha z} \left( \cos \kappa x + \frac{\delta}{\kappa} \sin \kappa x \right) \end{aligned} \quad (\text{A3})$$

where  $-2ik_g$  is the Wronskian and  $A_0(x)$  in (7) has been used for the grating region to represent  $TE$  modes. Then the total solution is

$$E_{gc}(x) = C_2 e^{ik_g x} + C_3 e^{-ik_g x} + \frac{k_0^2}{\kappa^2 - k_g^2} \tilde{B} A_y e^{-\alpha z} \left( \cos \kappa x + \frac{\delta}{\kappa} \sin \kappa x \right) \quad (\text{A4})$$

## Appendix B

### Sinusoidal Grating

For the sinusoidal grating, the coefficients in (1) are expressed

$$B_q = \begin{cases} -\frac{(n_2^2 - n_1^2)}{\pi q} \sin[q \cos^{-1}(\frac{2x}{t} - 1)] & 0 < x < t \\ 0 & x < 0, \ x > t, \ q \neq 0 \end{cases} \quad (\text{B1})$$

Then equation (13) is modified to

$$\frac{\partial^2 E_1}{\partial x^2} - \beta_1^2 E_1 + k_0^2 \bar{n}^2 E_1 - k_0^2 \frac{(n_2^2 - n_1^2)}{\pi q} \sin(q \cos^{-1}(\frac{2x}{t} - 1)) E_0(x) = 0 \quad (\text{B2})$$

Then the solution for  $E_g$  in the grating is written as

$$E_g(x, z) = C_2 e^{ik_g x} + C_3 e^{-ik_g x} + E_{gp} \quad (\text{B3})$$

and the particular solution can be obtained by following the procedure in Appendix A,

$$E_{gp} \equiv b = \frac{k_0^2}{2k_g^2} (n_2^2 - n_1^2) J_1(\frac{k_g t}{2}) \sin[k_g(x - \frac{t}{2})] A_{0g} e^{-\alpha z} \quad (\text{B4})$$

where  $J_1$  is the Bessel function of the first kind.

The remaining procedure and results are similar to those of the rectangular grating.

## Appendix C

Solution of the linear equations (22)-(32) for the approximate second order diffraction condition yield the following results for the parameter  $A', B', C', D'$ .

$$\begin{aligned}
 A' = & \left( \frac{k_2 + k_3}{k_2 - k_3} \right) \cos 2k_2(d-t) \left[ (1-\delta) \cos \kappa t + \left( \frac{\delta}{\kappa} + \kappa \right) \sin \kappa t \right] \\
 & - \left[ (1+\delta) \cos \kappa t + \left( \frac{\delta}{\kappa} - \kappa \right) \sin \kappa t \right] \\
 & + \frac{1}{2} \left[ \left( 1 - \frac{\delta k_g''}{k_g'^2 + k_g''^2} \right) \cos k_g' t + \frac{\delta k_g'}{k_g'^2 + k_g''^2} \sin k_g' t \right] \exp(-k_g'' t) \\
 & * \left[ 1 + \frac{k_g''}{k_2} - \left( \frac{k_2 + k_3}{k_2 - k_3} \right) \left( 1 - \frac{k_g''}{k_2} \right) \cos 2k_2(d-t) + \left( \frac{k_2 + k_3}{k_2 - k_3} \right) \frac{k_g'}{k_2} \sin 2k_2(d-t) \right] \\
 & + \frac{1}{2} \left[ \left( 1 - \frac{\delta k_g''}{k_g'^2 + k_g''^2} \right) \sin k_g' t - \frac{\delta k_g'}{k_g'^2 + k_g''^2} \cos k_g' t \right] \exp(-k_g'' t) \\
 & * \left[ \frac{k_g'}{k_2} + \left( \frac{k_2 + k_3}{k_2 - k_3} \right) \left( 1 - \frac{k_g''}{k_2} \right) \sin 2k_2(d-t) + \left( \frac{k_2 + k_3}{k_2 - k_3} \right) \frac{k_g'}{k_2} \cos 2k_2(d-t) \right] \\
 & + \frac{1}{2} \left[ \left( 1 + \frac{\delta k_g''}{k_g'^2 + k_g''^2} \right) \cos k_g' t + \frac{\delta k_g'}{k_g'^2 + k_g''^2} \sin k_g' t \right] \exp(k_g'' t) \\
 & * \left[ 1 - \frac{k_g''}{k_2} + \left( \frac{k_2 + k_3}{k_2 - k_3} \right) \left( 1 + \frac{k_g''}{k_2} \right) \cos 2k_2(d-t) - \left( \frac{k_2 + k_3}{k_2 - k_3} \right) \frac{k_g'}{k_2} \sin 2k_2(d-t) \right] \\
 & + \frac{1}{2} \left[ \left( 1 + \frac{\delta k_g''}{k_g'^2 + k_g''^2} \right) \sin k_g' t - \frac{\delta k_g'}{k_g'^2 + k_g''^2} \cos k_g' t \right] \exp(k_g'' t) \\
 & * \left[ \frac{k_g'}{k_2} - \left( \frac{k_2 + k_3}{k_2 - k_3} \right) \left( 1 + \frac{k_g''}{k_2} \right) \sin 2k_2(d-t) + \left( \frac{k_2 + k_3}{k_2 - k_3} \right) \frac{k_g'}{k_2} \cos 2k_2(d-t) \right]
 \end{aligned}$$

$$\begin{aligned}
 B' = & \left( \frac{k_2 + k_3}{k_2 - k_3} \right) \sin 2k_2(d-t) \left[ (1-\delta) \cos \kappa t + \left( \frac{\delta}{\kappa} + \kappa \right) \sin \kappa t \right] \\
 & - \frac{1}{2} \left[ \left( 1 - \frac{\delta k_g''}{k_g'^2 + k_g''^2} \right) \cos k_g' t + \frac{\delta k_g'}{k_g'^2 + k_g''^2} \sin k_g' t \right] \exp(-k_g'' t) \\
 & * \left[ \frac{k_g'}{k_2} + \left( \frac{k_2 + k_3}{k_2 - k_3} \right) \left( 1 - \frac{k_g''}{k_2} \right) \sin 2k_2(d-t) + \left( \frac{k_2 + k_3}{k_2 - k_3} \right) \frac{k_g'}{k_2} \cos 2k_2(d-t) \right] \\
 & + \frac{1}{2} \left[ \left( 1 - \frac{\delta k_g''}{k_g'^2 + k_g''^2} \right) \sin k_g' t - \frac{\delta k_g'}{k_g'^2 + k_g''^2} \cos k_g' t \right] \exp(-k_g'' t) \\
 & * \left[ 1 + \frac{k_g''}{k_2} - \left( \frac{k_2 + k_3}{k_2 - k_3} \right) \left( 1 - \frac{k_g''}{k_2} \right) \cos 2k_2(d-t) + \left( \frac{k_2 + k_3}{k_2 - k_3} \right) \frac{k_g'}{k_2} \sin 2k_2(d-t) \right] \\
 & - \frac{1}{2} \left[ \left( 1 + \frac{\delta k_g''}{k_g'^2 + k_g''^2} \right) \cos k_g' t + \frac{\delta k_g'}{k_g'^2 + k_g''^2} \sin k_g' t \right] \exp(k_g'' t)
 \end{aligned}$$

$$\begin{aligned}
& * \left[ \frac{k'_g}{k_2} - \left( \frac{k_2 + k_3}{k_2 - k_3} \right) \left( 1 + \frac{k''_g}{k_2} \right) \sin 2k_2(d - t) + \left( \frac{k_2 + k_3}{k_2 - k_3} \right) \frac{k'_g}{k_2} \cos 2k_2(d - t) \right] \\
& - \frac{1}{2} \left[ \left( 1 + \frac{\delta k''_g}{k'^2_g + k''^2_g} \right) \sin k'_g t - \frac{\delta k'_g}{k'^2_g + k''^2_g} \cos k'_g t \right] \exp(k''_g t) \\
& * \left[ 1 - \frac{k'_g}{k_2} - \left( \frac{k_2 + k_3}{k_2 - k_3} \right) \left( 1 + \frac{k''_g}{k_2} \right) \cos 2k_2(d - t) - \left( \frac{k_2 + k_3}{k_2 - k_3} \right) \frac{k'_g}{k_2} \sin 2k_2(d - t) \right]
\end{aligned}$$

$$\begin{aligned}
C' = & \left[ \left( 1 + \frac{k_1 k'_g}{k'^2_g + k''^2_g} + \frac{k''_g}{k_2} \right) \cos k'_g t + \left( \frac{k'_g}{k_2} + \frac{k_1}{k_2} + \frac{k_1 k''_g}{k'^2_g + k''^2_g} \right) \sin k'_g t \right] \exp(-k''_g t) \\
& + \left[ \left( 1 - \frac{k_1 k'_g}{k'^2_g + k''^2_g} - \frac{k''_g}{k_2} \right) \cos k'_g t + \left( \frac{k'_g}{k_2} - \frac{k_1}{k_2} + \frac{k_1 k''_g}{k'^2_g + k''^2_g} \right) \sin k'_g t \right] \exp(k''_g t) \\
& - \left( \frac{k_2 + k_3}{k_2 - k_3} \right) \left( 1 + \frac{k_1 k'_g}{k'^2_g + k''^2_g} - \frac{k''_g}{k_2} \right) \cos[2k_2(d - t) + k'_g t] \exp(-k''_g t) \\
& + \left( \frac{k_2 + k_3}{k_2 - k_3} \right) \left( \frac{k'_g}{k_2} + \frac{k_1}{k_2} - \frac{k_1 k''_g}{k'^2_g + k''^2_g} \right) \sin[2k_2(d - t) + k'_g t] \exp(-k''_g t) \\
& - \left( \frac{k_2 + k_3}{k_2 - k_3} \right) \left( 1 - \frac{k_1 k'_g}{k'^2_g + k''^2_g} + \frac{k''_g}{k_2} \right) \cos[2k_2(d - t) - k'_g t] \exp(k''_g t) \\
& - \left( \frac{k_2 + k_3}{k_2 - k_3} \right) \left( \frac{k'_g}{k_2} - \frac{k_1}{k_2} - \frac{k_1 k''_g}{k'^2_g + k''^2_g} \right) \sin[2k_2(d - t) - k'_g t] \exp(k''_g t)
\end{aligned}$$

$$\begin{aligned}
D' = & \left[ \left( 1 + \frac{k_1 k'_g}{k'^2_g + k''^2_g} + \frac{k''_g}{k_2} \right) \sin k'_g t - \left( \frac{k'_g}{k_2} + \frac{k_1}{k_2} + \frac{k_1 k''_g}{k'^2_g + k''^2_g} \right) \cos k'_g t \right] \exp(-k''_g t) \\
& - \left[ \left( 1 - \frac{k_1 k'_g}{k'^2_g + k''^2_g} - \frac{k''_g}{k_2} \right) \sin k'_g t + \left( \frac{k'_g}{k_2} - \frac{k_1}{k_2} + \frac{k_1 k''_g}{k'^2_g + k''^2_g} \right) \cos k'_g t \right] \exp(k''_g t) \\
& - \left( \frac{k_2 + k_3}{k_2 - k_3} \right) \left( 1 + \frac{k_1 k'_g}{k'^2_g + k''^2_g} - \frac{k''_g}{k_2} \right) \sin[2k_2(d - t) + k'_g t] \exp(-k''_g t) \\
& + \left( \frac{k_2 + k_3}{k_2 - k_3} \right) \left( \frac{k'_g}{k_2} + \frac{k_1}{k_2} - \frac{k_1 k''_g}{k'^2_g + k''^2_g} \right) \cos[2k_2(d - t) + k'_g t] \exp(-k''_g t) \\
& - \left( \frac{k_2 + k_3}{k_2 - k_3} \right) \left( 1 - \frac{k_1 k'_g}{k'^2_g + k''^2_g} + \frac{k''_g}{k_2} \right) \sin[2k_2(d - t) - k'_g t] \exp(k''_g t) \\
& - \left( \frac{k_2 + k_3}{k_2 - k_3} \right) \left( \frac{k'_g}{k_2} - \frac{k_1}{k_2} - \frac{k_1 k''_g}{k'^2_g + k''^2_g} \right) \cos[2k_2(d - t) - k'_g t] \exp(k''_g t)
\end{aligned}$$

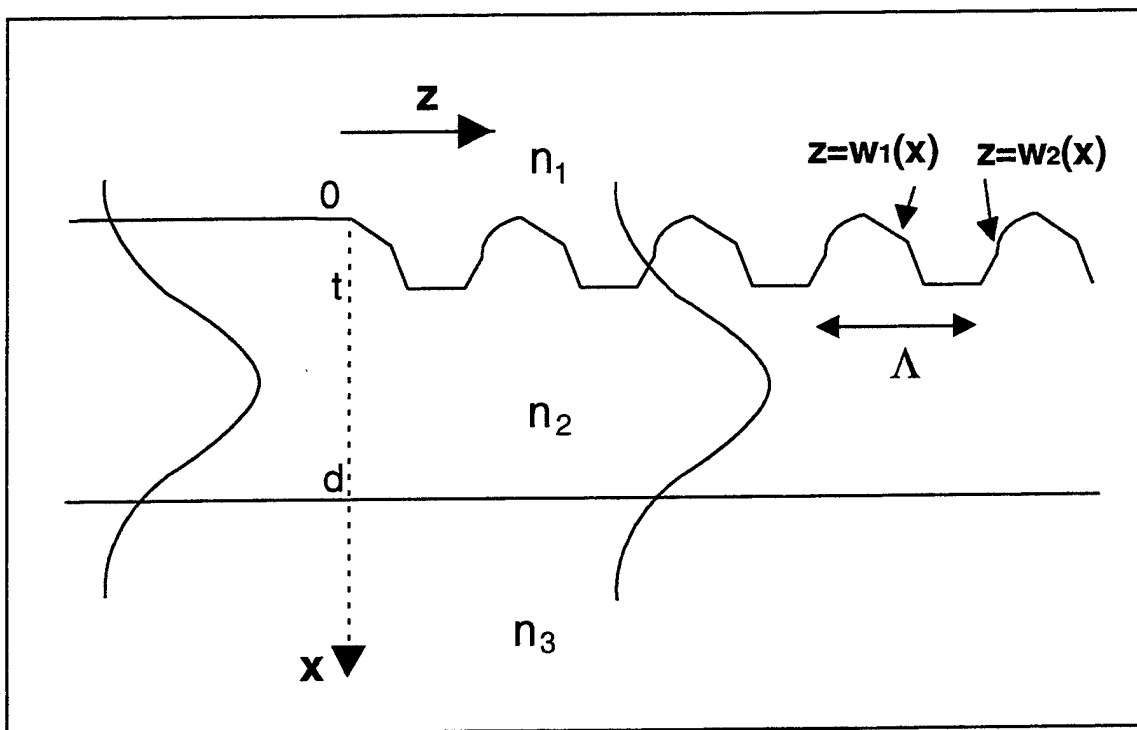


Fig 1 A slab waveguide with a grating of thickness  $t$

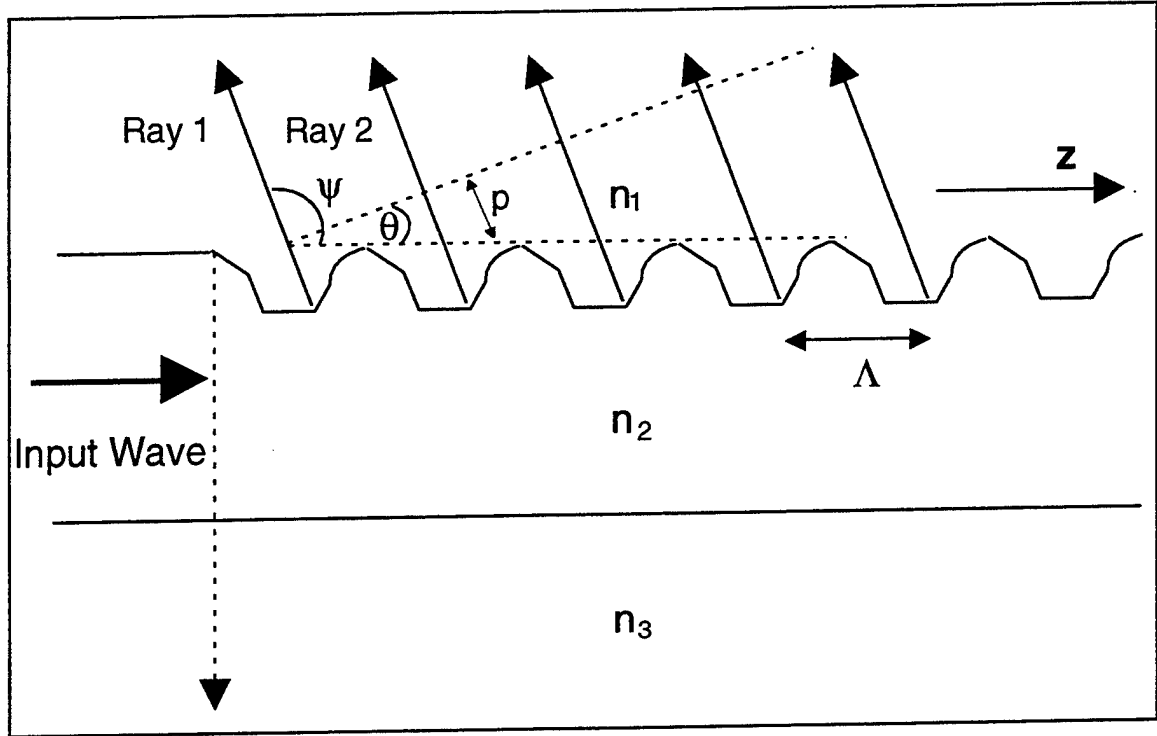


Fig. 2a Bragg diffraction scheme

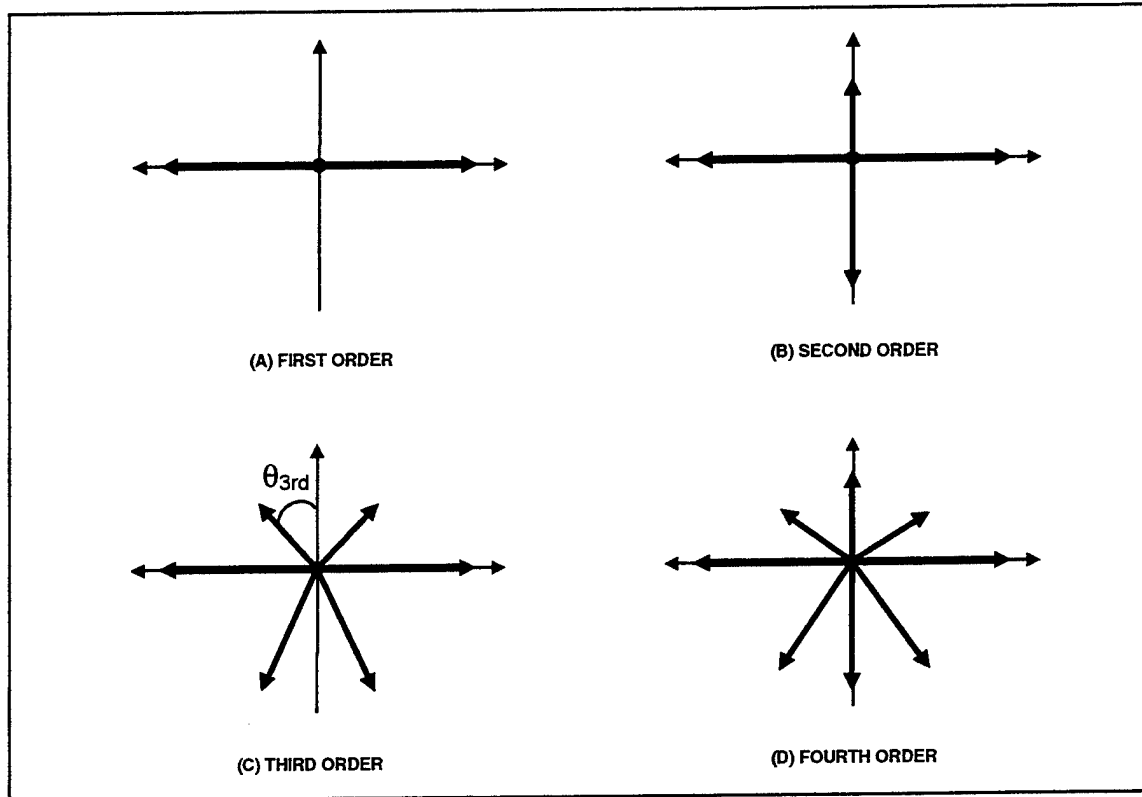


Fig. 2b Vector diagrams for Bragg gratings ( $\theta_{3rd}$  can be calculated from the standard formula[12] to yield  $19.47^\circ$ )

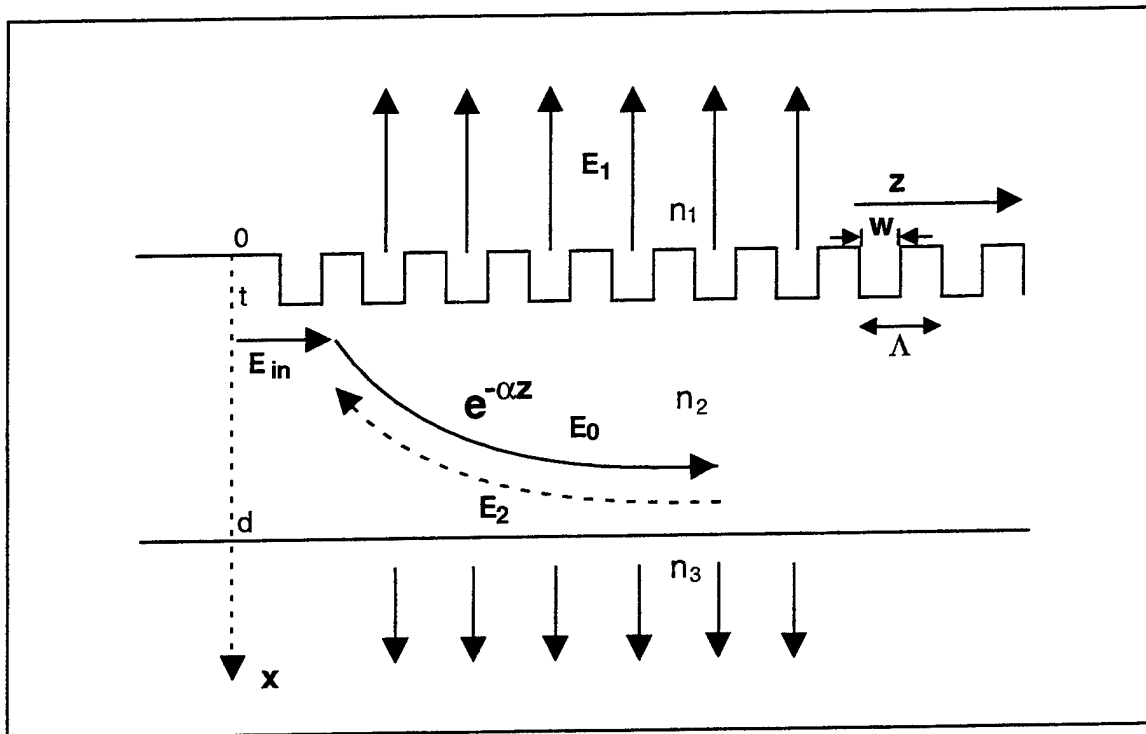


Fig. 3 Schematic of the incident wave producing transmitted wave, reflected wave and diffracted wave due to the grating



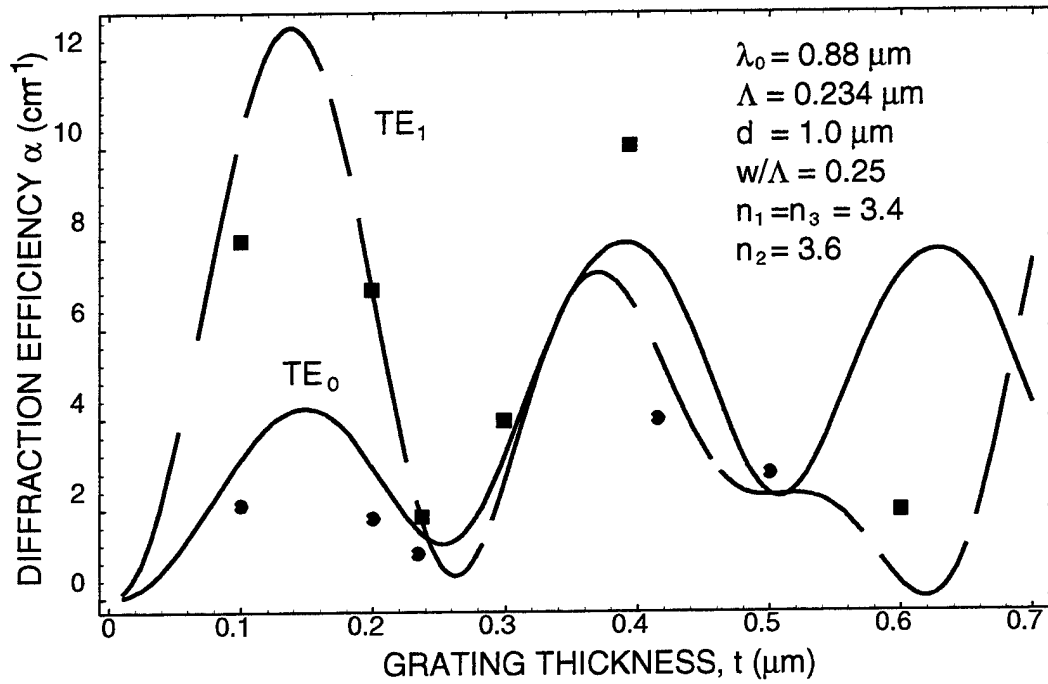


Fig. 4a Diffraction efficiency versus grating thickness for a rectangular grating. Discrete points are data of Streifer[10]. • TE<sub>0</sub> mode ■ TE<sub>1</sub> mode. Note that the individual points (from Streifer's paper) are not for the ideal second order case. Therefore, even though these should be larger than our ideal second order calculation, it is not because Streifer omits  $E_2$  from his perturbation (see text).

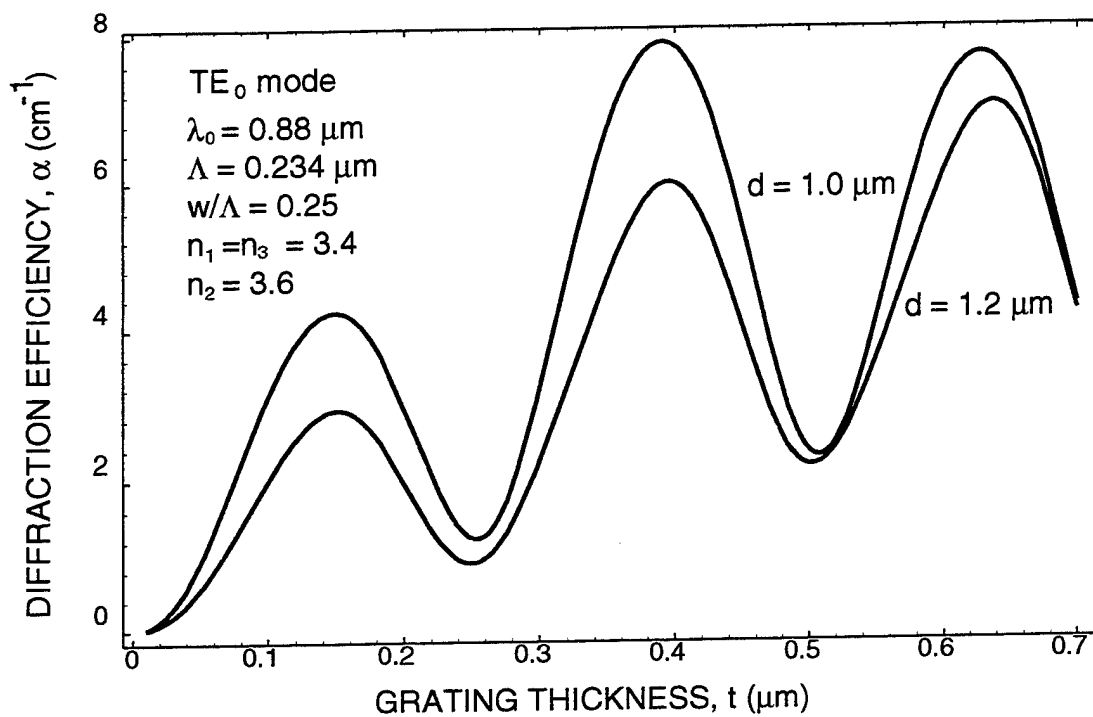


Fig. 4b Diffraction efficiency versus grating thickness for a rectangular grating with different waveguide thicknesses.

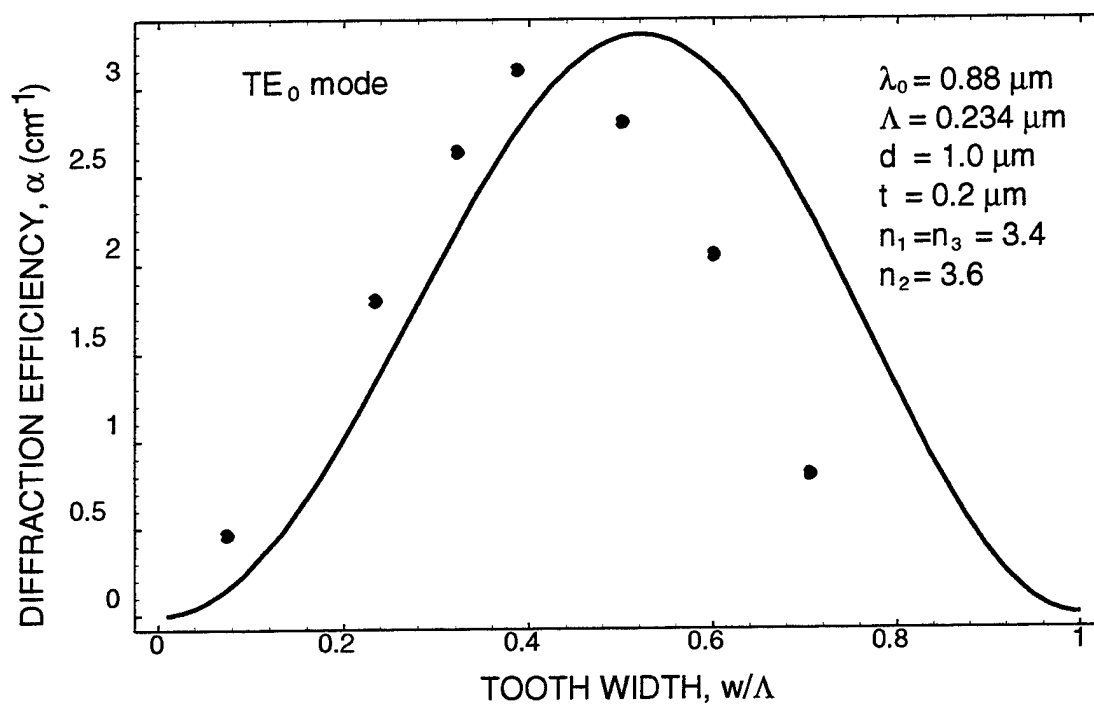


Fig. 5. Diffraction efficiency versus tooth width for a rectangular grating. Discrete points are calculations of Streifer[10].

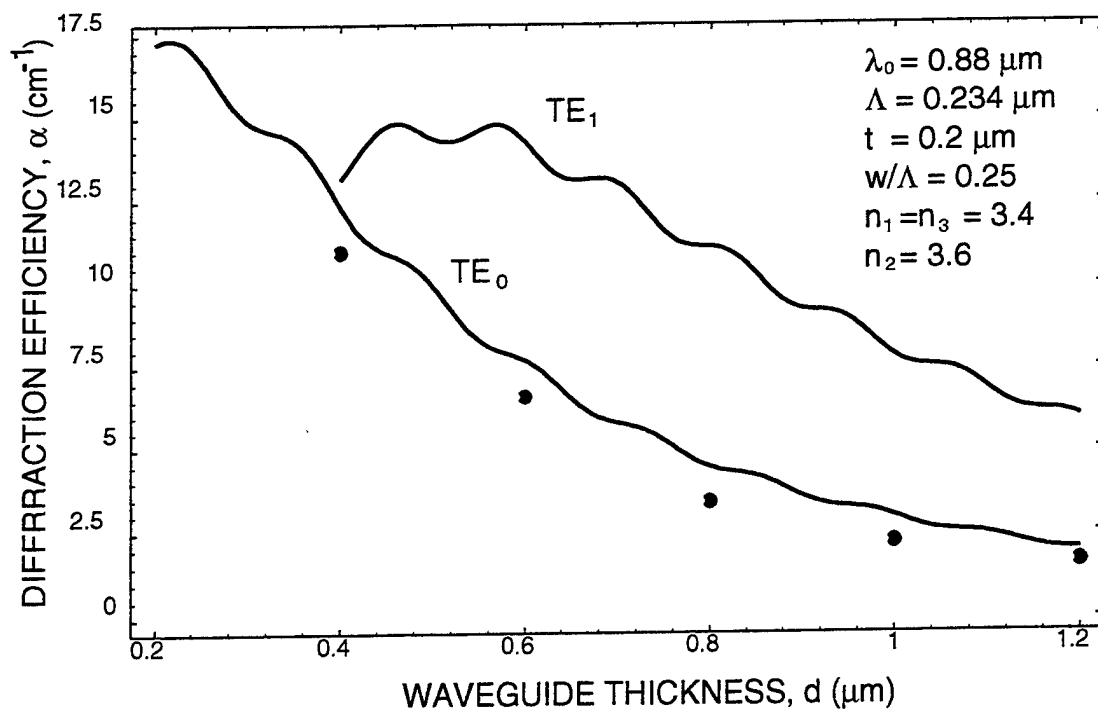


Fig. 6 Diffraction efficiency versus waveguide thickness for a rectangular grating. Discrete points are calculations of Streifer[10] for the TE<sub>0</sub> mode.

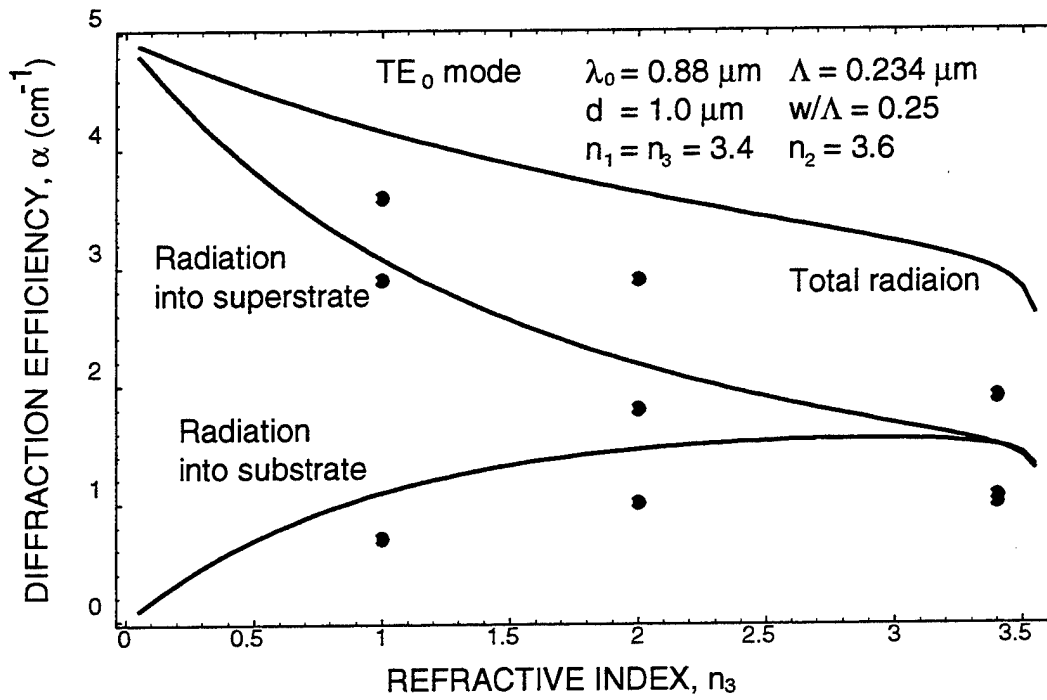


Fig. 7 TE<sub>0</sub> mode diffraction efficiency versus  $n_3$  for a rectangular grating. Discrete points are calculations of Streifer[10].

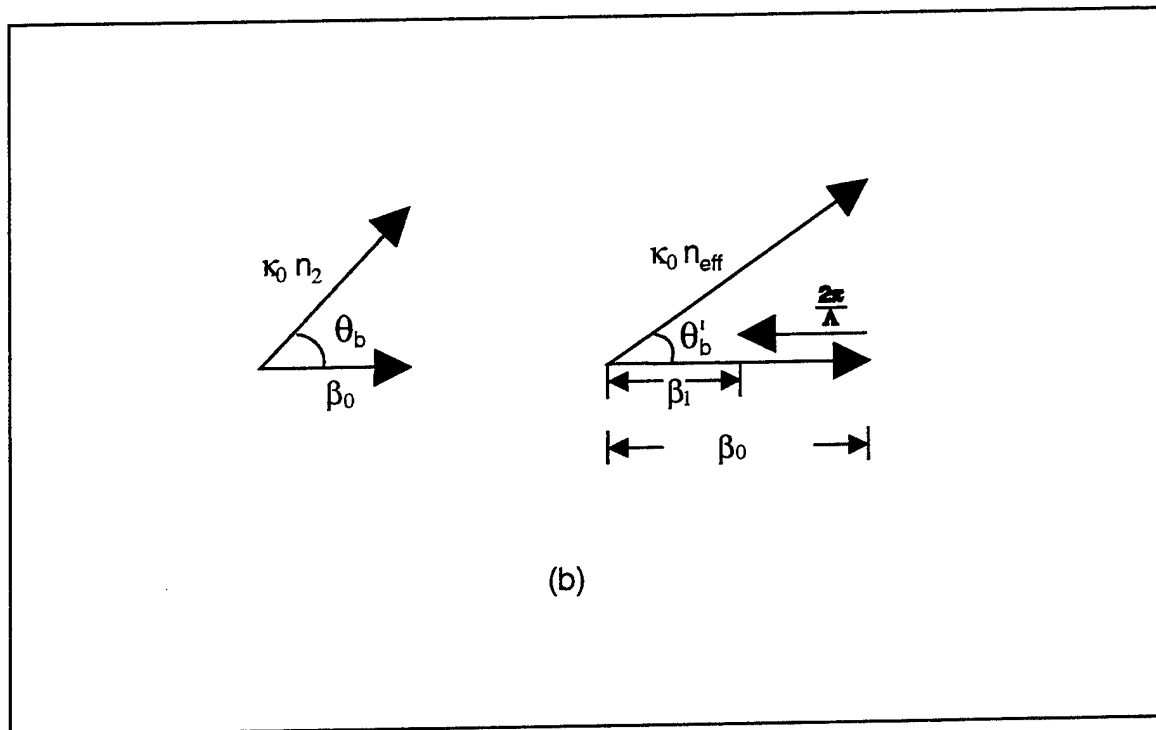
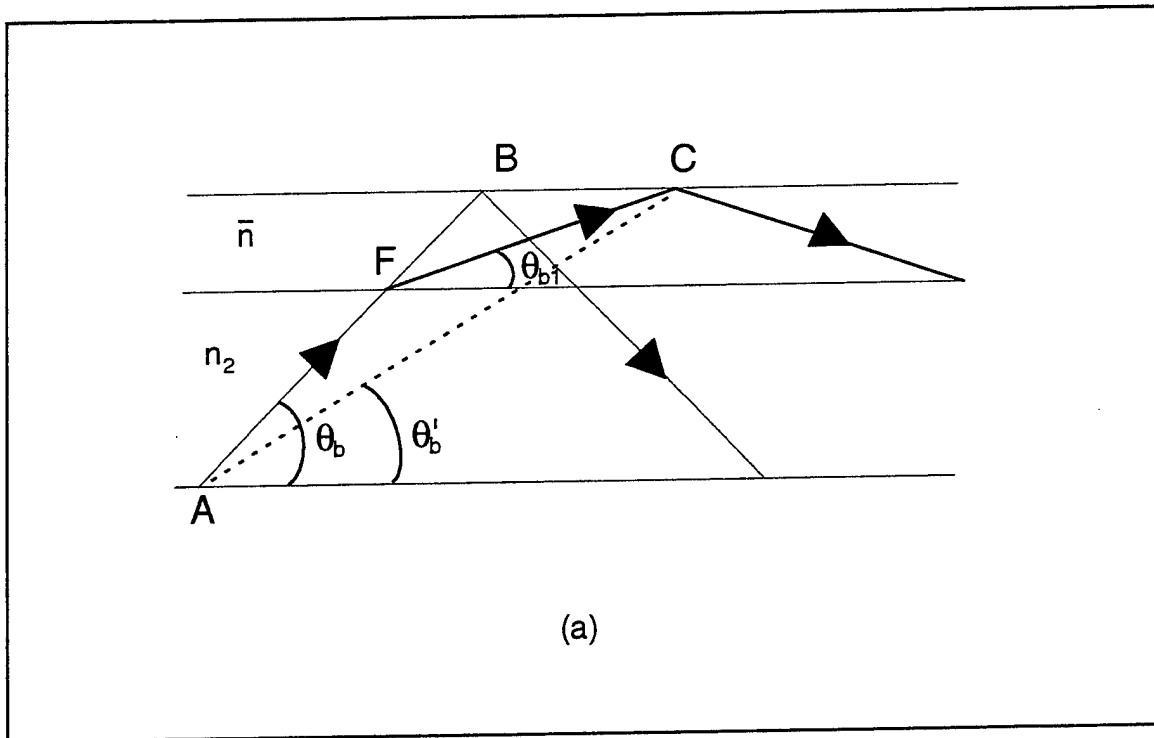


Fig. 8a, 8b Schematic of total internal reflection for a composite waveguide and wave vector.

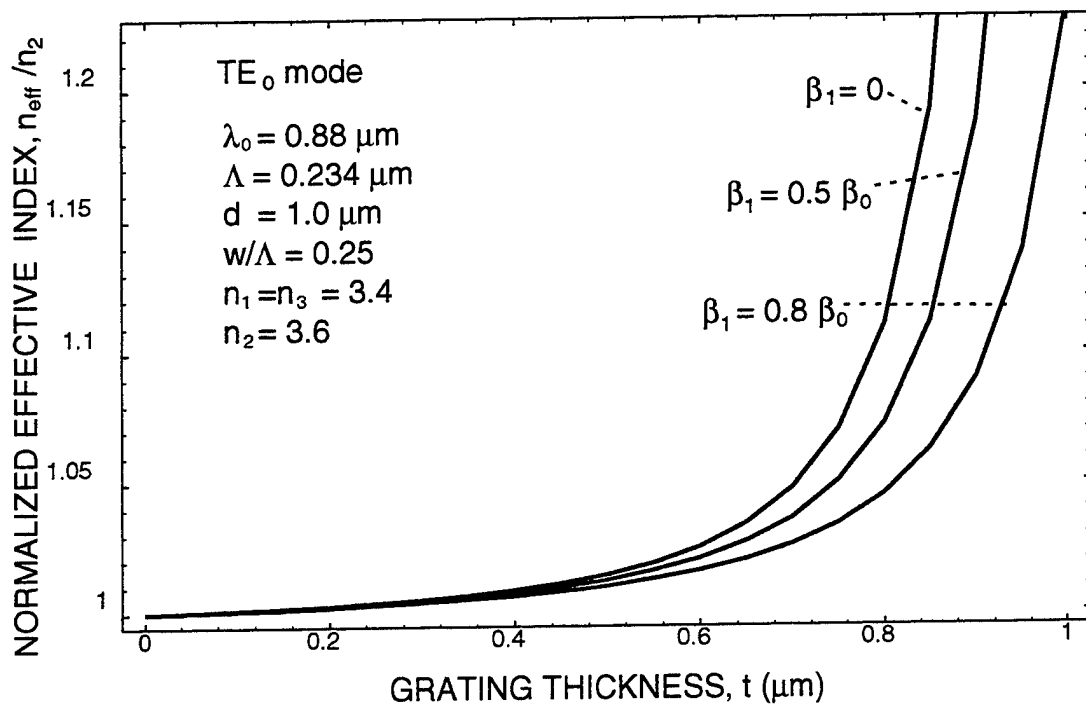


Fig. 9 Normalized effective index (with respect to  $n_2$ ) versus grating thickness with  $\beta_1$  as parameter.

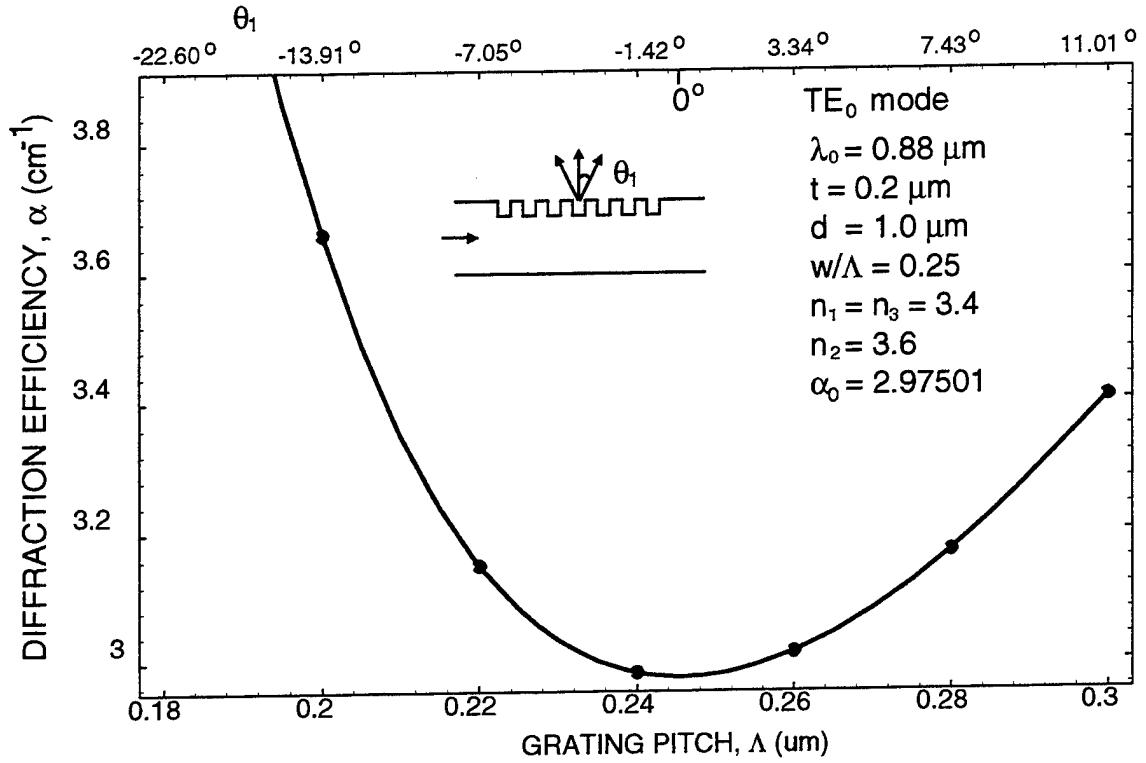


Fig. 10a Diffraction efficiency versus grating pitch for approximate second-order rectangular grating. Discrete points are solutions obtained with  $\alpha_0$  to represent  $\alpha$  in  $i \beta_1 d E_1 / dz (= i \beta_1 \alpha E_1)$  in (47).



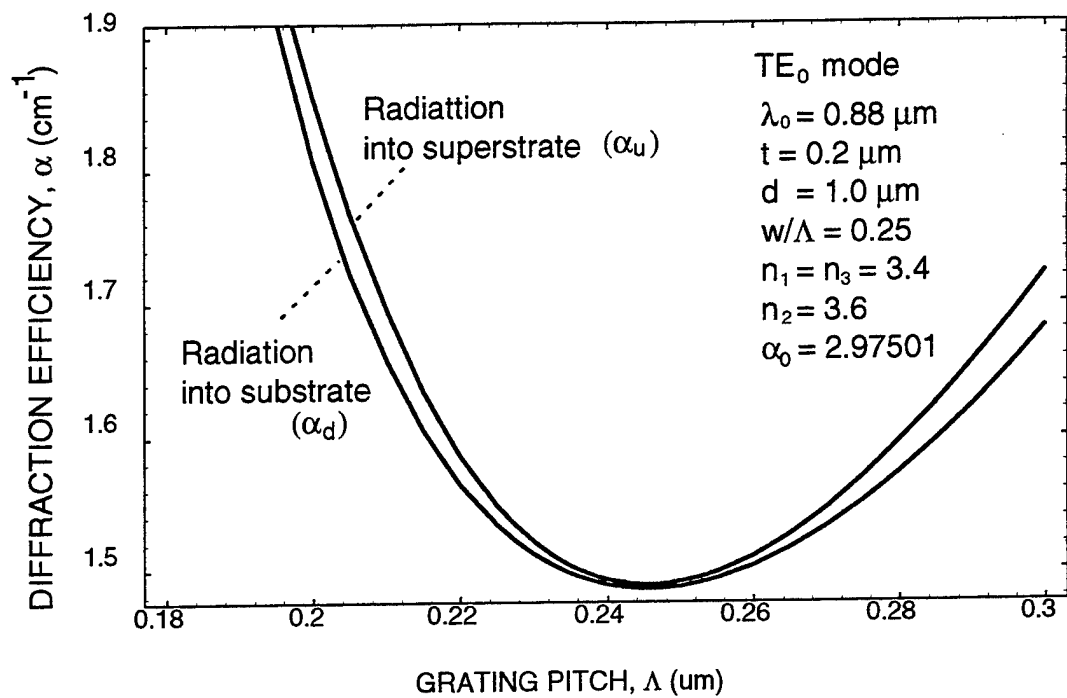


Fig. 10b Diffraction efficiency in the upward and downward directions versus grating pitch for the approximate second-order rectangular grating.

**Appendix B. Diffraction Into Corrugated Waveguide From Normally Incident Radiation**

# Diffraction Into a Corrugated Waveguide From Normally Incident Radiation

G. W. Taylor and C. Kwan

Electrical and Systems Engineering

University of Connecticut

Storrs, CT 06269

## **Abstract**

The diffraction of a plane wave normally incident upon a corrugated waveguide with a second order grating pitch is examined. Using a rectangular grating the efficiency of diffraction into the first order components in the form of guided waves is determined. Using simple approximations, closed form expressions are found from which the dependence of efficiency upon grating thickness, waveguide thickness, grating pitch and indices are predicted. The approach provides a useful simulation tool to predict the efficiency of coupling into a waveguide from an external or internal orthogonal source.

# I Introduction

Coupling into or out of a waveguide by the use of a grating has been studied by many researchers [1][2][3][4] as a simple method to transfer free space signals to waveguides in optical integrated circuits. In most cases [2][4] the input light is propagated at an angle to the guide to optimize the coupling since the tangential input component is launched more easily into the guide. However propagation normal to the guide is also important as a means to couple from a vertically emitting structure into a waveguide. With the emergence of the vertical cavity laser as a preferred embodiment to an integrated light source, the use of a normally incident diffraction grating becomes an interesting mechanism to create an optical source with high right angle mode output power[5][?]. Another new important application for diffraction from normally incident light to laterally propagating light is the detection of infrared light using intersubband transition[6]. It is therefore of considerable interest to develop predictions of the efficiency of the diffraction process in terms of the waveguide and grating parameters. The existing mathematical descriptions [1][3][4][7], which in general describe off normal incidence situations, are numerical, while our objective here is to obtain an analytical prediction.

Previously [8] we have reported an approach for describing diffraction from the guide into the superstrate or the substrate which enables a closed form solution. The same techniques will be applied here to characterize the diffraction in the reverse direction. For this derivation a symmetrical grating will be assumed.

## II Diffraction into guide

In the previous paper [8] Streifer's method [1] was used to describe the problem of ideal second order diffraction of a guided wave into a wave radiating at right angles to the guide. Here we adapt the same approach to the diffraction of a wave normally incident upon a corrugated guide, into a guided mode as illustrated in Fig. 1. The slab waveguide is corrugated to a thickness  $t$ , an arbitrary point in the corrugation is chosen for the origin of the  $z$  axis, the  $x$  axis origin is chosen at the top of the corrugation and  $x$  increases positively downwards. As previously, the periodic variation of the index within the grating is represented by the Fourier series

$$n_g^2(x, z) = \bar{n}^2(x) + \sum_{q=-\infty \text{ \& } q \neq 0}^{\infty} B_q(x) e^{i2\pi qz/\Lambda} \quad (1)$$

where  $\bar{n}$  is the average index over one grating period,  $B_q$  are the Fourier coefficients, and  $\Lambda$  is the grating period as illustrated in Fig. 1. For the rectangular grating, which is our main interest here, these coefficients have been evaluated as (see Streifer [1])

$$B_q = \begin{cases} -\frac{(n_2^2 - n_1^2)}{\pi q} \sin\left(\frac{\pi q w}{\Lambda}\right) & 0 < x < t \\ 0 & x < 0, \quad t < x, \quad q \neq 0 \end{cases} \quad (2)$$

where  $w$  is the grating tooth width (see Fig. 1). By restricting the discussion to include only the first and second diffraction orders, the index in the grating region corresponding to (1) is

$$n_g^2(x, z, q) = \bar{n}^2 - \frac{(n_2^2 - n_1^2)}{q\pi} \sin\left(\frac{\pi q w}{\Lambda}\right) e^{\frac{i2\pi q}{\Lambda} z}, \quad q = \pm 1 \quad (3)$$

where the average  $\bar{n}$  is given by

$$\bar{n}^2 = \{wn_1^2 + (\Lambda - w)n_2^2\}/\Lambda, \quad 0 < x < t \quad (4)$$

Overall, the index variation is summarized by region as

$$n^2(x, z) = \begin{cases} n_1^2 & x < 0 \\ n_g^2(x, z) & 0 < x < t \\ n_2^2 & t < x < d \\ n_3^2 & d < x \end{cases} \quad (5)$$

### III Second order grating calculation

Because we are restricting our discussion to the case of second order diffraction, then it was shown [8][9] that the problem is simplified because we need to consider only the first and second order diffracted waves. In Fig. 1 the normally incident radiation ( $\theta = 0$ ) corresponds to ideal second order diffraction and other waves for  $\theta \neq 0$ , represent approximate second order diffraction. By representing the total E field as the sum of the diffracted waves in the forward, the reverse and the surface normal directions and substituting into the two dimensional wave equation, it was shown that the diffraction is represented by three differential equations (D.E.'s) which are

$$\frac{\partial^2 E_0}{\partial x^2} - \beta_0^2 E_0 + k_0^2 \bar{n}^2 E_0 + 2i\beta_0 \frac{\partial E_0}{\partial z} + k_0^2 (\tilde{B}_1 E_1 + \tilde{B}_2 E_2) = 0, \quad m = 0 \quad (6)$$

$$\frac{\partial^2 E_1}{\partial x^2} - \beta_1^2 E_1 + k_0^2 \bar{n}^2 E_1 + 2i\beta_1 \frac{\partial E_1}{\partial z} + k_0^2 (\tilde{B}_{-1} E_0 + \tilde{B}_1 E_2) = 0, \quad m = 1 \quad (7)$$

$$\frac{\partial^2 E_2}{\partial x^2} - \beta_2^2 E_2 + k_0^2 \bar{n}^2 E_2 + 2i\beta_2 \frac{\partial E_2}{\partial z} + k_0^2 (\tilde{B}_{-1} E_1 + \tilde{B}_{-2} E_0) = 0, \quad m = 2 \quad (8)$$

It is noted that the coefficients  $q = -1$  and  $+1$  in (2) determine the coefficients for the waves with  $m = 0$  and  $2$  (i.e. waves  $E_0$  and  $E_2$ ) respectively. These will be represented by  $\tilde{B}_{-1} = \tilde{B}_1 \equiv \tilde{B} = -\frac{(n_2^2 - n_1^2)}{\pi} \sin(\frac{\pi w}{\Lambda})$ .

These three diffracted waves are indicated in Fig. 1 and the variation of the  $E_0$  and  $E_2$  components in the  $z$  direction is indicated. These components are the first order diffracted waves and are growing in the  $+z$  and  $-z$  directions respectively

due to diffraction into the guide from the normally incident wave. It is interesting to note however (and specified later) that second order diffraction is required to produce  $E_0$  and  $E_2$ , i.e. they would not exist with surface normal radiation for a first order diffraction grating.

The generalised Bragg condition which relates the propagation constants of the various diffraction orders  $m$  is  $\beta_m = \beta_0 - \frac{2\pi m}{\Lambda}$ . For the ideal second order case of  $\beta_1 = 0$ , it was shown that

$$\beta_0 = -\beta_2 \quad (9)$$

and since  $m = 1$  for this case, then we have  $\beta_0 = \frac{2\pi}{\Lambda}$ . Then the  $E_1$  D.E. (c.f.(7)) becomes

$$\frac{\partial^2 E_1}{\partial x^2} + k_0^2 \tilde{n}^2 E_1 + k_0^2 \tilde{B} (E_0 + E_2) = 0 \quad (10)$$

and we also note that for the symmetrical grating, we have  $E_0 = E_2$  (the case of asymmetry will be considered elsewhere). The  $E_1$  wave exists in the grating region and results from the wave  $C_0 e^{-ik_1 x}$  incident on the waveguide. Due to multiple reflections at the interfaces 0,  $t$  and  $d$ , there will be several other normally propagating waves within the structure which are shown in Fig. 1.

In regard to the waves  $E_0$  and  $E_2$ , we utilize the model of the previous paper for diffraction out of the guide. Thus  $E_0$  and  $E_2$  are assumed to be guided waves traveling in the  $\pm z$  directions in the guide and represented by

$$E_0 = A_0(x) e^{\alpha z} e^{-i\beta_0 z}, \quad E_2 = A_0(x) e^{-\alpha z} e^{i\beta_0 z} \quad (11)$$

where  $\beta_0$  is the propagation constant of the waveguide and  $\alpha$  is the growth constant of the wave. These waves are assumed to consist of  $TE$  modes in the guide with  $A_0(x)$  determined by

$$A_0(x) = \begin{cases} A_y e^{\delta x} & x \leq 0 \\ A_y \cos \kappa x + B_y \sin \kappa x & 0 \leq x \leq d \\ (A_y \cos \kappa d + B_y \sin \kappa d) e^{-\gamma(x-d)} & d \leq x \end{cases} \quad (12a)$$

where

$$\begin{aligned}
A_y & \text{ is the value of } A_0(0), \\
\kappa & = n_2 k_0 \sin \theta_b, \\
\delta & = \left[ (n_2^2 - n_1^2) k_0^2 - n_2^2 k_0^2 \sin^2 \theta_b \right]^{1/2}, \\
\gamma & = \left[ (n_2^2 - n_3^2) k_0^2 - n_2^2 k_0^2 \sin^2 \theta_b \right]^{1/2},
\end{aligned} \tag{12b}$$

and  $\theta_b$  is the bounce angle. As mentioned earlier these waves are assumed to grow in the  $\pm z$  directions due to the diffracted energy from the input wave and  $\alpha$ , the rate of growth will be determined from the solutions. The presence of the  $E_0$  and  $E_2$  waves represent an energy loss mechanism for the wave  $E_1$  in the grating region and (11) provides a representation for the perturbation terms in (10). Solving (10) using (11) with  $E_0, E_2 = 0$  to find the complementary solution, using (12a, b) to find a particular solution and then combining the two, a general solution (see Appendix A) is found to be

$$E_{gx}(x, z) = C_2 e^{ik_g x} + C_3 e^{-ik_g x} + b(\cos \kappa x + \frac{\delta}{\kappa} \sin \kappa x) \tag{13}$$

where

$$b(z) = \frac{2k_0^2}{\kappa^2 - k_g^2} \tilde{B} A_y e^{+\alpha z} \tag{14}$$

This solution introduces a factor of 2 in (10) because  $E_0 = E_2$  for the symmetrical situation. It is noted in this case that the presence of  $E_0$  and  $E_2$  in (10) represents a small loss term in the general  $E_1$  equation rather than a driving force in the out of the guide case, and it is therefore expected that  $E_0, E_2 \ll E_1$ . Thus  $E_1$  exists even if  $E_0, E_2 = 0$ . But for the  $E_0$  and  $E_2$  equations (6) and (7), the perturbation term  $E_1$  is a driving force and the waves  $E_0$  and  $E_2$  would not exist without it. It noted that both  $A_y$  and  $\alpha$  have been introduced as unknowns which depend on the input wave  $C_0$ .

It is noted that  $E_{gx}(x, z)$  represents the  $E_1$  wave solution in the grating region. In the work that follows we continue to use  $E_{gc}$  for the  $x$  directed wave in the grating and use  $E_{1x}, E_{2x}$ , and  $E_{gx}$  for the  $x$  directed waves in the other parts of

the guide which represent collectively the  $E_1$  wave. They are described by region as shown in Fig. 1 and in total the waves may then be written

$$E_{1x}(x, z) = C_0 e^{-ik_1 x} + C_1 e^{ik_1 x}, \quad k_1 = (k_0^2 n_1^2 - \beta_1^2)^{1/2} = k_0 n_1 \quad (15)$$

$$E_{gx}(x, z) = C_2 e^{ik_g x} + C_3 e^{-ik_g x} + E_{gp}, \quad k_g = (k_0^2 \bar{n}^2 - \beta_1^2)^{1/2} = k_0 \bar{n} \quad (16)$$

$$E_{2x}(x, z) = C_4 e^{ik_2(d-x)} + C_5 e^{-ik_2(d-x)}, \quad k_2 = (k_0^2 n_2^2 - \beta_1^2)^{1/2} = k_0 n_2 \quad (17)$$

$$E_{3x}(x, z) = C_6 e^{-ik_3(x-d)}, \quad k_3 = (k_0^2 n_3^2 - \beta_1^2)^{1/2} = k_0 n_3 \quad (18)$$

in which  $E_{gp}$  is the grating dependent contribution as described by (13) and  $\beta_1 = 0$  as given by (9).

We then perform the matching of these equations in both magnitude and derivative (continuity of  $H_z$ ) at the interfaces  $x = 0, x = t$  and  $x = d$ . In line with the previous derivations, the matching produces the equations

$$C_0 + C_1 = C_2 + C_3 + b, \quad x = 0 \quad (19)$$

$$-ik_1 C_0 + ik_1 C_1 = ik_g C_2 - ik_g C_3 + \delta \cdot b, \quad x = 0 \quad (20)$$

$$C_2 e^{ik_g t} + C_3 e^{-ik_g t} + b(\cos \kappa t + \frac{\delta}{\kappa} \sin \kappa t) = C_4 e^{ik_2(d-t)} + C_5 e^{-ik_2(d-t)}, \quad x = t \quad (21)$$

$$ik_g(C_2 e^{ik_g t} - C_3 e^{-ik_g t}) - b(\kappa \sin \kappa t - \delta \cos \kappa t) = -ik_2(C_4 e^{ik_2(d-t)} - C_5 e^{-ik_2(d-t)}), \quad x = t \quad (22)$$

$$C_4 + C_5 = C_6, \quad x = d \quad (23)$$

$$-ik_2 C_4 + ik_2 C_5 = -ik_3 C_6, \quad x = d \quad (24)$$

When these equations are solved we obtain the following results for  $C_1, C_2, C_3, C_6$ ,

$$\begin{aligned} C_1 &= -\frac{(1 - \frac{k_1}{k_g})a_1 + (1 + \frac{k_1}{k_g})a_2}{(1 + \frac{k_1}{k_g})a_1 + (1 - \frac{k_1}{k_g})a_2} C_0 + \frac{(1 - \frac{\delta}{ik_g})a_1 + (1 + \frac{\delta}{ik_g})a_2 + a_3}{(1 + \frac{k_1}{k_g})a_1 + (1 - \frac{k_1}{k_g})a_2} b \\ &\equiv r_1 C_0 + r_2 b, \end{aligned} \quad (25)$$

$$\begin{aligned} C_2 &= \frac{1}{2}[(1 - \frac{k_1}{k_g}) + (1 + \frac{k_1}{k_g})r_1] C_0 + \frac{1}{2}[(1 + \frac{k_1}{k_g})r_2 - (1 + \frac{\delta}{ik_g})] b \\ &\equiv r_3 C_0 + r_4 b \end{aligned} \quad (26)$$



$$C_3 = \frac{1}{2}[(1 + \frac{k_1}{k_g}) + (1 - \frac{k_1}{k_g})r_1]C_0 + \frac{1}{2}[(1 - \frac{k_1}{k_g})r_2 - (1 - \frac{\delta}{ik_g})]b \quad (27)$$

$$\equiv r_5C_0 + r_6b$$

$$C_6 = (r_3 \cdot e^{i[-k_2(d-t)+k_g t]} + r_5 \cdot e^{i[k_2(d-t)+k_g t]})C_0 + \quad (28)$$

$$\{ \frac{r_4}{2}(1 - \frac{k_g}{k_2})e^{i[-k_2(d-t)+k_g t]} + \frac{r_6}{2}(1 + \frac{k_g}{k_2})e^{i[k_2(d-t)+k_g t]} +$$

$$(\cos \kappa t + \frac{\delta}{\kappa} \sin \kappa t) \cosh[k_2(d-t)] - \frac{1}{k_2}(\kappa \sin \kappa t - \delta \cos \kappa t) \sinh[k_2(d-t)] \} b$$

$$\equiv r_7C_0 + r_8b$$

where the following functions have been defined

$$a_1 = [(1 + \frac{k_g}{k_2})\bar{x} - (1 - \frac{k_g}{k_2})e^{-2ik_2(d-t)}]e^{ik_g t} \quad (29)$$

$$a_2 = [(1 - \frac{k_g}{k_2})\bar{x} - (1 + \frac{k_g}{k_2})e^{-2ik_2(d-t)}]e^{-ik_g t} \quad (30)$$

$$a_3 = -2(\cos \kappa t + \frac{\delta}{\kappa} \sin \kappa t)(\bar{x} + e^{-2ik_2(d-t)}) + \frac{2i}{k_2}(\kappa \sin \kappa t - \delta \cos \kappa t)(-\bar{x} + e^{-2ik_2(d-t)}) \quad (31)$$

$$\bar{x} = \frac{1 + k_3/k_2}{1 - k_3/k_2} \quad (32)$$

In order to determine  $\alpha$  we apply the conservation of power, which demands that the difference between power input normal to the guide and the power output normal to the guide should equal the gradient in  $z$  of the guided wave power which is stated

$$2 \frac{d}{dz} (\frac{1}{2\eta_f} A_{0m}^2 e^{+2\alpha z} d') = \frac{1}{2\eta_1} C_0 \cdot C_0^* - \frac{1}{2\eta_1} C_1 \cdot C_1^* - \frac{1}{2\eta_3} C_6 \cdot C_6^* \quad (33)$$

Here 2 in the left hand side of (33) indicates the outputs in both + x and - x directions and  $A_{0m}$  is the maximum value of field of the guided wave, given by

$$A_{0m} = A_y \sqrt{\frac{\kappa^2 + \delta^2}{2\kappa^2}} \quad (34)$$

where  $d'$  is the effective guide thickness  $d' = d + \frac{1}{\delta} + \frac{1}{\gamma}$  and  $A_y$  was defined by (12a), (12b). As in the previous work [8] we assume that the index of the propagating wave

in the corrugated waveguide is  $n_2$  which was shown to be a good approximation until the grating thickness  $t$  becomes a substantial fraction of the guide thickness  $d$ .

To proceed further with the solution we need to express  $A_{0m}$  (or equivalently  $b$  as per (14)) as terms proportional to  $C_0$ , the input. Then all terms in  $b$  on both sides of (33), (i.e. in  $A_{0m}$ ,  $C_1$  and  $C_6$ ) can be cancelled out. This can be accomplished by solving (6), the D.E. for  $E_0$  corresponding to (11) and using the solution (13) with  $C_2$  and  $C_3$  given by (26) and (27) to represent  $E_1$  in the region of the grating. After matching this solution at all boundaries, the relation  $E_0(0) = A_y$  can be used to determine  $b$  in terms of  $C_0$ . This procedure will be implemented shortly.

However, in order to determine  $\alpha$  alone this procedure is not initially required if we note that in the absence of the grating, we would have  $b = 0$  and then (33) reduces to

$$\frac{1}{2\eta_1}C_0 \cdot C_0^* = \frac{1}{2\eta_1}C_1 \cdot C_1^* + \frac{1}{2\eta_3}C_6 \cdot C_6^* \quad (35)$$

It is therefore evident by inspection of (33) and (35), that only the terms in  $b$  on the right side of (25), (28) are required and so using (14), (25) and (28) in (33) we obtain

$$\frac{1}{\eta_2} \left( \frac{\kappa^2 + \delta^2}{2\kappa^2} \right) \left( \frac{\kappa^2 - k_g^2}{k_0^2 \tilde{B}} \right) \alpha d' = \frac{1}{\eta_1} r_2 \cdot r_2^* + \frac{1}{\eta_3} r_8 \cdot r_8^* \quad (36)$$

where  $r_2$  and  $r_8$  are defined by (25) and (28). It is noted in performing the complex conjugations to obtain (36) from (35) and (33), the terms in  $C_0$  and  $b$  in (25) and (28) represent waves travelling in orthogonal directions and therefore cross products are not required. The solution for the wave growth constant  $\alpha$  is obtained from (36) as

$$\alpha = \left( \frac{2\kappa^2}{\kappa^2 + \delta^2} \right) \left( \frac{k_0^2 \tilde{B}}{\kappa^2 - k_g^2} \right)^2 \frac{1}{d'} \left[ \frac{\eta_2}{\eta_1} r_2 \cdot r_2^* + \frac{\eta_2}{\eta_3} r_8 \cdot r_8^* \right] \quad (37)$$

Performing the complex conjugations a positive real value for  $\alpha$  is obtained and is expressed in terms of the constants  $A \rightarrow H$  where

$$\frac{A + iB}{C + iD} = r_2, \frac{E + iF}{G + iH} = r_8 \quad (38)$$

The expressions for  $A, B, C, D, E, F, G, H$  are determined in the Appendix B.

Comparison of the solution of  $A \rightarrow H$  with the solutions for diffraction out of the guide [8] reveals that the result obtained for  $\alpha$  is identical for the two cases. This may also be seen by inspection of (19) (24) since, if  $C_0$  is reduced to 0, this set becomes identical to that for diffraction out of the guide. In some sense, this result is expected as the natural reversibility of light propagating through a passive system since the decay in one direction becomes the growth in the opposite direction of propagation. However, this reversibility does not apply to the efficiency as described below.

In the previous derivation of diffraction out of the guide, the decay constant of the input wave times the effective guide width was the diffraction efficiency. For diffraction into the guide, this is no longer true due to the significant transmission through the guide. Furthermore, since the input normal to the guide is constant with position and yet the wave diffracted into the guide is growing with distance then the overall efficiency would appear to increase with increasing  $z$ . This is erroneous of course because the mode growing in the guide would also diffract back out of the guide to a radiating wave. Therefore to determine the efficiency of diffraction into the guide as an independent mechanism on a per unit length basis at an arbitrary position one should consider  $z = 0$ , since by definition this result could not be affected by any diffracted waves for  $z \leq 0$ .

$$\eta = \frac{\delta P_{TW}}{\delta P_{in}} \quad (39)$$

where  $\delta P_{TW}$  is the TW power generated in an increment  $dz$  and  $\delta P_{in}$  is the power incident in the corrugation in an increment  $dz$ . From the power components in (33), this is determined as

$$\eta = 2\alpha d' \frac{\eta_1}{\eta_2} \frac{A_y A_y^*}{C_0 C_0^*} \quad (40)$$

A expression similar to (40) can also been found in another publication[10].

An issue of importance is how to use the two independent results of diffraction into the guide and diffraction out of the guide in a practical application such as determining the length of guide. In general one must write a differential equation incorporating both effects separately in addition to other losses or sources in the guide. In the absence of these, the two results can be readily combined to find a length dependent efficiency  $\eta(L)$ .

To determine  $\eta$  we require  $A_y$  and this means a solution of (6) is required in all regions of the guide. We therefore write the equations for the top cladding and the grating as

$$E_{01} = D_1 e^{ik'_1 x}, \quad k'_1 = (k_0^2 n_1^2 - \beta_0^2)^{1/2} \quad (41)$$

and

$$E_{0g}(x, z) = D_2 e^{ik'_g x} + D_3 e^{-ik'_g x} + \frac{k_0^2 \tilde{B} C_2 e^{ik_g x}}{k_g^2 - k_g'^2} + \frac{k_0^2 \tilde{B} C_3 e^{-ik_g x}}{k_g^2 - k_g'^2} \quad (42)$$

Noting that the constants can be rewritten as

$$\beta_0^2 = k_0^2 n_2^2 \cos^2 \theta_b, \quad k_g'^2 = k_0^2 \bar{n}^2 - \beta_0^2 + 2i\alpha\beta_0, \quad k_g^2 - k_g'^2 \cong \beta_0^2$$

and if we ignore the term  $2i\alpha\beta_0$  since  $\alpha \ll \beta_0$  then (42) becomes

$$E_{0g}(x, z) = D_2 e^{ik'_g x} + D_3 e^{-ik'_g x} + B'(C_2 e^{ik_g x} + C_3 e^{-ik_g x}) \quad (43)$$

where  $B' = \frac{\tilde{B}}{n_2^2 \cos^2 \theta_b}$ . For the waveguide core and lower cladding, the equations are

$$E_{02}(x, z) = D_4 e^{ik'_2(d-x)} + D_5 e^{-ik'_2(d-x)}, \quad k'_2 = (k_0^2 n_2^2 - \beta_0^2)^{1/2} \quad (44)$$

$$E_{03}(x, z) = D_6 e^{-ik'_3(x-d)}, \quad k'_3 = (k_0^2 n_3^2 - \beta_0^2)^{1/2} \quad (45)$$

Equations (41)-(45) are matched at each interface in both magnitude and derivation as implemented for the  $E_1$  wave. Then it is possible to express  $D_1$  in terms of  $C_2$  and  $C_3$

$$D_1 = \frac{y_1 \cdot C_2 + y_2 \cdot C_3}{y_0} \quad (46)$$

where

$$y_0 = \frac{1}{2}(1 + \frac{k'_1}{k'_g})(1 + \frac{k'_g}{k'_1})x'e^{i2k'_2(d-t)+ik'_g t} + \frac{1}{2}(1 - \frac{k'_1}{k'_g})(1 - \frac{k'_g}{k'_1})x'e^{i2k'_2(d-t)-ik'_g t} \quad (47)$$

$$- \frac{1}{2}(1 + \frac{k'_1}{k'_g})(1 - \frac{k'_g}{k'_2})e^{ik'_g t} - \frac{1}{2}(1 - \frac{k'_1}{k'_g})(1 + \frac{k'_g}{k'_2})e^{-ik'_g t}$$

$$y_1 = B'\{(1 - \frac{k_g}{k'_2})e^{ik_g t} - (1 + \frac{k_g}{k'_2})e^{ik_g t}x'e^{i2k'_2(d-t)} \quad (48)$$

$$+ \frac{1}{2}(1 + \frac{k_g}{k'_g})e^{ik'_g t}[(1 + \frac{k'_g}{k'_2})x'e^{ik'_2(d-t)} - (1 - \frac{k'_g}{k'_2})]$$

$$+ \frac{1}{2}(1 - \frac{k_g}{k'_g})e^{-ik'_g t}[(1 - \frac{k'_g}{k'_2})x'e^{ik'_2(d-t)} - (1 + \frac{k'_g}{k'_2})]\}$$

$$y_2 = B'\{(1 + \frac{k_g}{k'_2})e^{-ik_g t} - (1 - \frac{k_g}{k'_2})e^{-ik_g t}x'e^{i2k'_2(d-t)} \quad (49)$$

$$+ \frac{1}{2}(1 - \frac{k_g}{k'_g})e^{ik'_g t}[(1 + \frac{k'_g}{k'_2})x'e^{ik'_2(d-t)} - (1 - \frac{k'_g}{k'_2})]$$

$$+ \frac{1}{2}(1 + \frac{k_g}{k'_g})e^{-ik'_g t}[(1 - \frac{k'_g}{k'_2})x'e^{ik'_2(d-t)} - (1 + \frac{k'_g}{k'_2})]\}$$

$$b' = \frac{2k_0^2 \tilde{B}}{(k_g^2 - k_g'^2)}, \quad x' = \frac{1 + k'_3/k'_2}{1 - k'_3/k'_2} \quad (50)$$

From the solutions of the  $E_1$  equation, as described by (25) through (28), we have determined that  $C_2$  and  $C_3$  are functions of the input  $C_0$  and the perturbation term  $b$ , (c.f. (14)) so (46) is expressed

$$D_1 = (\frac{y_1 \cdot r_3 + y_2 \cdot r_5}{y_0})C_0 + (\frac{y_1 \cdot r_4 + y_2 \cdot r_6}{y_0})b \quad (51)$$

We now make the observation that since  $D_1$  is the value of  $E_0(x, z)$  at  $x = 0$  and since we are representing the total wave propagating in the waveguide by (11), then we have

$$D_1 = A_y \quad (52)$$

However, we already have expressed  $b$  in terms of  $A_y$  and  $\alpha$  through (14) and since  $\alpha$  has been found independently by (37) then we may substitute these results into (51) and (52) to determine an expression for  $A_y$  in terms of the input  $C_0$  as

$$A_y = \frac{(y_1 \cdot r_3 + y_3 \cdot r_5)C_0}{y_0 - (y_1 \cdot r_4 + y_3 \cdot r_6) \frac{k_0^2 \tilde{B}}{(\kappa^2 - k_g^2)} e^{\alpha z}} \quad (53)$$

Note that if we ignore the  $b$  terms in (26) and (27) since these will be much smaller than the input wave, then we obtain

$$A_y = \frac{(y_1 \cdot r_3 + y_2 \cdot r_5)}{y_0} C_0 \quad (54)$$

Then the efficiency is found from (31) and (45) as

$$\eta = 2\alpha d' \frac{\eta_1}{\eta_2} \frac{A_y A_y^*}{C_0 C_0^*} = 2\alpha d' \frac{\eta_1}{\eta_2} \frac{(y_1 \cdot r_3 + y_2 \cdot r_5)(y_1 \cdot r_3 + y_2 \cdot r_5)^*}{y_0 y_0^*} \quad (55)$$

## IV Illustration of Results and Interpretation

First we plot the variation of both  $\alpha$  and  $\eta$  as a function of thickness  $t$  for a given thickness  $d$  for both small and large index variation in Fig. 2a, 2b and 2c respectively. For all these plots  $\alpha$  gives the growth of the field (the growth of the power would be  $2\alpha$ ). It is noted that the efficiency and the diffraction do not track each other as was the case for diffraction out of the guide [8]. This results from the matching procedure and the presence of standing waves in the structure. The result for  $\eta$  shows twice as many peaks as the result for  $\alpha$  because two matching procedures are involved. The peaks in  $\alpha$  occur for  $t = \lambda/2$  and the peaks in  $\eta$  occur for  $t = \lambda/4$ . In Fig. 2b the values of  $\eta$  increase dramatically with the increase of index change as one would expect. As the index difference increases the range of validity of the calculation decreases and in Fig. 2b it is indicated to be  $t_{cr} \simeq 0.07 \mu m$ . The determination of  $t_{cr}$  is shown in Fig. 2c where we plot the variation of the effective bounce angle.

As explained previously [8], the calculation is based upon the constancy of  $\beta_0$  the propagation constant in the waveguide both with and without the grating. When the effective bounce angle goes to zero, it implies that the loss has become so great that no effective propagation can occur. Therefore in the case of a large index change of 1.6 the grating should be etched to no more than  $0.07 \mu m$  for a  $1.0 \mu m$  guide. In Fig. 3, the efficiency is compared for the  $TE_0$  and  $TE_1$  modes for the weak grating case with a significant apparent increase for the higher order mode because of stronger grating interaction.

It is interesting to note that the energy is being diffracted into the first order wave  $E_0$  and  $E_2$  (see Fig. 1). As shown by (41)-(45) the second order wave  $E_1$  in the grating must first be excited to provide the perturbative driving force for the  $E_0$  and  $E_2$  waves and the wave  $E_1$ , being the solution of (10), is excited only by a grating with a second order pitch. This means that  $E_0$  and  $E_2$  would not be produced if the grating pitch was the first order.

In Fig. 4, the  $\eta$  and  $\alpha$  are shown as a function of the tooth width. There is a broad maximum for both parameters with the result for  $\alpha$  showing symmetry but the result for  $\eta$  showing a slight displacement to values of  $w/\Lambda < 0.5$ .

In Fig. 5,  $\eta$  and  $\alpha$  are shown versus guide thickness  $d$  and the same behavior is noted as for diffraction out of the guide. However, the efficiency shows more oscillatory behavior, which evidence of additional standing wave effects resulting from the second matching procedure for  $\eta$ .

## V Approximate Second Order Grating Pitch

For diffraction into the guide, we need to consider both the angle  $\theta$  and the grating pitch  $\Lambda$ . For any combination of parameters, the phase matching condition

$$\beta_0 - \frac{2\pi}{\Lambda} = \beta_1 \quad (56)$$

must be satisfied where  $\beta_1$  is the component of the input wave vector in the  $z$  direction, i.e.

$$\beta_1 = k_0 n_1 \sin \theta$$

Clearly, for non-zero  $\theta$ , then  $\beta \neq 0$  and if (56) is satisfied, then  $\Lambda \neq \Lambda_{s.o.}$  where  $\Lambda_{s.o.}$  is the second order value for the chosen wavelength. Stated alternately, for  $\Lambda = \Lambda_{s.o.}$ , the incident wave must be normal to the guide for a diffracted wave to build up in the guide. Also for each value of  $\Lambda$  ( $\neq \Lambda_{s.o.}$ ), there is an unique value of  $\theta$  for which diffraction into the guide will occur, which increases continuously as  $\Lambda$  is made larger or smaller than  $\Lambda_{s.o.}$ . Fig. 6 shows the situation for an oblique angle  $\theta$  and a grating pitch  $\Lambda \neq \Lambda_{s.o.}$ . Then if  $\Lambda < \Lambda_{s.o.}$  the phase matching condition (56) indicates that the diffracted wave propagates in the opposite direction to the  $z$  component of the input and if  $\Lambda > \Lambda_{s.o.}$ , the propagation is in the same direction as the  $z$  component of the input wave (symmetrical propagation in both directions can only occur for normal incidence). These comments apply to approximate second order grating pitches, and approximate solutions are found as below. For third and higher order approximate grating pitches, there will be more than one value of  $\theta$  to satisfy the phase match condition.

Therefore for diffraction into the guide we need the solution to

$$\frac{\partial^2 E_1}{\partial x^2} + (k_0^2 \bar{n}^2 - \beta_1^2) E_1 + 2i\beta_1 \frac{\partial E_1}{\partial z} + k_0^2 \tilde{B} E_0(z) = 0$$

This equation is solved as in the out-of-the-guide case in which the propagation con-



stant in the grating layer

$$k'_g = k'_{gr} + ik'_{gi}$$

and the parameter  $b$  in the particular solution (given by (14) for ideal second order)

$$b = b_r - ib_i$$

now have real and imaginary parts. However to the extent that  $\alpha_1 \ll \beta_1$  we can ignore the imaginary part so that

$$k'_g = (k_0^2 \bar{n}^2 - \beta_1^2)^{1/2}$$

$$b = \frac{k_0^2}{\kappa^2 - k_g'^2} \bar{n}^2 \tilde{B} A_y e^{\alpha z}$$

The remainder of the solution follows the calculations of (15) through (32) to produce modified values of  $C_1$ ,  $C_2$ ,  $C_3$  and  $C_6$ . These modified values are used to predict modified values of  $r_2$ ,  $r_8$  and  $\alpha$  by comparison with (37).

The calculation of the nonideal second order grating is performed in the same way, with the alteration in (41) -(45) that modified values of  $C_2$  and  $C_3$  are used. The results are shown in Fig. 6 for the weak grating case and here, for the chosen  $t = 0.2 \mu m$ ,  $\eta$  and  $\alpha$  essentially track each other.

## VI Summary

A model has been presented to describe diffraction into a waveguide from a normally incident beam. A closed form method to obtain the diffraction efficiency of the grating from the beam to the guided wave has been described that can be implemented easily on a PC Platform. The calculation shows reversible behavior in terms of the diffraction constant when compared to diffraction out of the guide. This is a result of the conservation of energy in both situations. However, the efficiencies are

dramatically different due to the significant energy passing through the guide in the present situation.

In the context of simple phase matching, there is no deviation of the input angle allowed to obtain diffraction i.e. the phase matching condition states that if the grating pitch and incident angle are not matched for a given wavelength then no diffraction into the guide would occur. This is an idealization and would not be expected experimentally because of parameter variations, specifically the refractive indices which are generally temperature and background dependent. It is noted in our discussion that the particular solution for the wave in the grating region,  $E_{gx}$ , corresponds to the calculation of the coupling coefficient in the coupled mode theory.

## References

- [1] W. Streifer, D. R. Scifres, and R. Burnham. "Analysis of grating-coupled radiation in GaAs:GaAlAs lasers and waveguides". *IEEE J. Quantum Electronics*, vol. 12, no. 7, pp. 422-428, July 1976.
- [2] K. Ogawa, W. S. C. Chang, B. L. Soporì, and Rosenbaum F. J. "A theoretical analysis of etched grating couplers for integrated optics". *IEEE Journal of Quantum Electronics*, vol. 9, No. 1, pp. 29-42, Jan. 1973.
- [3] I. I. Mokhun' and M. O. Sopin. "Geometric-optical approach to the problem of excitation of a corrugated optical waveguide at near-normal angles of incidence". *Quantum Electronics*, vol. 26, No. 9, pp. 836-838, Sep. 1996.
- [4] C. Ghizoni, B. Chen, and C. Tang. "Theory and experiments on grating couplers for thin-film waveguides". *IEEE Journal of Quantum Electronics*, Vol. 12, No. 2, pp. 69-73, Feb. 1976.
- [5] Y. and Kubota T. and Takeda M. Nakaya, T. and Katoh. "Diffraction efficiency of a grating coupler for an array illuminator ". *Applied Optics*, vol. 35, No. 20, pp. 3891-3898, Jul. 1996.
- [6] J. Y. Duboz, V. Berger, N. Laurent, D. Adam, and J. Nagle. "Grating coupled infrared modulator at normal incidence based on intersubband transitions". *Appl. Phys. Lett.*, vol. 70, No. 12, pp. 1569-1571, Mar. 1997.
- [7] H. Nishihara, M. Haruna, and T. Suhara. *Optical integrated circuits*. McGraw-Hill, 1987.
- [8] G. W. Taylor and C. Kwan. "Determination of diffraction efficiency for a second-order corrugated waveguide ". *IEEE J. Quantum Electronics*, vol. 33, No. 2, pp. 176-186, Feb. 1997.

- [9] G. W. Taylor and C. Kwan. "Correction to Determination of diffraction efficiency for a second-order corrugated waveguide". *IEEE J. Quantum Electronics*, vol. 33, No. 6, pp. 1041, Jun. 1997.
- [10] E. G. Loewen and E. Popov. *Diffraction gratings and application*. New York:M. Dekker, 1997.

## List of figures

**Fig. 1** Schematic of the incident wave producing transmitted wave, reflected wave and diffracted wave due to periodic grating.

**Fig. 2a** Diffraction efficiency  $\eta$  (dash line) and diffraction constant  $\alpha$  (solid line) versus grating thickness for a rectangular grating ( $\Delta n = 0.2$ ).

**Fig. 2b** Diffraction efficiency  $\eta$  (dash line) and diffraction constant  $\alpha$  (solid line) versus grating thickness for a rectangular grating ( $\Delta n = 1.6$ ). In the shaded region  $t > t_{cr}$  and the calculation is not valid.

**Fig. 2c** Diffraction efficiency versus grating thickness for a rectangular grating. Solid line present  $TE_0$  mode and dash line is  $TE_1$  mode.

**Fig. 3** Effective bounce angle  $\theta_{eff}$  and effective waveguide index  $n_{eff}$  versus normalized grating depth,  $t/d$ .

**Fig. 4** Diffraction constant and diffraction efficiency versus tooth width for a rectangular grating. Solid line represents diffraction constant  $\alpha$  and dash line is diffraction efficiency  $\eta$ .

**Fig. 5** Diffraction constant and diffraction efficiency versus waveguide thickness for a rectangular grating. Solid line is diffraction constant  $\alpha$  and dash line is diffraction efficiency  $\eta$ .

**Fig. 6** Diffraction constant and diffraction efficiency versus grating pitch for the approximate second-order rectangular grating. Solid line is diffraction constant  $\alpha$  and dash line is diffraction efficiency  $\eta$ .

## Appendix A

### Particular Solution of Wave Equation

The  $x$  dependent differential wave equation in the grating is obtained from (12) and (13) as

$$\frac{\partial^2 E_g}{\partial x^2} + k_g^2 E_g = -k_0^2 \tilde{B} A_0(x) e^{-\alpha z} \quad (\text{A1})$$

The complementary solution (RHS=0) is

$$E_{gc}(x) = C_2 e^{ik_g x} + C_3 e^{-ik_g x} \quad (\text{A2})$$

the particular solution is

$$\begin{aligned} E_{gp} &= k_0^2 \tilde{B} e^{ik_g x} \int \frac{A_0(x) e^{-\alpha z} e^{-ik_g x}}{-2ik_g} dx - k_0^2 \tilde{B} e^{-ik_g x} \int \frac{A_0(x) e^{-\alpha z} e^{ik_g x}}{-2ik_g} dx \\ &= \left( \frac{k_0^2}{\kappa^2 - k_g^2} \right) \tilde{B} A_y e^{-\alpha z} \left( \cos \kappa x + \frac{\delta}{\kappa} \sin \kappa x \right) \end{aligned} \quad (\text{A3})$$

where  $-2ik_g$  is the Wronskian and  $A_0(x)$  in (7) has been used for the grating region to represent TE modes. Then the total solution is

$$E_{gc}(x) = C_2 e^{ik_g x} + C_3 e^{-ik_g x} + \frac{k_0^2}{\kappa^2 - k_g^2} \tilde{B} A_y e^{-\alpha z} \left( \cos \kappa x + \frac{\delta}{\kappa} \sin \kappa x \right) \quad (\text{A4})$$

## Appendix B

Solution of the linear equations (15)-(24) for the ideal second order diffraction condition yield the following results for the parameters  $A, B, C, D$ .

$$\begin{aligned}
 A = & \cos(k_g t) + \frac{\delta}{k_g} \sin(k_g t) - [\cos(\kappa t) + \frac{\delta}{\kappa} \sin(\kappa t)] \\
 & - \frac{1}{2} \left( \frac{k_2 + k_3}{k_2 - k_3} \right) \left( 1 + \frac{k_g}{k_2} \right) \{ \cos[2k_2(d - t) + k_g t] + \frac{\delta}{k_g} \sin[2k_2(d - t) + k_g t] \} \\
 & - \frac{1}{2} \left( \frac{k_2 + k_3}{k_2 - k_3} \right) \left( 1 - \frac{k_g}{k_2} \right) \{ \cos[2k_2(d - t) - k_g t] - \frac{\delta}{k_g} \sin[2k_2(d - t) - k_g t] \} \\
 & + (\cos \kappa t + \frac{\delta}{\kappa} \sin \kappa t) \left( \frac{k_2 + k_3}{k_2 - k_3} \right) \cos[2k_2(d - t)] \\
 & + \left( \frac{\delta}{k_2} \cos \kappa t - \frac{\kappa}{k_2} \sin \kappa t \right) \left( \frac{k_2 + k_3}{k_2 - k_3} \right) \sin[2k_2(d - t)]
 \end{aligned}$$

$$\begin{aligned}
 B = & -\frac{k_g}{k_2} \sin(k_g t) + \frac{\delta}{k_g} \cos(k_g t) - \left[ \frac{\delta}{k_2} \cos(\kappa t) - \frac{\kappa}{k_2} \sin(\kappa t) \right] \\
 & - \frac{1}{2} \left( \frac{k_2 + k_3}{k_2 - k_3} \right) \left( 1 + \frac{k_g}{k_2} \right) \{ \sin[2k_2(d - t) + k_g t] - \frac{\delta}{k_g} \cos[2k_2(d - t) + k_g t] \} \\
 & - \frac{1}{2} \left( \frac{k_2 + k_3}{k_2 - k_3} \right) \left( 1 - \frac{k_g}{k_2} \right) \{ \sin[2k_2(d - t) - k_g t] + \frac{\delta}{k_g} \cos[2k_2(d - t) - k_g t] \} \\
 & + (\cos \kappa t + \frac{\delta}{\kappa} \sin \kappa t) \left( \frac{k_2 + k_3}{k_2 - k_3} \right) \sin[2k_2(d - t)] \\
 & - \left( \frac{\delta}{k_2} \cos \kappa t - \frac{\kappa}{k_2} \sin \kappa t \right) \left( \frac{k_2 + k_3}{k_2 - k_3} \right) \cos[2k_2(d - t)]
 \end{aligned}$$

$$\begin{aligned}
 C = & 2 \left( 1 - \frac{k_1}{k_2} \right) \cos(k_g t) - \left( 1 + \frac{k_1}{k_g} \right) \left( 1 + \frac{k_g}{k_2} \right) \left( \frac{k_2 + k_3}{k_2 - k_3} \right) \cos[k_g t + 2k_2(d - t)] \\
 & - \left( 1 - \frac{k_1}{k_g} \right) \left( 1 - \frac{k_g}{k_2} \right) \left( \frac{k_2 + k_3}{k_2 - k_3} \right) \cos[k_g t - 2k_2(d - t)]
 \end{aligned}$$

$$\begin{aligned}
 D = & 2 \left( \frac{k_1}{k_g} - \frac{k_g}{k_2} \right) \sin(k_g t) - \left( 1 + \frac{k_1}{k_g} \right) \left( 1 + \frac{k_g}{k_2} \right) \left( \frac{k_2 + k_3}{k_2 - k_3} \right) \sin[k_g t + 2k_2(d - t)] \\
 & + \left( 1 - \frac{k_1}{k_g} \right) \left( 1 - \frac{k_g}{k_2} \right) \left( \frac{k_2 + k_3}{k_2 - k_3} \right) \sin[k_g t - 2k_2(d - t)]
 \end{aligned}$$





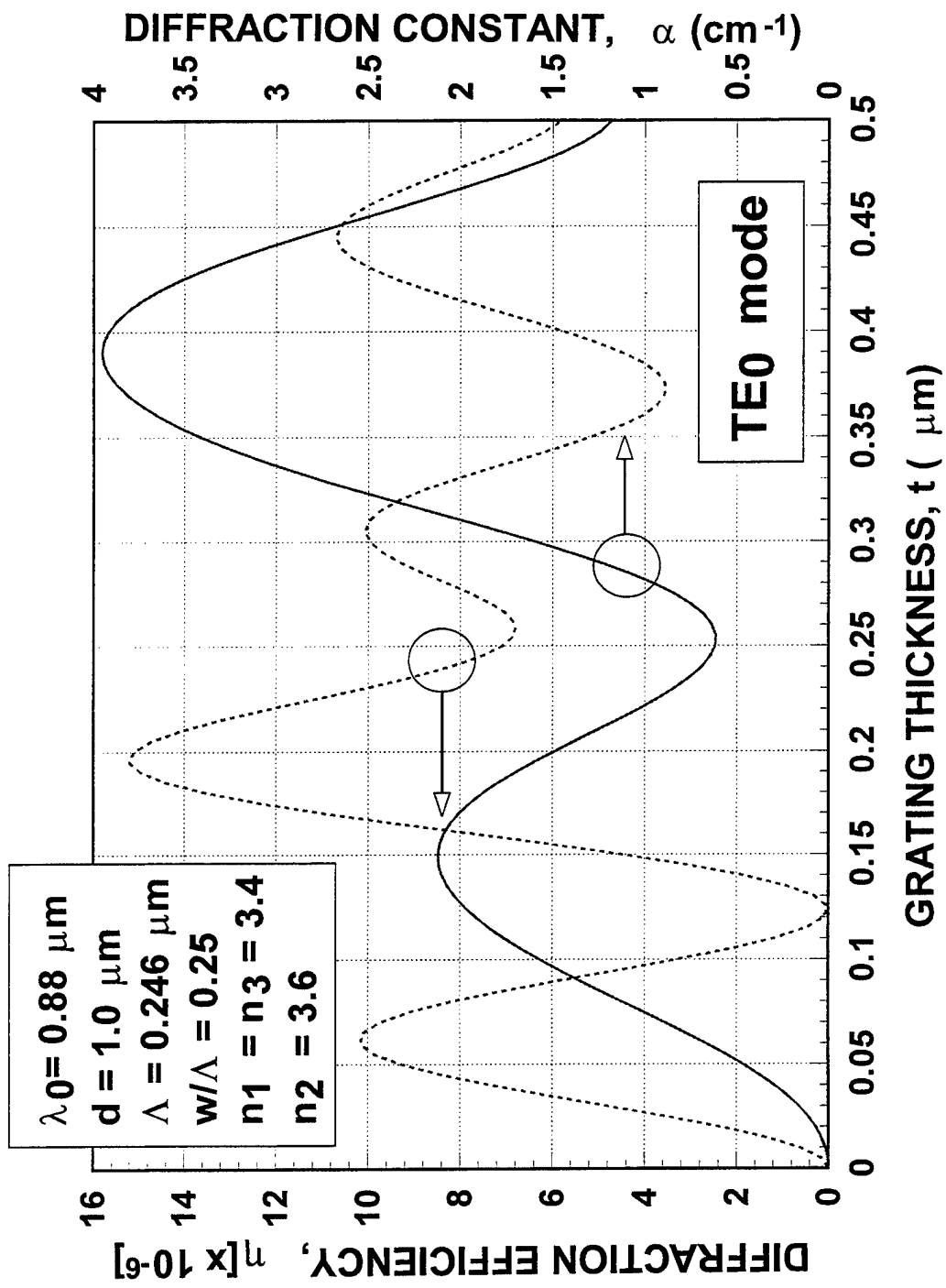


Fig. 2a

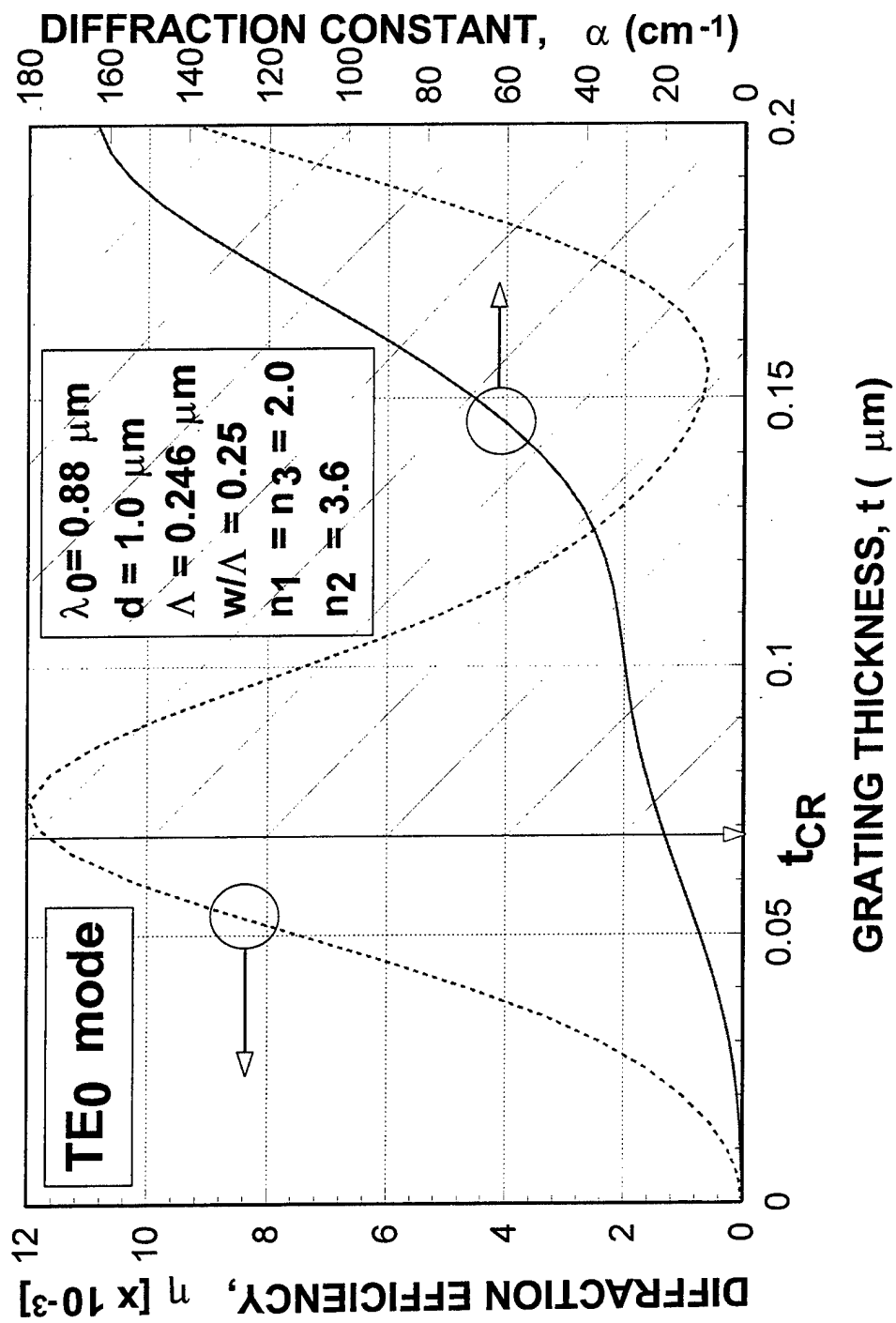


Fig. 2b

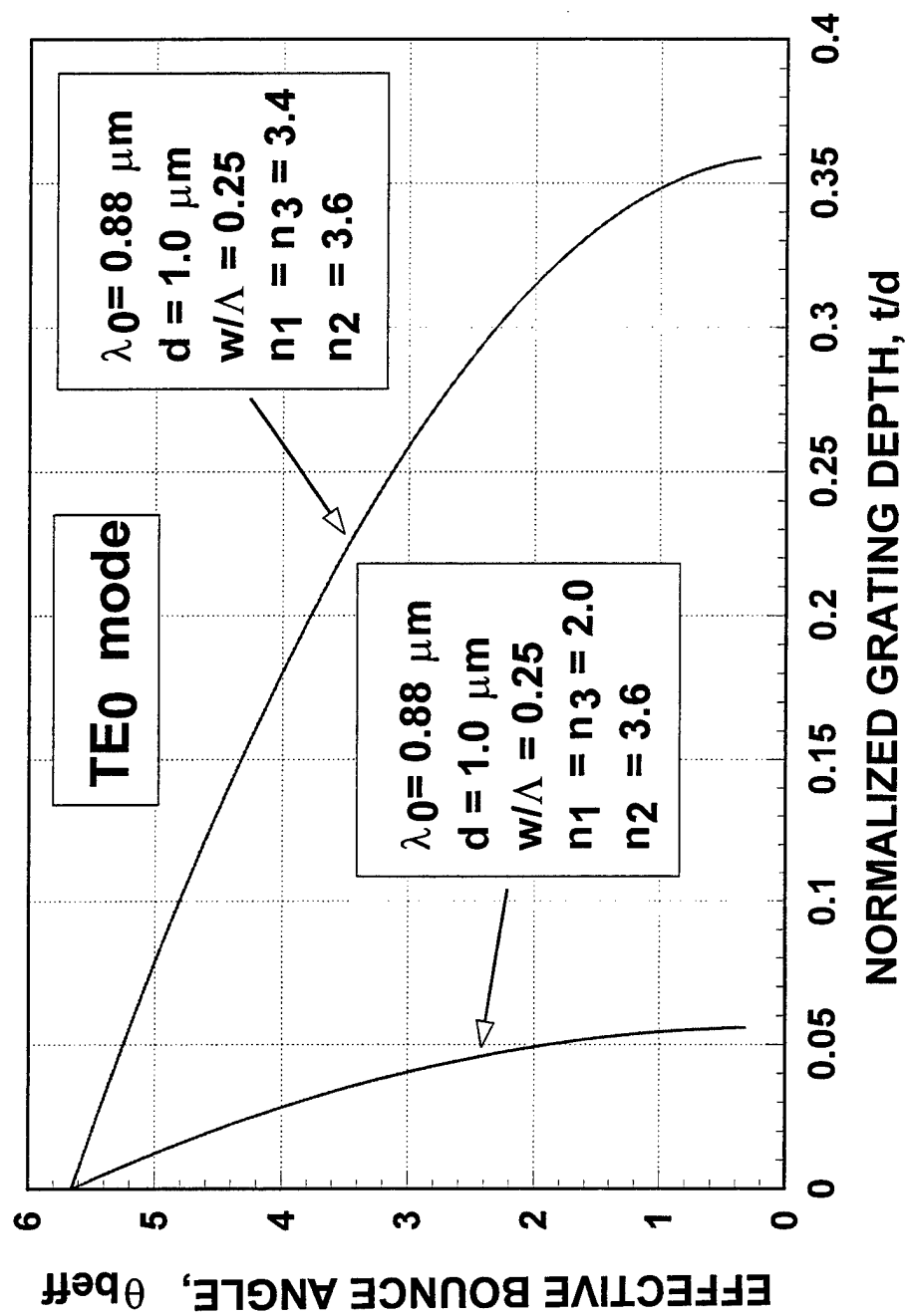


Fig. 2c

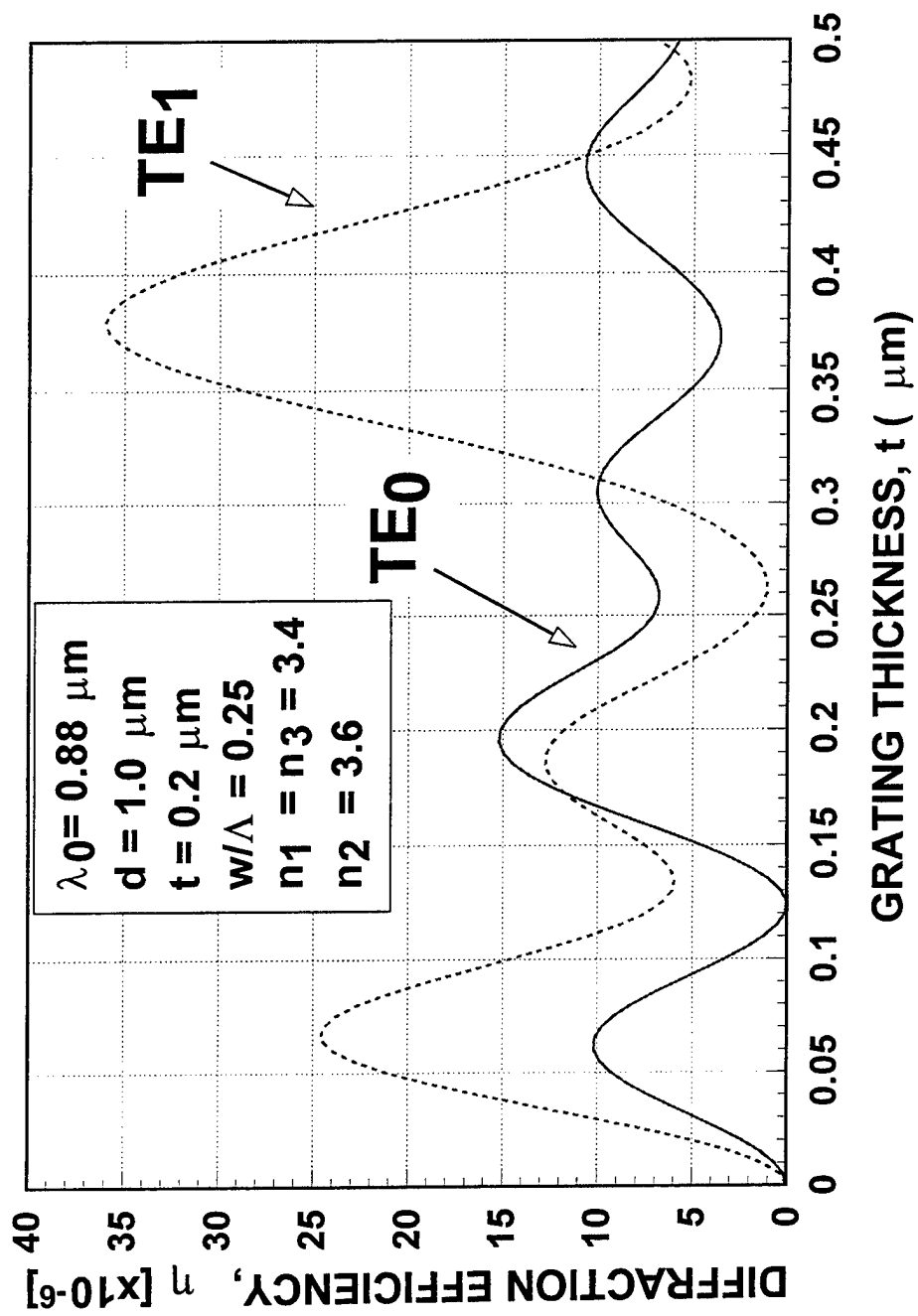


Fig. 3

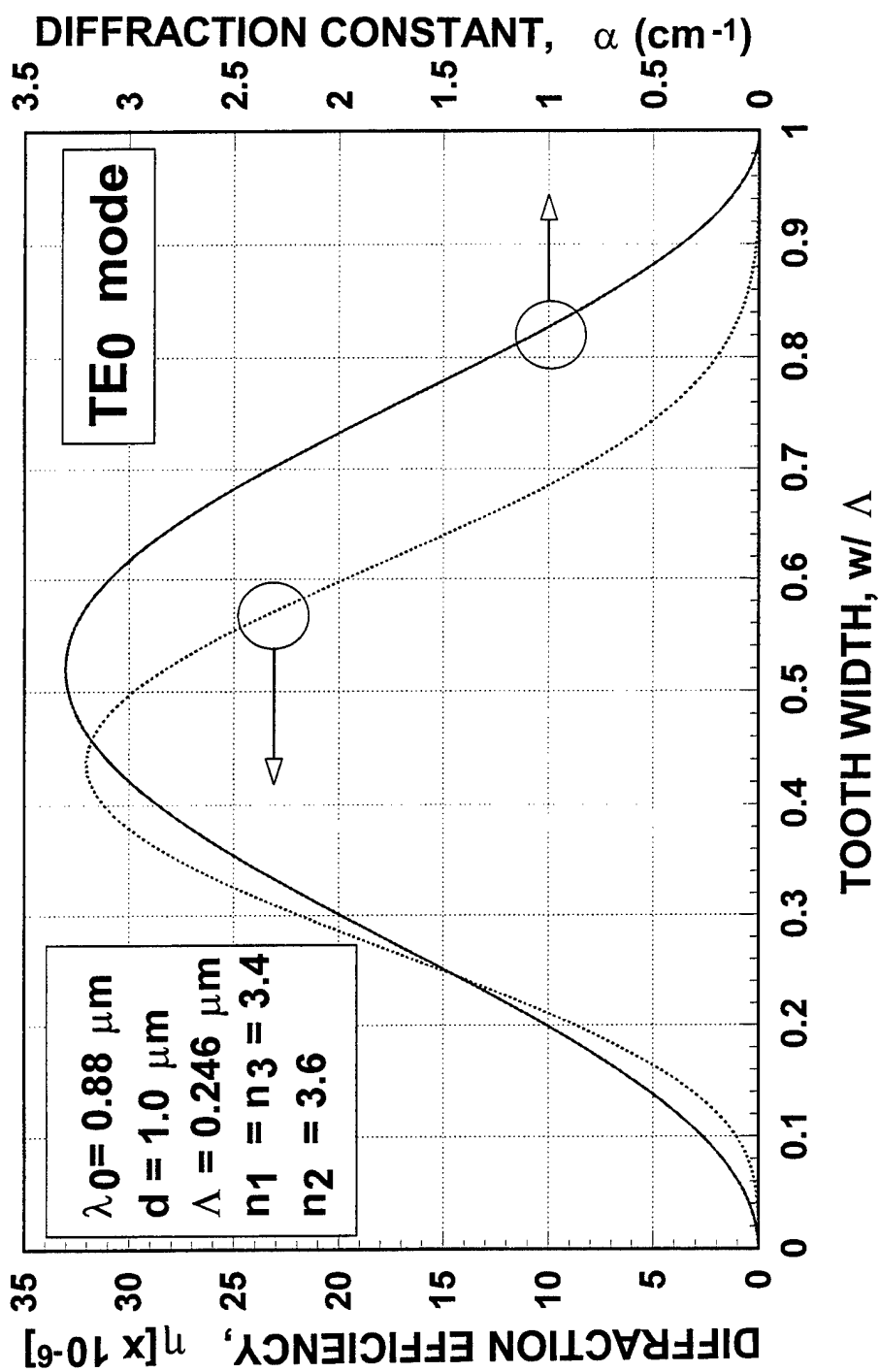


Fig. 4

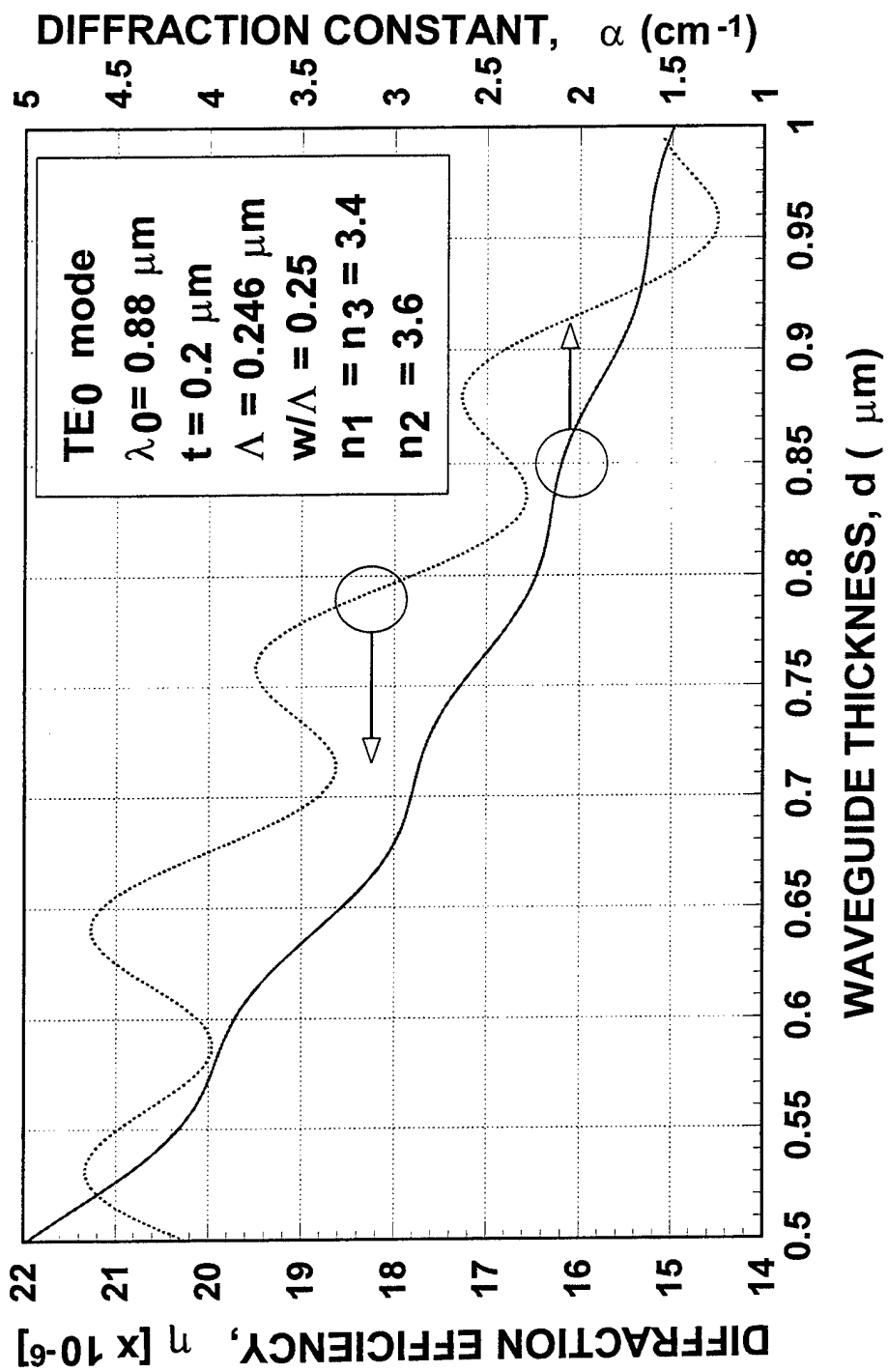
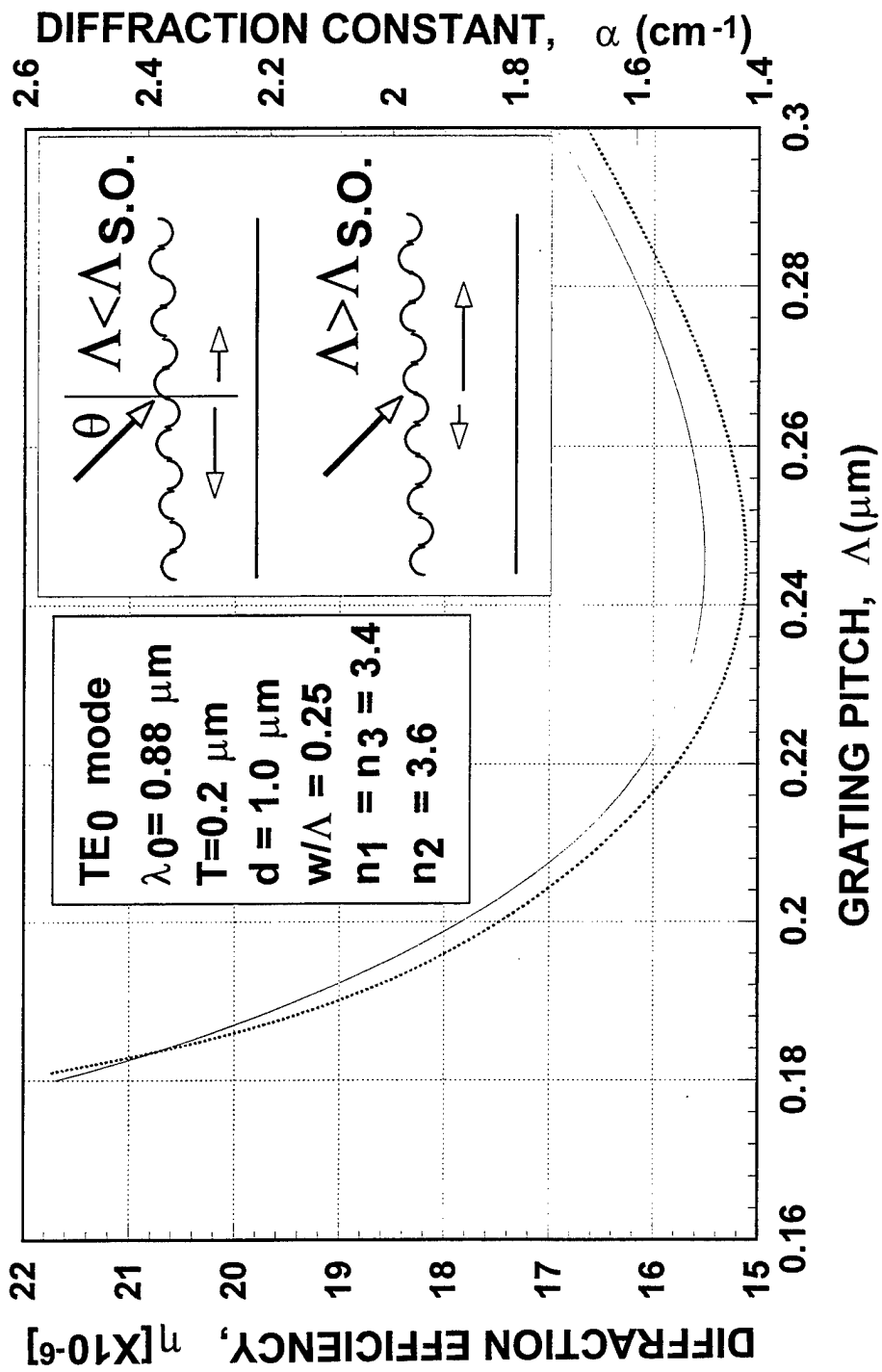


Fig. 5



**Fig. 6**